Detection of Fungal Infections of Different Durations in Canola, Wheat, and Barley and Different Concentrations of Ochratoxin A Contamination in Wheat and Barley using Near-Infrared (NIR) Hyperspectral Imaging

By

THIRUPPATHI SENTHILKUMAR

A Thesis

Submitted to the Faculty of Graduate Studies of

The University of Manitoba

in partial fulfilment of the requirements for the degree of

DOCTOR OF PHILOSOPHY

Department of Biosystems Engineering
University of Manitoba
Winnipeg, Canada,
R3T 5V6

Abstract

Fungal infection and mycotoxin contamination in agricultural products are a serious food safety issue. The detection of fungal infection and mycotoxin contamination in food products should be in a rapid way. A Near-Infrared (NIR) hyperspectral imaging system was used to detect fungal infection in 2013 crop year canola, wheat, and barley at different periods after inoculation and different concentration levels of ochratoxin A in wheat and barley. Artificially fungal infected (Fungi: *Aspergillus glaucus*, *Penicillium* spp.) kernels of canola, wheat and barley, were subjected to single kernel imaging after 2, 4, 6, 8, and 10 weeks post inoculation in the NIR region from 1000 to 1600 nm at 61 evenly distributed wavelengths at 10 nm intervals. The acquired image data were in the three-dimensional hypercube forms, and these were transformed into two-dimensional data. The two-dimensional data were subjected to principal component analysis to identify significant wavelengths based on the highest principal component factor loadings. Wavelengths 1100, 1130, 1250, and 1300 nm were identified as significant for detection of fungal infection in canola kernels, wavelengths 1280, 1300, and 1350 nm were identified as significant for detection of fungal infection in wheat kernels, and wavelengths 1260, 1310, and 1360 nm were identified as significant for detection of fungal infection in barley kernels. The linear, quadratic and Mahalanobis statistical discriminant classifiers differentiated healthy canola kernels with > 95% and fungal infected canola kernels with > 90% classification accuracy. All the three classifiers discriminated healthy wheat and barley kernels with > 90% and fungal infected wheat and barley kernels with > 80% classification accuracy.

The wavelengths 1300, 1350, and 1480 nm were identified as significant for detection of ochratoxin A contaminated wheat kernels, and wavelengths 1310, 1360, 1480 nm were identified as significant for detection of ochratoxin A contaminated barley kernels. All the three statistical classifiers differentiated healthy wheat and barley kernels and ochratoxin A contaminated wheat and barley kernels with a classification accuracy of 100%. The classifiers were able to discriminate between different durations of fungal infections in canola, wheat, and barley kernels with classification accuracy of more than 80% at initial periods (2 weeks) of fungal infection and 100% at the later periods of fungal infection. Different concentration levels of ochratoxin A contamination in wheat and barley kernels were discriminated with a classification accuracy of > 98% at ochratoxin A concentration level of ≤ 72 ppb in wheat kernels and ≤ 140 ppb in barley kernels and with 100% classification accuracy at higher concentration levels.

Acknowledgements

First I would like to thank my advisor Dr. Digvir. S. Jayas (Vice-President Research and International), for accepting me as his student, encouraging me towards my research goal, helping me all the time even in the middle of his extremely busy administrative job and a special thanks for his extreme patience. Second, I would like to thank Dr. N.D.G. White for providing me with all the samples required for this study, and for his unconditional support for attaining my research goals. I would like to thank my committee members Dr. Paul G. Fields and Dr. Tom Gräfenhan for providing excellent feedback on my research, and their help during manuscript submission is extraordinary.

I would like to extend my gratitude to Dr. C.B. Singh for sharing his expert knowledge in handling NIR hyperspectral imaging systems. My special thanks to Mr. C. Demianyk for helping me prepare fungal cultures throughout my research. I would like to extend my gratitude to my colleagues V. Chelladurai, Dr. L. Ravikanth, K. Kannan, and Dr. F. Jian.

I thank the Cereal Research Centre, Agriculture and Agri Food Canada, Winnipeg, for providing me with canola, wheat and barley and the Canadian Grain Commission, Winnipeg for providing me with the fungal cultures. I thank University of Manitoba Graduate Fellowship program, the Graduate Enhancement of Tri-Council Stipends program, Canola Council of Canada, Natural Sciences and Engineering Research Council of Canada for providing financial support for my research and I also thank Canada Foundation for Innovation, and Manitoba Research Innovation Fund and several industry partners for creating research infrastructure.

I would like to thank my CHET mentor Barbara for improving my presentation skills, her constant support and positive words helped me attain my career goals. I would like to thank my numerous friends and relatives for their constant encouragement and support. I also thank visiting researchers, Dr. M. Loganathan, and Dr. M.R. Srinivasan for sharing their research expertise. And a special mention to my undergraduate advisor, Dr. K. Alagusundaram, for what I am today. At last, I would like to thank my wife Suganya for her moral support.

THIS THESIS IS FONDLY DEDICATED TO MY PARENTS
T. SUBBULAKSHMI AND L. THIRUPPATHI FOR BEING MY PILLARS OF STRENGTH

Table of Contents

List of Figures

List of Tables

Chapter 1

Introduction and background

1.1 Food Security

World population at the start of 2014 was estimated to be at 7.2 billion and it is growing every year at an average rate of 1.2% from 2010 to 2014 (United Nations, 2014). It is estimated that 795 million people are chronically undernourished due to socio-economic factors (United Nations, 2014). It is important to feed the growing world population with limited land availability and growing demand for biofuels. Nearly 1300 million tonnes (Mt) or one third of the edible food products destined for human consumption are either lost or wasted due to losses occurring during production, post-harvest storage and handling, or during industrial processes; or wastage occurring during consumption. The losses occurring in developed countries are smaller compared to less developed countries, but wastage during consumption is more in developed countries compared to less developed countries (Gustavsson et al., 2011).

Cereals and oilseeds are major source of carbohydrates, proteins, and fats for human beings. Average world cereal grain and oil seed crop production for the five year period 2009 to 2013 is 2580 Mt and 178 Mt, respectively. The major cereal grains based on production are maize, rice, wheat, and barley and on utilization are rice, wheat, maize, and barley, respectively (Awika, 2011). The major oilseed crops produced are, soybean, palm, and rapeseed (canola) and utilized are palm, soybean and rapeseed (Mba, 2015). The losses occurring in cereals after harvest and before consumption are in the range from 14.5% in the developed world to 22.5% in the less developed world. The losses vary from year to year due to changes in environmental factors, and the losses occurring in oilseeds are in the range from 6% to 22% (Gustavsson et al., 2011). Storing the produced food materials without any losses is one of the important factors to increase arm economy, eradicate hunger, increase food security, and food safety for the world population.

1.2 Cereal grains and oilseeds in Canada

Canada is the fifth largest exporter of agricultural and agri-food products to the world market with an economic value of CAD $46 billion and a world share of 3.5% (Statistics Canada, 2013). The agri-food sector in Canada contributes 6.7% of total GDP and employs 2.2 million people. The total cash receipts of agricultural products including all cereals and oilseeds stood at CAD $31 billion dollars. Canola is the most valuable crop with the cash receipts of $7.3 billion followed by wheat at CAD $6.9 billion. Canadian barley (feed and malting) brings in CAD $1 billion as cash receipts. The total economic value of canola, wheat, and barley in Canada were CAD $19.3, 11.0, and 13.8 billion, respectively in 2013 (Canola Council of Canada, 2013; NRC Canada, 2013; Palladini and Armstrong, 2013).

Canada ranked eighth among the world countries producing cereal grains with a total cereal grains production of 66 Mt in 2013. Canada is the sixth largest producer and second largest exporter of wheat with total production of 37.5 Mt (27.3 Mt of spring, 6.5 Mt of durum, and 3.8 Mt of winter wheat) and total exports of 19.8 Mt in 2013 (FAOSTAT, 2013). Canada is the largest producer and exporter of durum wheat with annual export of 4.8 Mt (Statistics Canada, 2013). Canada is the fourth largest producer of barley grains with total production of 10.23 Mt and second largest exporter of malt with total export of 0.5 Mt in 2013 (FAOSTAT, 2013).

Canola (rapeseed) is one of the highest oil yielding crops in the world with an average of 44.5% oil content and the canola meal is used as animal feed that has 39.6% crude protein content. Canola oil is the third most consumed edible oil after palm oil and soybean oil with an annual production of 24.6 Mt (FAOSTAT, 2013). Canola is an oilseed crop developed by the

University of Manitoba and Agriculture and Agri-Food Canada researchers from rapeseed using normal plant breeding techniques. The difference between rapeseed and canola is the latter has low erucic acid (less than 2%), and glucosinolates (less than 30 micromoles) but the former has more than 50% of erucic acid and more than 90 micromoles of glucosinolates. The word canola is derived from its origin Canada and Ola meaning oil. Canada produced 17.9 Mt of canola in 2013 and ranked number one among all the rapeseed producing countries. Canada exports nearly 90% of its canola to the world market as seed, oil, and meal.

1.3 Storage losses

The major reason for spoilage of stored grains and oilseeds are moisture content and temperature at which grain is stored. The high moisture content and temperature facilitate the granivorous insects, mites, and fungi to grow and multiply and can result in total spoilage of stored grains. The other pests like rats, mice, and birds can feed on stored grains if there are few control or preventive measures for these pests.

1.3.1 Insects

The major insects causing damage to stored grains are of the orders Coleoptera, Lepidoptera, and Psocoptera and they can grow in the optimum temperature range between 18 and 38ºC, moisture content range between 13 and 15%, and relative humidity between 60 and 70% (Rees and Rangsi, 2004). The most common insects found in Canadian storage structures are *Tribolium castaneum* (Herbst), the red flour beetle, and *Cryptolestes ferrugineus* (Stephens), the rusty grain beetle (Fig 1.1) and they can survive even at lower humidity levels compared to other species.

A

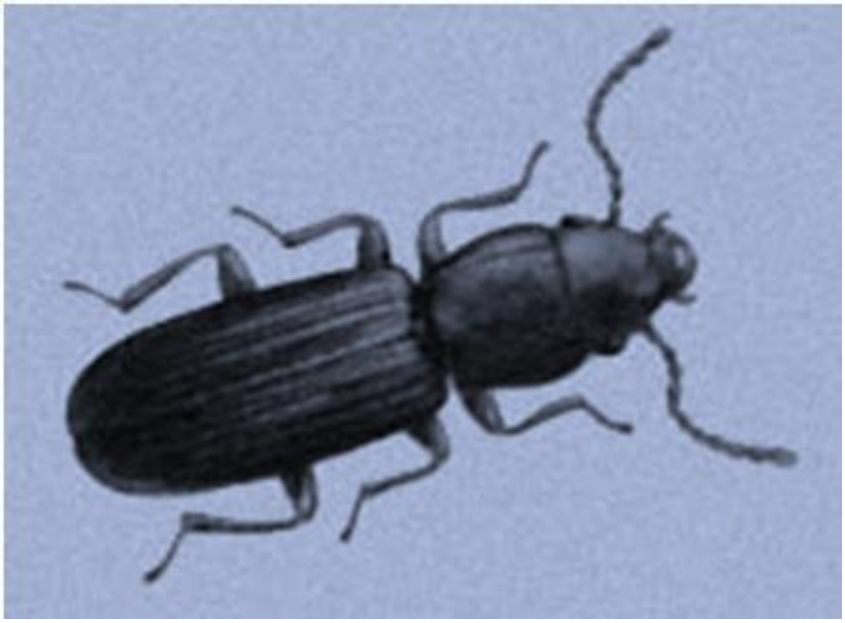

B

Fig. 1.1. *Tribolium castaneum*, the red flour beetle (A), and *Cryptolestes ferrugineus*, the rusty grain beetle (B).

The major losses occurring due to insect infestations are:

1. Quantity loss due to consumption by insects
2. Reduction in quality grade
3. Helps fungi to grow and multiply
4. Allergies to consumers
5. Contamination with insect parts and feces
6. Economic loss due to consumer rejection of infested grain products
7. Increase in pesticide levels in grains
8. Risk for pesticide applicators
9. Loss of farmers effort and energy to grow the crop
10. The allergic reactions associated with insect infestations are not fully documented and can be significant, but not as fatal as fungal infection and eventual mycotoxin production in stored grains.

1.3.2 Mites

The mites are very delicate organisms and are hard to see inside stored grain bulks. The major genera of mites found in Canada causing damage to stored grains and oilseeds are *Acarus, Glycyphagus, Tarsonemus, Lepidoglyphus* (predator) (Anonymous, 2009). The mites thrive at relative humidity above 60% and can survive even at lower temperature levels prevailing in Canada (Mills, 1989). The major losses occurring due to mites in stored grains are:

1. Mite infestations can taint the grains
2. Reduce germination
3. Can be allergenic to consumers

4. Can help fungi transportation

5. Highly infested grains become unfit for animal feed

6. Imparts bad odours to the grains.

1.3.3 Fungi

The fungi have the potential to cause more damage than insects and mites under unsuitable storage conditions. Fungi can deteriorate the grains and oilseeds (Fig.1.2.) and can contaminate the grains with its secondary metabolites, mycotoxins, which are a serious food safety issue. Consumption of mycotoxin contaminated grains can be fatal to both human beings and animals. There are two kinds of fungi causing damage to grains; one is the field fungi causing damage in the field, which can be controlled by properly drying the grains before storage, and another is storage fungi causing damage in the stored grains. The major fungal genera causing spoilage and contamination to stored grains are *Penicillium* and *Aspergillus.*

The major losses to stored grains due to fungal infection are:

1. Degrading of grains due to dull appearance and unacceptable odors caused by fungi
2. Appearance of visible mold
3. Rejection for seed usage due to loss of germination from the damaged germ
4. Rejection at processing level due to increase in free fatty acid values
5. Storage bin collapse due to uneven pressure points created by aggregation of grains
6. Bin burning and damage to premises caused by fungi induced heating
7. Contamination of products by mycotoxins
8. Respiratory problems to humans caused by fungal spores

Fig. 1.2. Fungal infection and aggregation in canola seeds stored at higher moisture content of 14% in plastic bags over the period of ten months.

9. Livestock poisoning due to mycotoxins
10. Economic loss due to feed refusal
11. Can cause potential health problems to human beings
12. Allergies for consumers
13. Rejection of shipments
14. Loss of well-established markets
15. Storage facilities can be unusable and need professional cleaning
16. Dangerous air space created by fungi inside the storage structures.

1.4 Mycotoxins

Mycotoxins are secondary metabolites (molecular weight less than 700) naturally produced by fungi under favorable temperature and humidity levels. Mycotoxins are both beneficial and harmful to human beings; the major benefits of mycotoxins are they can be used as immunosuppressant, antibiotics, medicine for hemorrhage and migraine headaches (Etzel, 2002). There are approximately 400 known mycotoxins, but only some of them are harmful to human beings and animals (Etzel, 2002). The death of 100,000 turkey poults in England in the year 1960 awakened the scientists about the harmful effects of mycotoxins and later the mycotoxins which killed turkey poults were identified as aflatoxins (Sargeant, 1961). The further research on the mycotoxins led to the identification of other harmful mycotoxins, Fumonisins, Deoxynivalenol (DON), T-2 toxin, Zearalenone, and Ochratoxin A. The major genera of fungi producing mycotoxins are *Aspergillus* and *Penicillium* at storage level, and *Fusarium* at field level. Mycotoxin contamination in agricultural products all over the world is estimated to be 25% (Kabak et al., 2006). Mycotoxin contamination is widely found in many agricultural crops and fruits all over the world. The illness outbreaks caused by mycotoxins can occur rarely in

developing countries, but the major concern is about long term ingestion of low levels of mycotoxin in food products and its health implications to consumers. The major mycotoxins found in food products are described below.

1.4.1 Aflatoxins

Aflatoxins are mainly produced by *Aspergillus flavus* Link and *Aspergillus parasiticus* Speare and are found mostly in peanuts, soybeans, maize, dried fruits, spices and other cereals. Aflatoxin contamination occurs mostly in tropical countries with hot and humid conditions and occasionally in temperate regions. There are different aflatoxins, B_1, B_2, G_1, G_2, M_1, and M_2, and the most potent among them is aflatoxin B_1. The milk obtained from cows consuming aflatoxin contaminated grains transforms aflatoxin B_1 into aflatoxin M_1 (Van Egmond, 1989). Aflatoxin B_1 can cause hepatocellular cancer in humans, damage to embryonic development, acute hepatitis, mutational changes and lethal dose of 10 to 20 mg of aflatoxin can cause death (Etzel, 2002). The aflatoxin had been classified as group 1 carcinogen by International Agency on Cancer Research (IARC) in 1993 and again confirmed in 2002 (IARC, 1993; 2002).

1.4.2 Ochratoxin A

Ochratoxin A (OTA) is produced by different species of the *Aspergillus* and *Penicillium* genera. In Canada, ochratoxin A is predominantly produced by *Penicillium verrucosum* Dierckx. ochratoxin A is mostly found in barley, wheat, rye, and coffee. ochratoxin A occurs in both tropical and temperate regions, species of *Aspergillus* genera are major producers of ochratoxin A in tropical regions and species of *Penicillium* genera are major producers of ochratoxin A in temperate regions (Duarte et al., 2010). Ochratoxin A is a very stable compound and it cannot be eliminated completely in normal industrial processing.

The OTA is a potent carcinogen in many animal species and classified as group 2B carcinogen by International Agency on Cancer Research (IARC, 2002; Duarte et al., 2011; Bui-Klimke and Felicia, 2015). The OTA is considered to be hepatotoxic, immunotoxic and teratogenic (Ringot et al., 2006; Bui-Klimke and Felicia, 2015). The OTA is a major mycotoxin found in Canadian stored grains and after analyzing the potential health hazards associated with OTA contamination, Health Canada proposed allowable maximum limits for ochratoxin A in grains and processed food products (Health Canada, 2009) as 0.5 µg/ kg in baby foods to 7 µg/ kg in wheat bran.

1.4.3 Fusarium toxins

The mycotoxins like Deoxynivalenol (DON), Zearalenone (ZEN), Fumonisins, and T-2 toxin are produced by *Fusarium* spp. in the field, if grains are not dried properly before storage, *Fusarium* spp. can also grow during storage. The fumonisins are mostly found in maize and are produced by *Fusarium verticillioides* (Sheldon) and *Fusarium proliferatum* (Matsush.) (Bryla et al., 2014). The major fumonisins are fumonisins B_1, B_2, and B_3; the most potent among them is fumonisins B_1 and are classified as group 2B carcinogens (IARC, 2002). Fumonisins can cause hepatic cancer in rats, esophageal cancer in humans, and pulmonary edema in pigs (Van Egmond, 2013). Deoxynivalenol also called as vomitoxin is produced by *Fusarium graminearum* (Schwabe) *and Fusarium subglutinans* (Wollen W. and Reinking) and they are predominantly found in wheat, barley, oats, rye, and maize (Clear and Abramson, 1986). Deoxynivalenol is considered to be immunosuppressive, embryotoxic and teratogenic, and neurotoxic (Piacentini et al., 2015).

Zearalenone (ZEN), mostly found in corn, wheat, barley, and oats, is produced by *F. graminearum, F. subglutinans, F. culmorum* (W.G. Smith) Sacc., and *F. cerealis*(Cooke)Sacc.

(Zinedine et al., 2007). Zearalenone can cause teratogenic, carcinogenic, neurotoxic, and estrogenic effects in both humans and animals (Liu et al., 2014). T-2 toxin, mostly found in corn, is produced by *Fusarium sporotrichioides* Sherb (Abramson et al., 2004). T-2 toxin can decrease feed consumption, cause diarrhea, skin problems, and hemorrhage in animals (Bennett and Klich 2003; Abramson et al., 2004).

1.4.4 Mycotoxins in Canada

The field level mycotoxins like Deoxynivalenol (DON), Zearalenone (ZEN), Fumonisins, and T-2 toxin are produced by *Fusarium* spp. and storage level mycotoxin ochratoxin A are of major concern. The presence of aflatoxin in Canadian stored products are not reported in the literature, but are reported to be found in imported food products and in exported Durum wheat at 10 ppb (CFIA, 2014). Canada has regulations for deoxynivalenol with a maximum allowable limit of 1.0 mg/kg, regulations stipulating maximum limits for ochratoxin A in food products are proposed by Health Canada at 0.5 to 7 µg/ kg, which is currently under consultation (Health Canada, 2009; 2012).

1.4.5 Occurrence of ochratoxin A in Canada

The ochratoxin A was found to be in 37 % of the Canadian wheat shipments above the Limit of Quantification (LOQ) during the period 2010-2012 (Tittlemier et al., 2014). The occurrence of ochratoxin A in durum wheat shipments was significantly higher than in spring wheat shipments (Tittlemier et al., 2014). Forty samples out of the 1970 samples analyzed for ochratoxin A contamination contain more than 5 µg/ kg, which is more than the maximum limit proposed by Health Canada (Tittlemier et al., 2014). The ochratoxin A occurrence increased with decrease in grain grade in all types of wheat (Tittlemier et al., 2014). Scudamore et al. (1999)

and Tittlemier et al. (2014) reported that occurrence of ochratoxin A increased with increase in storage time of wheat.

1.5 Fungal detection methods

The traditional microscopic-culture method to detect fungal infection is time-consuming (need 7 to 15 days from isolation to detection) and tedious process, and need professionals to detect different species. Soft X-ray imaging technique was used to detect fungal infection in corn with a classification accuracy more than 80% (Pearson and Wicklow, 2006), and in wheat (Narvankar et al., 2009) with classification accuracy more than 90%, however there is a risk from radiation emitted from the soft X-ray equipment. Thermal imaging was used to detect fungal infection in wheat at an advanced stage with classification accuracy more than 95%, but biggest disadvantage is we cannot differentiate between different fungal species due to more similar temperature profiles created by different fungal species, and fungal detection at early stage is yet to be studied (Chelladurai et al., 2010). Electronic nose was utilized to detect fungal infected cereals and it provided satisfactory results, but took a longer time for extraction and further volatile detection using Gas Chromatography-Mass Spectrometry (GC-MS). The new Polymerase Chain Reaction (PCR) based methods can detect fungal species and can also differentiate between different species but requires 24 h (Hayat et al., 2012). Fungal infections should be detected as soon as possible, to avoid further damage to the grains and to take necessary corrective measures.

1.6 Mycotoxin detection methods

The traditional methods employed to detect mycotoxins are a three-step process, the first is a time-consuming extraction procedure, followed by a cleanup procedure, and finally the

detection and quantification of mycotoxins using chromatographic methods. There are different extraction procedures currently used to extract compounds of interest from the samples, the time-consuming solvent extraction using methanol, acetonitrile or acetone, the costly and cumbersome supercritical fluid extraction, or the solid phase extraction, a promising technique with 95% recovery rate but it needs to be standardized (Turner et al., 2009). Immunoaffinity column (IAC) chromatography is used to purify and concentrate the extracted compounds. The last procedure involving detection and quantification are carried out by thin-layer chromatography (TLC), high performance liquid chromatography (HPLC), gas chromatography (GC), and ultra-performance liquid chromatography (UPLC). The chromatographic detection methods coupled with mass spectrometry quantification methods require at least 30 min to detect and quantify mycotoxins. ELISA is the fastest method when compared to traditional three-step chromatographic methods, but their quantification levels are lower when compared to chromatographic methods (Turner et al., 2009). The presence of mycotoxins in food products should be detected in a rapid way to avoid any serious food safety issues.

1.7 Near-Infrared (NIR) hyperspectral imaging

NIR imaging technique is a combination of both spectroscopy and conventional imaging and it is a promising method to detect various quality parameters associated with cereal grains and oilseeds (Vadivambal and Jayas, 2015). NIR hyperspectral imaging has been extensively used in many applications from its initial use in remote sensing applications in 1960s to its usage in biological materials in recent years (Vadivambal and Jayas, 2015). Fungal infection in stored products should be detected at a very short time; the time taken by NIR hyperspectral imaging system to acquire, process and analyze the image data corresponding to fungal infection in wheat only takes 2 min (Singh et al., 2007). The NIR hyperspectral imaging has been used to detect

fungal infection in stored grains at advanced stages of infection and obtained more than 95% classification accuracy, the NIR hyperspectral imaging technique was not used to detect fungal infection at an early stage. NIR hyperspectral imaging has not been used to its full potential to detect mycotoxins in stored products. Detection of ochratoxin A, the major storage mycotoxin in Canada, using NIR hyperspectral imaging has not been reported in the literature. Therefore, we decided to determine the potential of NIR hyperspectral imaging system to detect fungal infection in barley, canola and wheat (most valuable crops of Canada) at an earlier stage and to detect ochratoxin A contamination in stored barley and wheat with the following objectives. Ochratoxin A contamination in canola has not been reported to occur, so we decided to detect ochratoxin A contamination using NIR hyperspectral imaging only in wheat and barley.

1.8 Objectives

1. To assess the potential of NIR hyperspectral imaging to detect fungal infection in high oil content canola,
2. To detect different periods of fungal infection in stored canola using NIR hyperspectral imaging system, and to identify significant wavelengths corresponding to fungal infection in canola,
3. To detect different periods of fungal infection and different concentrations of ochratoxin A contamination in stored wheat using NIR hyperspectral imaging system, and to identify significant wavelengths corresponding to fungal infection and ochratoxin A contamination in wheat,
4. To detect different periods of fungal infection and different concentrations of ochratoxin A contamination in stored barley using NIR hyperspectral imaging system, and to

identify significant wavelengths corresponding to fungal infection and ochratoxin A contamination in barley,

5. To identify the classification accuracy between healthy and fungal infected samples of barley, canola, and wheat; and to determine classification accuracy between different species of fungal infected samples, and
6. To determine the classification accuracy between healthy and ochratoxin A contaminated samples of barley and wheat.

1.9 Organization of the Thesis

The thesis constitutes seven chapters:

Chapter 1

The first chapter deals with General Introduction and Objectives.

Chapter 2

The second chapter deals with the principals of near-infrared (NIR) hyperspectral imaging and its utilization in fungal and mycotoxin detection.

Chapter 3 to Chapter 6

The third to sixth chapters deal with the six objectives of this research thesis, chapter three deals with the first objective, chapter four the second objective, chapter five the third objective, chapter six the fourth objective; objective five is addressed in all the four chapters (chapter 3 to 6), and the sixth objective is addressed in chapter five and chapter six. Each chapter has its own Abstract, Introduction, Objectives, Materials and Methods, Results and Discussion, Conclusions and References.

Chapter 7

The seventh chapter summarizes the final conclusions of the research reported in this thesis comprising six objectives.

References

Abramson, D., B. McCallum, A. Tekauz, and D. M. Smith. 2004. HT-2 and T-2 toxins in barley inoculated with *Fusarium sporotrichioides*. *Canadian Journal of Plant Science* 84: 1189-1192.

Anonymous. (2009). Canadian Grain commission- Identifying the organisms. Available from: https://www.grainscanada.gc.ca/barley-orge/bom-mbo-eng.htm. Accessed 11.11.2015.

Awika, J.M. 2011. Major Cereal Grains Production and Use around the World. In Advances in Cereal Science: Implications to Food Processing and Health Promotion. American Chemical Society: Washington, DC.

Bennett, J. W. and M. Klich. 2003. Mycotoxins. *Clinical Microbiology Reviews* 16: 497–516.

Bryla, M., M. Roszko, K. Szymczyk, R. Jędrzejczak, E.S. Lowik, and M.W. Obiedzinski. 2014. Effect of baking on reduction of free and hidden fumonisins in gluten-free bread. *Journal of Agricultural and Food Chemistry* 62: 10341-10347.

Bui-Klimke, T.R. and W. Felicia. 2015. ochratoxin A and human health risk: a review of the evidence. *Critical Reviews in Food Science and Nutrition,* 55:1860-1869.

CFIA. 2014. 2010-2011 Aflatoxins in Dried Fruits, Nuts and Nut Products, and Corn Products.

Chelladurai, V., D.S. Jayas, and N.D.G. White. 2010. Thermal imaging for detecting fungal infection in stored wheat. *Journal of Stored Products Research* 46: 174-179.

Clear, R.M. and D. Abramson. 1986. Occurrence of fusarium head blight and deoxynivalenol

(vomitoxin) in two samples of Manitoba wheat in 1984. *Canadian Plant Disease Survey* 66(1): 9-11.

Etzel, R. A. 2002. Mycotoxins. *Journal of American Medical Association* 287:425-427.

FAOSTAT. 2013. Food and Agricultural commodities production. Food and Agricultural Organization of the United Nations. Available from: http://faostat3.fao.org/browse /Q/QC/Accessed 11.11.15

Gustavsson, J., C. Cederberg, U. Sonesson, R.V. Otterdijk, and A. Meybeck. 2011. Global food losses and food waste extent, causes and prevention. FAO: Rome.

Hayat, A., N. Paniel, A. Rhouati, J.L. Marty, and L. Barthelmebs. 2012. Recent advances in ochratoxin A-producing fungi detection based on PCR methods and ochratoxin A analysis in food matrices. *Food Control* 26(2): 401-415.

Health Canada. 2012. Canadian Standards (Maximum Levels) for Various Chemical Contaminants in Foods. Ottawa, Canada: Health Canada.

Health Canada. 2009. Proposed maximum limits for Ochratoxin A in food products. Ottawa, Canada: Health Canada.

IARC. 1993. Some naturally occurring substances: food items and constituents, heterocyclic aromatic amines and mycotoxins. In Monographs on the Evaluation of Carcinogenic Risks to Humans, Vol. 56. pp. 245–395. Lyon: IARC Press.

IARC. 2002. Some traditional herbal medicines: mycotoxins, naphthalene and styrene. In Monographs on the Evaluation of Carcinogenic Risks to Humans, Vol. 82, pp. 171-274.

Lyon : IARC Press.

Kabak, B., A. Dobson, and V. Isil. 2006. Strategies to prevent mycotoxin contamination of food and animal feed: a review. *Critical Reviews in Food Science and Nutrition* 46: 593-619.

Liu, J., Y. Hu, G. Zhu, X. Zhou, L. Jia, and T. Zhang. 2014. Highly sensitive detection of Zearalenone in feed samples using competitive surface-enhanced Raman scattering immunoassay. *Journal of Agricultural and Food Chemistry* 62: 8325-8332.

Mba, O.I., M.J. Dumont, and M. Ngadi. 2015. Palm oil: Processing, characterization and utilization in the food industry – A review. *Food Bioscience* 10: 26-4.

Mills, J.T. 1989. Spoilage and heating of stored agricultural products. Ottawa, Canada: Canadian Government Publishing Centre Supply and Services Canada.

Narvankar, D.S., C.B. Singh, D.S. Jayas, and N.D.G. White. 2009. Assessment of soft X-ray imaging for detection of fungal infection in wheat. *Biosystems Engineering*, 103: 49-56.

Pearson, T.C. and D.T. Wicklow. 2006. Detection of kernels infected by fungi. *Transactions of the ASABE* 49(4): 1235-1245.

Piacentini, K.C., G.D. Savi, M. E.V. Pereira, and V. M. Scussel. 2015. Fungi and the natural occurrence of deoxynivalenol and fumonisins in malting barley (*Hordeum vulgare* L.). *Food Chemistry* 187: 204-209.

Rees, D. P., and T.V. Rangsi. 2004. Insects of stored products. Collingwood, Vic : CSIRO.

Scudamore, K.A., S. Patel, and V. Breeze. 1999. Surveillance of stored grain from the 1997 harvest in the United Kingdom for ochratoxin A. *Food Additives & Contaminants: Part A* 16(7): 281-290.

Singh, C.B., D.S. Jayas, J. Paliwal, and N.D.G. White. 2007. Fungal detection in wheat using near-infrared hyperspectral imaging. *Transactions of the ASAE* 50: 2171-2176.

Statistics Canada. 2013. Table 002-0001 - Farm cash receipts, annual (dollars), CANSIM (database). (Accessed: 2015-09-20).

Tittlemier, S.A., M. Roscoe, R. Blagden and C. Kobialka. 2014. Occurrence of ochratoxin A in Canadian wheat shipments, 2010–12. *Food Additives & Contaminants: Part A* 31(5): 910-916.

Turnera, N.W., S. Subrahmanyam, and S.A. Piletsky. 2009. Analytical methods for determination of mycotoxins: A review. *Analytica Chimica Acta* 632: 168‑180.

United Nations. 2014. *Concise Report on the World Population Situation in 2014*. UN: New York.

Vadivambal, R., and D.S. Jayas. 2015. *Bio-Imaging: Principles, Techniques and Applications*. CRC Press, Taylor and Francis Group Ltd: Oxford, UK.

Van Egmond, H.P. 1989. Aflatoxin M1: occurrence, toxicity, regulation. In: Van Egmond, H.P. (Ed.), Mycotoxins in Dairy Products. pp. 11–55. London: Elsevier Applied Science.

Van Egmond, H.P. 2013. Mycotoxins: Risks, regulations and European co-operation. *Journal of Natural Sciences* 125: 7-20**.**

Zinedine, A., J. M. Soriano, J.C. Molto, and J. Manes. 2007. Review on the toxicity, occurrence, metabolism, detoxification, regulations and intake of Zearalenone: An oestrogenic mycotoxin. *Food and Chemical Toxicology* 45: 1-18.

Chapter 2

Near-Infrared (NIR) hyperspectral imaging: theory and applications to detect fungal infection and mycotoxin contamination in food products

Abstract

Near-Infrared hyperspectral imaging system is a promising technique to detect various quality parameters associated with food products. NIR hyperspectral imaging system can collect both spectral and spatial information of any given object and it can detect chemical constituents of food products, therefore it is also called chemical imaging. The image data obtained from hyperspectral imaging system are in the hypercube form, two spatial dimensions and third spectral dimension. The image data in the hypercube form cannot be directly used for analyzing, so the three-dimensional data is transformed into two-dimensional data using automatic thresholding, labelling, and reshaping. The transformed two-dimensional data subjected to principal component analysis provided significant wavelengths. Statistical features and histogram features extracted from the significant wavelengths were used in the statistical classification models. Fungal infection and mycotoxin contamination in food products disturb the original chemical composition of food products, the NIR hyperspectral imaging or chemical imaging has the potential to detect the chemical changes occurring in the sample. The NIR hyperspectral imaging system has the potential to detect fungal infection and mycotoxin contamination in food products.

2.1 Introduction

Quality of food is determined by its physical, chemical, and biological attributes. The physical attributes are usually assessed by visual inspection, chemical, and biological attributes are determined using tedious, and time consuming processes. The traditional methods involve use of many laboratory chemicals, need for professional experience, and they are disruptive to the samples. The need for safe food compelled scientists and engineers to develop instruments to measure various quality attributes associated with food products using economical methods that are fast, non-destructive, chemical-free and requiring only simple steps to operate. With the advent of digital imaging using black white or color cameras, the measurement of physical attributes by extracting spatial information made the physical attributes measurements easier and requires very little human attention. The development of NIR spectroscopy is really a boon to the food processors, by giving them a fast and chemical-free method by collecting the spectral information of an object. The biggest disadvantage of digital imaging is it cannot collect spectral information and the biggest disadvantage of NIR spectroscopy is it cannot collect spatial information. These disadvantages led to a new system called NIR hyperspectral imaging, which can provide both spatial and spectral information of an object.

Near-Infrared region of the electro-magnetic spectrum was discovered by Frederick William Herschel in 1800 (Manely, 2014), but its use in biological applications was realized after the arrival of NIR spectroscopy in 1970. The hyperspectral imaging was first developed for remote sensing applications, then later extended to agriculture, pharmaceuticals, food industry, and medical applications (Vadivambal and Jayas, 2015). The applications of NIR hyperspectral imaging in various fields and its application for cereal quality assessment were reported in the literature (Mahesh et al., 2015; Vadivambal and Jayas, 2015). The objective of this review is to

synthesize the applications of NIR hyperspectral imaging system to detect fungal infection and mycotoxin contamination in food products.

2.2 Principle of NIR hyperspectral imaging

A NIR hyperspectral imaging system utilizes the physical and chemical nature of a material to emit, absorb, transmit and reflect electromagnetic energy in a unique way at different wavelengths. The image acquired by the NIR hyperspectral imaging is in a three-dimensional hypercube form, two spatial and the third spectral dimension (wavelength) (Fig. 2.1.). There are three types of NIR hyperspectral imaging systems, the first is a staring system or area scan, the second is a push-broom or line scan system and the third is a whisk-broom or point scan. The staring system can capture two-dimensional images of a stationary sample at different wavelength for each spatial location (pixels). The push-broom system captures images of moving sample (or moving camera over stationary sample) and the image data obtained have the spectral information along one line. The whisk-broom system captures one spectrum at a time. The NIR hyperspectral imaging system is comprised of NIR camera with indium gallium arsenide (InGaAs) or mercury cadmium telluride (HgCdTe)-based array detector, liquid crystal tunable filters (LCTFs) to tune on to desired wavelengths, a light source in the NIR range, the most common light source is tungsten halogen lamps, and a computer with software to capture and analyze the image data.

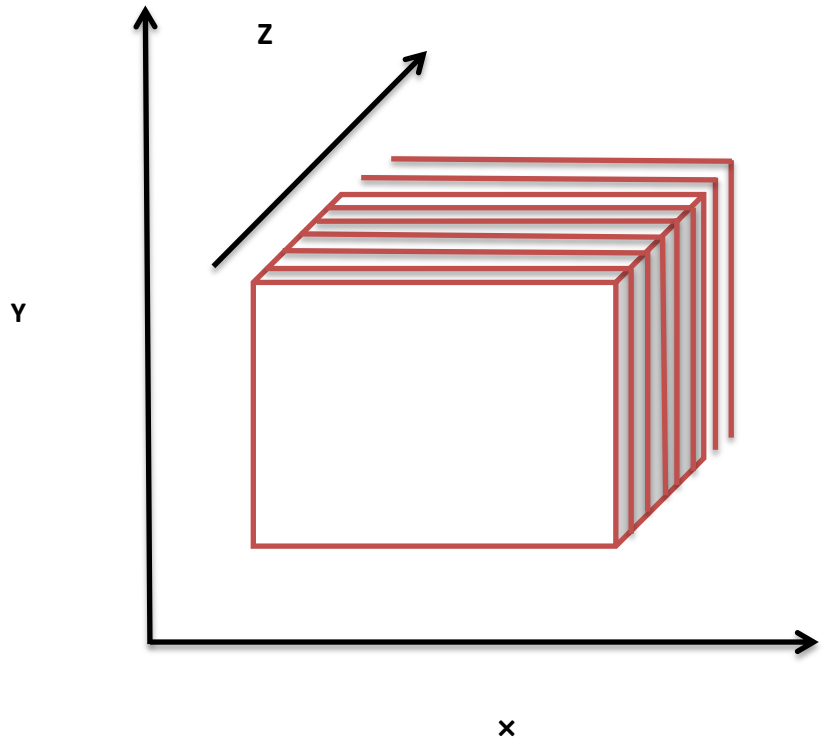

Fig. 2.1 Three-dimensional hypercube data obtained from NIR hyperspectral imaging system. (X, Y : spatial data; Z: spectral data (wavelength)).

2.3 Detection of fungal infection using NIR hyperspectral imaging

Staring or area scan and push-broom or line-scan NIR hyperspectral imaging systems in the range between 700 and 2500 nm have been used to detect fungal infection in various food products.

2.3.1 Staring system

Staring NIR hyperspectral imaging system in the range from 1000 to 1600 nm was used to detect *Aspergillus glaucus group*, *Aspergillus niger*Van Tieghan, and *Penicillium* spp. infected wheat samples, the image data subjected to principal component analysis provided 1284.2, 1315.8, and 1347.4 nm as significant wavelengths to detect fungal infection in wheat. Statistical and histogram features were extracted from significant wavelengths and were used in the classification models. Pair-wise and two-class models discriminated healthy kernels and fungal infected kernels with a classification accuracy of 95% (Singh et al., 2007). *Aspergillus flavus* infection in dates was detected using staring NIR hyperspectral imaging system in the range from 960 to 1700 nm (Teena et al., 2014). The principal component analysis applied to the image data provided 1120, 1300, 1610, 1650 nm as significant wavelengths to identify fungal infection in dates 48 h post inoculation. Statistical and histogram features corresponding to the significant wavelengths were extracted and used in the classification models. Linear and quadratic discriminant classifiers differentiated healthy dates from fungal infected dates with a classification accuracy of more than 90% (Teena et al., 2014).

Staring NIR hyperspectral imaging system was used to detect *A. flavus* and *Penicillium commune* Thom,C. infected pinto beans, chickpeas, kidney beans, green peas, and lentils in the NIR range from 960 to 1700 nm (Karuppiah et al., 2016). The wavelengths 1110, 1250, 1300,

1440, 1550 nm were significant to detect fungal infection in five different pulses. Histogram and statistical features extracted from significant wavelengths were used in the classification algorithms. The two-class and six-class discriminant statistical models developed to discriminate fungal infected samples from healthy samples provided more than 90% classification accuracy (Karuppiah et al., 2016). Staring shortwave NIR hyperspectral imaging system was used to detect *A. glaucus, A.niger,* and *Penicillium* spp. infected wheat kernels in the short wave NIR range from 700 to 1100 nm (Singh et al., 2012). The wavelength 870 nm was identified as significant wavelength to detect fungal infection in wheat. Statistical and histogram features corresponding to 870 nm wavelength were used in the two-class classification models. Linear, quadratic, and Mahalanobis discriminant classifiers differentiated fungal infected samples from healthy samples with a classification accuracy of more than 97% (Singh et al., 2012).

2.3.2 Push-broom system

Maize kernels infected with *Fusarium verticillioides* were subjected to push-broom NIR hyperspectral imaging in NIR range from 1000 to 2498 nm (Williams et al., 2012). The wavelengths 1900 and 2136 nm was identified as significant to detect fungal infection in maize based on highest factor loadings in the principal component analysis. The fungal infected maize samples were differentiated from healthy kernels at an early stage (48 h after inoculation) (Williams et al., 2012).

Push-broom NIR hyperspectral imaging system was used to detect *Alternaria alternata* (Fr.) Keissl, *A. brassicae* (Berk.) Sacc., and *A. brassicicola* (Schwein.) Wiltshire infected rapeseed kernels in the NIR region of 1000-2500 nm (Baranowski et al., 2015). The classification models differentiated healthy samples from fungal infected samples with

classification accuracy more than 80% at early stage (2 days) and more than 90 at later stages of infection (Baranowski et al.,2015).

Aspergillus oryzae (Ahlburg) E.Cohninfected brown rice were differentiated from healthy brown rice using push-broom NIR hyperspectral imaging system in the NIR range from 750 to 1000 nm. The NIR system detected fungal infected brown before the visible mold growth (Siripatrawan and Makino, 2015).

2.4 Detection of mycotoxins using NIR hyperspectral imaging

Ergot alkaloids (produced by *Claviceps purpurea* (Fr.) Tul.) contaminated rye, oats, and wheat were subjected to staring NIR hyperspectral imaging system in the range from 970-2500 nm (Vermeulen et al., 2013). The wavelengths 1573 and 2399 nm were identified to be significant in detecting ergot alkaloids in rye, oat, and wheat. There was a correlation of 0.94 between predicted and supplied values (Vermeulen et al., 2013).

Aflatoxin B_1 contaminated maize kernels were subjected to push-broom NIR hyperspectral imaging system in the range from 1000 to 2500 nm (Wang et al., 2015). The wavelengths 1729 and 2344 nm were identified to be significant in detecting Aflatoxin B_1 in maize kernels. The classification models differentiated contaminated samples from healthy samples with classification accuracy more than 80% (Wang et al., 2015).

2.5 Discussion

NIR hyperspectral imaging system used to detect fungal infection in food products mostly used staring and push-broom methods. The wavelength 1300 nm was attributed as the significant wavelength in most of the studies dealing with the detection of fungal infection in food products (Singh et al., 2007; Teena et al., 2014; Karuppiah et al., 2016). Principal

component analysis was the most common method to identify significant wavelengths corresponding to fungal infection and mycotoxin contamination in grains. NIR hyperspectral imaging system discriminated different fungal infected species with a classification accuracy of more than 90% (Singh et al., 2007). Statistical features in addition to histogram features extracted from significant wavelengths provided better classification accuracy than studies which used either statistical features or histogram features. Linear, quadratic and Mahalanobis statistical discriminant classifiers were mostly used to find classification accuracies between different samples. The NIR hyperspectral imaging system to detect fungal infection at an early stage and at different fungal infection periods is yet to be explored. The NIR hyperspectral imaging system was used to detect ergot alkaloids and aflatoxins in food products with excellent classification accuracies between healthy and mycotoxin contaminated samples, but other storage mycotoxins like ochratoxin A, which is more prevalent in temperate regions is yet to be studied. The literature on detection of fungal infection and mycotoxin contamination in food products using NIR hyperspectral imaging system is minimal, which indicates that this system has not yet been fully researched and its full potential not yet fully realized.

References

Baranowski, P., M. Jedryczka, W. Mazurek, D. B. Skowronska, A. Siedliska, and J. Kaczmarek. 2015. Hyperspectral and Thermal Imaging of Oilseed Rape (*Brassica napus*) Response to Fungal Species of the Genus Alternaria, PloS one 10: 1-19.

Karuppiah, K., T. Senthilkumar, D.S. Jayas, and N.D.G. White. 2016. Detection of fungal infection in five different pulses using near-infrared hyperspectral imaging. *Journal of Stored Products Research* 65: 13-18.

Manley, M. 2014. Near-infrared spectroscopy and hyperspectral imaging: non-destructive analysis of biological materials. *Chemical Society Review* 43: 8200-8214.

Mahesh, S., D.S. Jayas, J. Paliwal and N.D.G. White. 2015. Hyperspectral imaging to classify and monitor quality of agricultural materials. *Journal of Stored Products Research* 61: 17-26.

Singh, C.B., D.S. Jayas, J. Paliwal, and N.D.G. White. 2007. Fungal detection in wheat using near-infrared hyperspectral imaging. *Transactions of the ASAE* 50: 2171-2176.

Singh, C.B., D.S. Jayas, J. Paliwal, and N.D.G. White. 2012. Fungal damage detection in wheat using short-wave near-infrared hyperspectral and digital colour imaging. *International Journal of Food Properties* 15: 11-24.

Siripatrawan, U. and Y. Makino. 2015. Monitoring fungal growth on brown rice grains using rapid and non-destructive hyperspectral imaging. *International Journal of Food Microbiology* 199: 93-100.

Teena, M.A., A. Manickavasagan, L. Ravikanth, and D.S. Jayas. 2014. Near-infrered (NIR)

hyperspectral imaging to classify fungal infected dates. *Journal of Stored Products Research* 59: 306-313.

Vadivambal, R., and D.S. Jayas. 2016. *Bio-Imaging: Principles, Techniques and Applications*. CRC Press, Taylor and Francis Group Ltd: Oxford, UK.

Vermeulen, P.H., J. A. F. Pierna, H. P. Van-Egmond, J. Zegers, P. Dardenne, and V. Baeten. 2013. Validation and transferability study of a method based on near-infrared hyperspectral imaging for the detection and quantification of ergot bodies in cereals. *Analytical and Bioanalytical Chemistry* 405(24): 7765-7772.

Wang, W., X. Ni, K. C. Lawrence, S.C. Yoon, G. W. Heitschmidt, P. Feldner. 2015. Feasibility of detecting Aflatoxin B_1 in single maize kernels using hyperspectral imaging. *Journal of Food Engineering* 166: 182-192.

Williams, P. J., P. Geladi, T.J. Britz, and M. Manley. 2012. Investigation of fungal development in maize kernels using NIR hyperspectral imaging and multivariate data analysis. *Journal of Cereal Science* 55(3): 272-278.

Chapter 3

Detection of fungal infection in canola using near-infrared hyperspectral imaging

Abstract

Canada is the largest exporter of canola to the world market. It is very important to maintain the quality of canola to get good price for the seed. Fungal infection is the most significant problem to stored canola because of high oil content and it can reduce oil quality, seed germination, and impart unacceptable odors. Near-infrared (NIR) hyperspectral imaging was used in this study to detect the presence of fungal infection in stored canola. Artificially fungal infected (*Aspergillus glaucus* group) canola was subjected to single kernel imaging every two weeks after incubation using an NIR imaging system in the wavelength range of 1000 to 1600 nm at 61 evenly distributed wavelengths. Three wavelengths 1100, 1250 and 1300 nm were identified as significant wavelengths and were used in the analysis. Statistical discriminant classifiers (Linear and Quadratic) were used to classify healthy, two, four, six, eight, and ten week fungal incubated samples. The linear and quadratic statistical classifiers gave maximum accuracy of 99% for healthy samples and 100% for fungal infected samples at later stages of infection levels and 90 to 95% for the first four weeks of *A. glaucus* infected samples.

3.1 Introduction

Average canola (*Brassica napus L.*, low erucic acid oil) production in Canada during the 2005-2010 crop years was 10.7 Mt; and 6.3 Mt of canola seeds were exported to the world market making Canada the largest exporter of canola (Statistics Canada, 2011). Canola is the second most valuable crop after wheat as it adds $14 billion to the Canadian economy (Canola Council of Canada, 2008). High oil content present in canola makes it unfavorable for the insects to multiply but, creates a more conducive environment for the fungi and mites to grow (Sinha and Wallace, 1977; Brogan, 1986), however, fungi cause more damage to the canola seeds than mites (Mills et al., 1978). There are two types of fungi, pre-harvest or field fungi and post-harvest or storage fungi. Field fungi can be eliminated by drying before storage, but storage fungi under favourable temperature and moisture conditions inside the storage facilities grow exponentially.

The storage fungal species usually found in Canadian canola seeds are *Aspergillus glaucus* group, *Aspergillus candidus* Link, and *Penicillium* spp.; the *A. glaucus* can grow even at low relative humidity (Pronyk et al., 2004). The fungi consume the dry matter, and release carbon dioxide, water and energy. The reduction in dry matter content, which is an indicator of seed quality loss affects the market price of canola. The fungal infection in canola reduces the germination capacity and oil quality; increases fat acidity values and ergosterol content; causes discolouration and can impart unacceptable odours. It is very important to protect the oilseeds from any quality degradation, for providing safe products to the consumers, and good returns to the farmers. Discrimination of fungal-infected seeds from healthy seeds can help in reducing the quality related problems, and if identified in initial stages, can avoid further damage to the canola.

The identification of fungal-infected canola should be a rapid method to eliminate the infected seeds and to protect the healthy seeds. The traditional microbial culture methods and microscopic detection and quantification methods take a long time (Magan, 1993; Williams, 1989). Different techniques have been investigated to detect the presence of fungi such as ultra sound (Walcott *et al*., 1998) and machine vision (Paulsen, 1990) but the major issue is the low accuracy in detecting fungi in incipient growth stages. Soft X-rays was used to classify the fungal infected wheat kernels with the classification accuracy more than 90 % (Narvankar *et al*., 2009), but soft X-ray can be harmful to humans.

The NIR hyperspectral imaging (chemical or spectral imaging) is an emerging technology that combines spectroscopy and conventional imaging to get both spatial and spectral information about an object. Researchers have used NIR hyperspectral imaging in remote sensing (Goetz et al., 1985), agriculture (Monteiro et al., 2007) and pharmaceuticals (Gowen et al., 2008). The flexible and non-destructive nature of hyperspectral imaging makes it a suitable technique for assessing food quality (Naganathana et al., 2008).

The NIR hyperspectral imaging has been used in determining many quality parameters of grains: to differentiate Canadian wheat classes with classification accuracy between 86-100% using statistical classifiers (Mahesh et al., 2008); midge damage in wheat kernels with high classification accuracy (Singh et al., 2010a); insect damaged wheat kernels with classification accuracy of more than 90% (Singh et al., 2010b); and detection of fungal-infected wheat samples with a classification accuracy of more than 90% from healthy samples (Singh et al., 2007). The later study did not identify the fungal infection at different stages. The NIR hyperspectral imaging technique has not been explored to detect quality parameters in canola.

Therefore, the objectives of this study were:

1. To assess the potential of NIR hyperspectral imaging system for detecting fungal (*A. glaucus*) infection in high oil content canola, and

2. To determine the classification accuracy of five different infection stages of fungal-infected canola and healthy samples.

3.2 Materials and Methods

3.2.1 Culture preparation

Four kilogram sample at 14.5% moisture content after surface sterilization using 1% sodium hypochlorite solution of a high oil content (over 45% wet weight basis) canola (variety InVigor 5440), was used to prepare fungal-infected samples. The cultures of *A. glaucus* group were obtained from the Cereal Research Centre, Agriculture and Agri-Food Canada, Winnipeg, MB. The pure fungal lines were placed on potato dextrose agar (PDA) medium for 1 week at 30°C. The agar medium with fungal spores was sprayed on the canola seeds after diluting the medium with 200 mL sterilized water and one drop of Polysorbate 20. The canola seeds were placed in a plastic bag with provision for air movement in an environmental chamber (CONVIRON, Controlled Environments Limited, Winnipeg, MB) at 30°C and the fungal infected samples were collected after 2, 4, 6, 8 and 10 weeks for imaging. Proper safety measures like disposable respirator with valve (Fig. A.7), disposable gloves (Fig. A.8) and 95% ethanol solution were used when handling fungal cultures and fungal infected samples.

3.2.2 NIR hyperspectral imaging

The NIR hyperspectral imaging system consisted of a camera with liquid crystal tunable filters (LCTFs), a mount lens, a sample stage, and a light source and a computer system for image analysis as shown in Fig. 3.1.The camera (Model No. SU640-1.7RT-D, Sensors Unlimited Inc., Princeton, NJ) had an Indium Gallium Arsenide (InGaAs) detector and was used for acquiring images in the 1000-1600 NIR wavelength region at 10 nm intervals. The camera had the spatial resolution of 640×480 pixels with 27 μm pitch. The LCTFs attached to the camera helps to effortlessly tune on to the desired wavelengths. The LCTFs had a 20 mm aperture size and a 10 mm transmission bandwidth. The filters coupled to the camera produced 12-bit multispectral images. The samples were illuminated by a pair of 300 W tungsten-halogen lights which had the capacity to emit light in a wavelength range of 400-2500 nm (Ushio Lighting Inc., Cypress, CA) and were placed 0.5 m away from the imaging area at 45° angles, The data acquisition board (NI PCI-1422, National Instruments Corp., Austin, TX) was attuned to RS-422 signals generated from the camera system for image acquisition.

3.2.3 Image acquisition

Three hundred canola seeds from each fungal-infected sample and healthy sample were subjected to imaging. The dark count and baseline images (99% reflectance) were taken at regular intervals. Five randomly selected seeds were manually placed without touching each other on a black plastic board in the field of view (FOV) of the NIR imaging system and imaged (Fig. 3.2). The images were acquired by utilizing a Lab VIEW program (Version 7.1, National Instruments Corp., Austin, TX). The camera was aligned to the centre wavelength of 1300 nm in

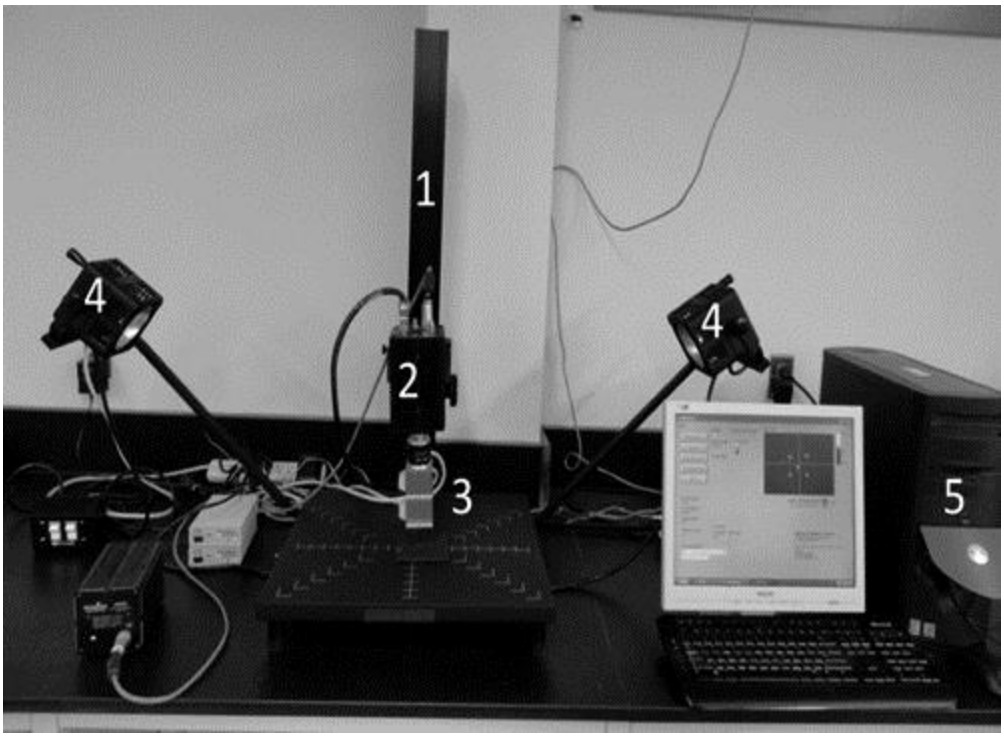

Fig. 3.1. NIR hyperspectral imaging system 1. Camera Stand, 2. NIR Camera, 3. LCTF Filters, 4.Tungsten- Halogen Lamps, 5. Data Acquisition and Processing System

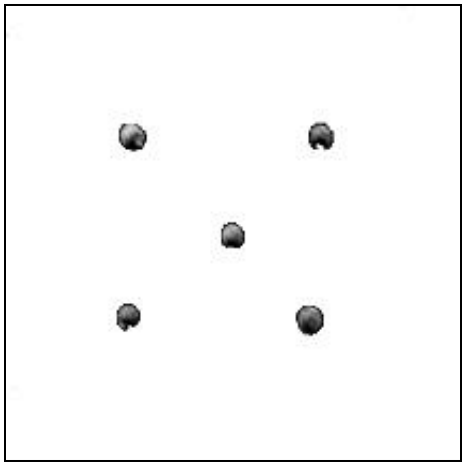

Fig. 3.2. Five non-touching canola seeds for imaging

the NIR camera's usable wavelength region of 1000-1600 nm. The total number of images used in the analysis were 1800.

3.2.4 Data analysis

The acquired image files were imported into MATLAB (Mathworks Inc., Natick, MA, USA) to display and analyze the hyperspectral data using a program written in MATLAB. The NIR camera had a few insensitive pixels called dead pixels due to a sensor defect. A 3X3 median filter was used to remove the dead pixels. The signal-to-noise ratio was improved by automatically co-adding 10 images at each of 61 wavebands. Single-seed canola images from five non-touching seeds in the original images were separated and labelled using an image processing code developed in MATLAB (Singh et al., 2007). First greyscale intensity images were obtained by converting original hypercube data from matrix to image format. Then greyscale images were converted to binary image using automatic thresholding and each seed was labelled (1-5) based on all connected pixels in a seed (Fig. 3.3).

The five labelled seeds in an image were analyzed using a multivariate image analysis (MVI) program written in MATLAB. The principal component analysis (PCA) was used to perform MVI (Geladi and Grahn, 1996). The simple multivariate image (hyperspectral data) obtained had width and height as two pixel coordinates and a wavelength value as variable index making it a three-dimensional array (hypercube). The three-dimensional array data were reshaped into a two-dimensional array by means of pixel intensities (reflectance) rearrangement of a seed into a column at all the 61 wavelengths. The k x 61 sized two-dimensional arrays were obtained as a result of the above process, (k is the total number of pixels in a labelled seed at each waveband). Finally, PCA was applied to the two-dimensional data set of each seed. The

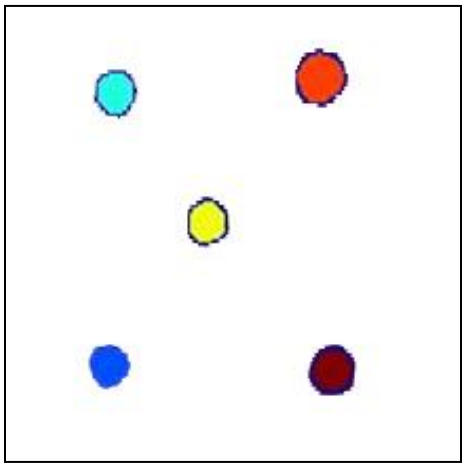

Fig. 3.3. Labelled seeds excluding the background after applying image processing program

highest factor loadings in the first principal component were selected as the most significant wavelengths. The mean, maximum, and minimum reflectance intensities from the image slices corresponding to identified significant wavelengths were used in classification algorithms.

3.3 Results and Discussion

Three wavelengths 1100, 1250, and 1300 nm had the highest factor loadings in the total range of 1000 to 1600 nm corresponding to the first principal component (Fig. 3.4). These three most significant wavelengths were used for further classification by discriminant analysis. Singh et al. (2007) identified 1315.8 and 1347.4 nm as the most significant wavelength to classify fungal-damaged wheat kernels and Wang et al. (2003) found 1330 nm as the significant wavelength for fungal-infected soybean seeds and related it to C-H bond representing fibre and starch content in soybean. In previous studies, it was reported that NIR absorptions at 960 and 1420 nm wavelengths were corresponding to water content; 1470, 1480, and 1500 nm were related to protein content; 1200, 1250, 1310, 1360, 1610 and 1700 nm were related to carbohydrate content; 960, 1060, 1330, 1390, 1480, and 1680 nm were related to kernel hardness; and 1390 nm was related to oil content in wheat (Wang et al., 1999; Delwiche and Massie, 1996; Murray and Williams, 1987). In this study, peaks were observed at 1100 and 1250 which can be related to water content and carbohydrate content respectively. The 1300 nm can be attributed to fungal infection. In this study we analyzed 61 wavebands that took nearly 2 min in scanning, pre-processing, labelling, reshaping, and applying PCA to all five seeds of an image. However, future analysis would take less time, as we would need only three scans at the above mentioned significant wavelengths for classification.

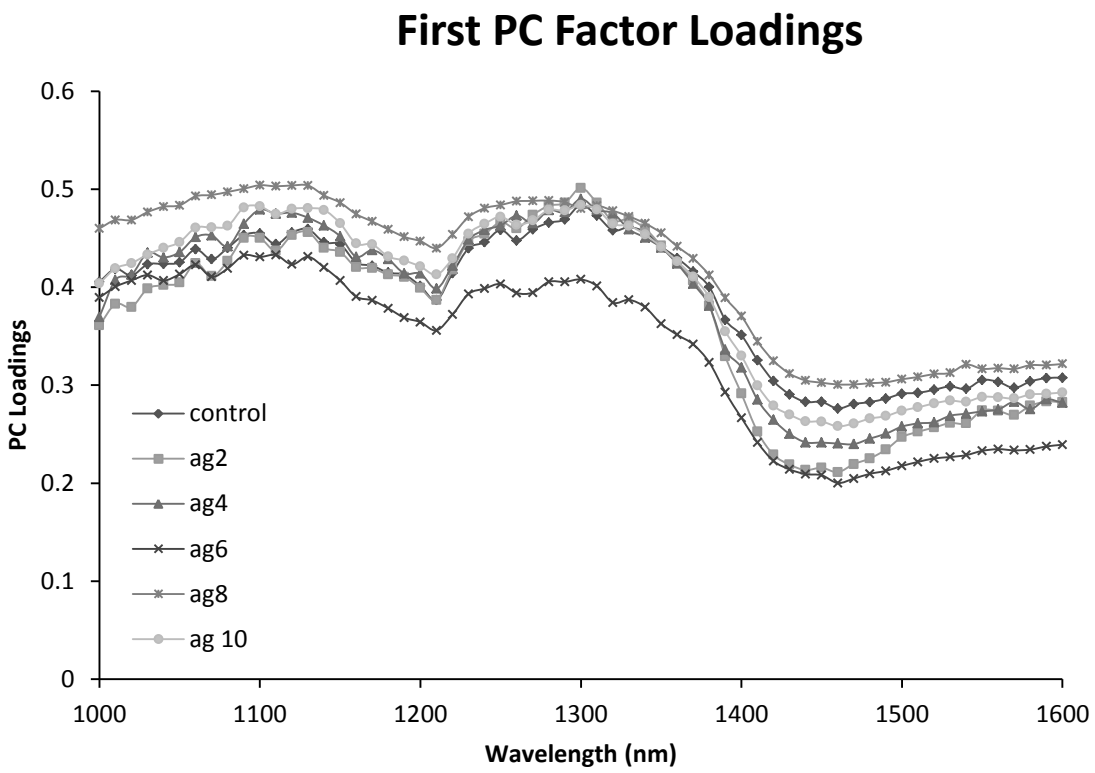

Fig. 3.4. First PC factor loadings of healthy and fungal infected samples (ag 2 to 10: *Aspergillus glaucus* second to tenth week)

We made an attempt to see if the seeds infected by *A. glaucus* could be differentiated from healthy seeds. A pair-wise model was tested using 600 seeds (300 from one of the five fungi-incubated samples and 300 healthy seeds) for each analysis; *A. glaucus* second week infected versus healthy, *A. glaucus* four week infected versus healthy, A. *glaucus* six week infected versus healthy, *A. glaucus* eight week infected versus healthy, and *A. glaucus* ten week infected versus healthy (Table 3.1). The linear pair-wise classification classified healthy samples and second week *A. glaucus* infected samples with classification accuracy of 96.3% and second week *A. glaucus* infected samples with 91.3% accuracy, the remaining pair-wise classifications between healthy and other four different fungal infected samples were classified with 100% accuracy. The quadratic pair-wise classification classified healthy and second week *A. glaucus* infected samples with accuracy of 92.7% and 95.3%, respectively. The classification accuracy was the lowest for healthy and second week *A. glaucus* infected samples because at the end of second week the infection level was lower, after that the classification accuracy increased between healthy and other four different stages of *A. glaucus* infected samples due to high infection level over the seeds. The quadratic pair-wise discriminant classifier classified all the remaining four *A. glaucus* infected samples with classification accuracy between 99.0 to 100%, and healthy samples were classified with an accuracy of 100%.

Then we made an attempt to find the classification accuracy between five different fungal infected stages as shown in Table 3.2. The linear pair-wise classification between different weeks of *A. glaucus* infected samples provided highest classification accuracy of 100% between six, eight, and ten week fungal infected samples. This higher classification accuracy can be the related to the increase in infection level after certain period of time (after four weeks). The classification accuracy was the least for second week and fourth week *A. glaucus* infected

Table 3.1. LDA and QDA classification accuracies (%) for healthy and fungal infected samples of different stages.

Sample	Statistical Discriminant Classification (%) using statistical features of 1100, 1250 and 1300 nm wavelengths*	
	LDA	**QDA**
Healthy	96.0	92.7
***A. glaucus* week 2**	91.3	95.3
Healthy	100	100
***A. glaucus* week 4**	100	99.3
Healthy	100	100
***A. glaucus* week 6**	100	99.7
Healthy	100	100
***A. glaucus* week 8**	100	100
Healthy	100	100
***A. glaucus* week 10**	100	100

Sample size for each class was 300.

Table 3.2. LDA and QDA classification accuracies (%) between fungal infected samples at different stages.

Sample	Statistical Discriminant Classification (%) using statistical features of 1100, 1250 and 1300 nm wavelengths*	
	LDA	**QDA**
***A. glaucus* week 2**	88.7	95
***A. glaucus* week 4**	94.7	84
***A. glaucus* week 2**	99.3	98.7
***A. glaucus* week 6**	97.3	98.7
***A. glaucus* week 2**	100	100
***A. glaucus* week 8**	100	100
***A. glaucus* week 2**	100	100
***A. glaucus* week 10**	100	100
***A. glaucus* week 4**	94.7	99.3
***A. glaucus* week 6**	98.7	98.7
***A. glaucus* week 4**	100	100
***A. glaucus* week 8**	100	100
***A. glaucus* week 4**	100	100
***A. glaucus* week 10**	100	100
***A. glaucus* week 6**	100	100
***A. glaucus* week 8**	100	100
***A. glaucus* week 6**	100	100
***A. glaucus* week 10**	100	100
***A. glaucus* week 8**	100	100
***A. glaucus* week 10**	100	100

Sample size for each class was 300.

Table 3.3. Six–class classification (%) of canola seeds by LDA and QDA discriminant classifier

	Healthy	Second week	Fourth week	Sixth week	Eighth week	Tenth week
LDA						
Healthy	**95.3**	4.7	0	0	0	0
Second week	18	**75.3**	6.7	0	0	0
Fourth week	0	14.7	**85.3**	0	0	0
Sixth week	0	0	4.7	**95.3**	0	0
Eighth week	0	0	0	0	**100**	0
Tenth week	0	0	0	0	0	**100**
QDA						
Healthy	**92**	6.7	1.3	0	0	0
Second week	15.3	**67.3**	17.3	0	0	0
Fourth week	0.7	4.7	**94.7**	0	0	0
Sixth week	0	0	1.3	**98.7**	0	0
Eighth week	0	0	0	0	**100**	0
Tenth week	0	0	0	0	0	**100**

samples; this can be attributed to the smaller difference in infection between second and fourth week. The quadratic pair-wise classification followed the same pattern. The LDA and QDA of six-class classification provided highest classification accuracy for sixth, eight and tenth week *A. glaucus* infected samples, and lowest for second and fourth week *A. glaucus* infected samples (Table 3.3). The results from the six-class LDA and QDA classification s showed classification accuracy increased with increase in infection level. In the linear six-class classification we can easily discriminate healthy, sixth, eighth and tenth week *A. glaucus* infected samples with high classification accuracy (95.3 to 100%). The quadratic six-class classification results indicate that we can easily discriminate healthy, fourth, sixth, eighth, and tenth week *A. glaucus* infected samples (Classification accuracy: 92 to 100%).

3.4 Conclusion

Healthy and fungal infected canola seeds can be easily discriminated using near-infrared (NIR) hyperspectral imaging in the 1000 to 1600 nm wavelength range. The different stages of fungal infected samples can also be discriminated using the NIR hyperspectral imaging. The results from this study indicated that NIR hyperspectral imaging holds promise for detecting fungal infection in canola seeds at various stages of fungal growth. Three wavelengths (1100, 1250, and 1300 nm) identified as most significant wavelengths corresponding to the highest factor loadings of the first principal component were used in the analysis. A linear pair-wise discriminant classifier classified 96.3% of healthy samples and 91.3% of second week *A. glaucus* infected samples. The linear pair-wise classifier classified all the remaining four different stages of *A. glaucus* infected and healthy canola samples with 100% classification accuracy. The quadratic pair-wise discriminant classifier classified 92.67% of healthy samples and 95.33% of second week *A. glaucus* infected samples. The quadratic pair-wise discriminant classifier

classified all the four remaining fungal infected samples with 99 to 100 % classification accuracy, and healthy samples with 100% accuracy. The linear discriminant analysis (LDA) and quadratic discriminant analysis (QDA) classification between different *A. glaucus* infected samples gave highest classification accuracy for sixth, eight and tenth week samples and the lowest accuracy for second and fourth week *A. glaucus* infected samples. The six-class LDA and QDA classification also followed the trend of highest classification accuracy for highly infected samples and lowest accuracy for least infected samples.

References

Brogan, I. W. 1986. Control of rapeseed quality for crushing. In Oilseed Rape, eds. Scarisbrick D H; Daniels R W. Collins, London, UK, 282-300.

Canola Council of Canada. 2008. Socio-Economic Value Report. Available online: http://www.canolacouncil.org/uploads/Canola_in_Canada_Socio_Economic_Value_Report_January_08.pdf**.**

Delwiche, S. R., and D.R. Massie. 1996. Classification of wheat by visible and near-infrared reflectance from single kernels. *Cereal Chemistry* 73: 399-405.

Geladi, P., and H. Grahn. 1996. Multivariate Image Analysis. John Wiley and Sons: Chichester, UK.

Goetz, A.F.H., G. Vane, T.E. Solomon, and B.N. Rock. 1985. Imaging spectrometry for earth remote sensing. *Science* 228: 1147-1153.

Gowen, A.A., C.P. O'Donnell, P.J. Cullen, and S.E.J. Bell. 2008. Recent applications of chemical imaging to pharmaceutical process monitoring and quality healthy. *European Journal of Pharmaceutics and Biopharmaceutics* 69: 10-12.

Magan, N. 1993. Early detection of fungi in stored grain. *International Biodeterioration and Biodegradation* 32: 145-160.

Mahesh, S., A. Manickavasagan, D.S. Jayas, J. Paliwal, and N.D.G. White. 2008. Feasibility of near-infrared hyperspectral imaging to differentiate Canadian wheat classes. *Biosystems Engineering* 101: 50-57.

Mills, J.T., R.N. Sinha, H.A.H. Wallace. 1978. Assessment of quality criteria of stored rapeseed-a multivariate study. *Journal of Stored Products Research* 14: 121-133.

Monteiro, S., Y. Minekawa., Y. Kosugi, T. Akazawa, K. Oda. 2007. Prediction of sweetness and amino acid content in soybean crops from hyperspectral imagery. *ISPRS Journal of Photogrammetry and Remote Sensing* 62(1): 2-12.

Murray, I., and P.C. Williams**.** 1987. Chemical principles of near-infrared technology. In Near-infrared Technology in the Agricultural and Food Industries, eds. Williams P C; Norris K H. American Association of Cereal Chemists Inc, St. Paul, MN, pp. 17-34.

Naganathana, G.K., L.M. Grimesb, J. Subbiah, C.R. Calkinsb, A. Samalc, and G.E. Meyera. 2008. Visible/near-infrared hyperspectral imaging for beef tenderness prediction. *Computer and Electronics in Agriculture* 64(2): 225-233.

Narvankar, D.S., C.B. Singh, D.S. Jayas, and N.D.G. White. 2009. Assessment of soft X-ray imaging for detection of fungal infection in wheat. *Biosystems Engineering* 103: 49-56.

Paulsen, M.R. 1990. Using machine vision to inspect oilseeds. *Inform. American Oil Chemists' Society* 1(1): 50-55.

Pronyk, C., W.E. Muir, N.D.G. White, and D. Abramson. 2004. Carbon dioxide production and deterioration in stored canola. *Canadian Biosystems Engineering* 46: 3.25-3.33.

Singh, C.B., D.S. Jayas, J. Paliwal, and N.D.G. White. 2007. Fungal detection in wheat using near-infrared hyperspectral imaging. *Transactions of ASABE* 50(6): 2171-2176.

Singh,C.B., D.S. Jayas, J. Paliwal, and N.D.G. White. 2010a. Detection of midge-damaged

wheat kernels using short-wave near-infrared hyperspectral and digital colour imaging. *Biosystems Engineering* 105: 380-387.

Singh, C.B., D.S. Jayas, J. Paliwal, and N.D.G. White. 2010b. Identification of insect-damaged wheat kernels using soft-wave near-infrared hyperspectral and digital colour imaging. *Computers and Electronics in Agriculture* 73: 118-125.

Sinha, R.N., and H.A.H. Wallace. 1977. Storage stability of farm-stored rapeseed and barley. *Canadian Journal of Plant Science* 57: 351-365.

Statistics Canada. 2011. Cereals and Oilseeds Review. Catalogue number: 22-007-X.

Walcott, R.R., D.C. McGee, and M.K. Misra. 1998. Detection of asymptomatic fungal infections of soybean seeds by ultrasound analysis. *Plant Disease* 82(5): 584-589.

Wang, D., F.E. Dowell., and R.E. Lacey. 1999. Single wheat kernel color classification using neural networks. *Transactions of ASAE* 42: 233-240.

Wang, D., F.E. Dowell, M.S. Ram, and W.T. Schapaugh. 2003. Classification of fungal-damaged soybean seeds using near-infrared spectroscopy. *International Journal of Food Properties* 7: 75-82.

Williams, A.P. 1989. Methodology developments in food mycology. *Journal of Applied Bacteriology* 67(S): 612-617.

Chapter 4

Detection of different periods of fungal infection in stored canola using near-infrared hyperspectral imaging

This chapter is based on the following publication:

Senthilkumar, T., D.S. Jayas, and N.D.G. White. 2015. Detection of different stages of fungal infection in stored canola using near-infrared hyperspectral imaging. *Journal of Stored Products Research,* 63: 80-88.

Abstract

Near-infrared (NIR) hyperspectral imaging system was used to detect different stages of fungal infections in stored canola. Artificially infected canola seeds (Fungi: *Aspergillus glaucus* and *Penicillium* spp.) were subjected to hyperspectral imaging in the range between 1000 to 1600 nm at 61 evenly distributed wavelengths. Four wavelengths 1100, 1130, 1250 and 1300 nm were identified as significant wavelengths and were used in statistical discriminant analysis. Pair-wise, two-class and six-class classification models were developed to classify the healthy and different stages of fungal infected samples. Linear, quadratic and Mahalanobis discriminant classifiers were used to classify healthy, five stages of *A. glaucus* and five stages of *Penicillium* spp. infected canola seeds. All the three classifiers classified healthy and fungal infected canola seeds with a classification accuracy of more than 95% for healthy canola seeds and more than 90% for the initial stages of *A. glaucus* and *Penicillium* spp. infected canola seeds. The classification accuracy increased to 100% with increase in fungal infection level (length of time since inoculation). All the samples subjected to imaging were tested for seed germination and free fatty acid value (FAV). The germination decreased with increase in amount of fungal infection, whereas FAV increased with increase in amount of fungal infection.

4.1 Introduction

Canada produced an average of 15 million tonnes (Mt) of Canola (*Brassica napus* L. and *B. campestris* L. cultivars of low erucic acid oil and low glucosinolates meal) and exported an average of 8 Mt of canola seeds per year in the last five years (2010 to 2014). The economic value of canola in Canada is CAD $20 billion and it is the most valuable crop in Canada by surpassing wheat in recent years (Statistics Canada, 2015). It is important to store the canola properly before it reaches the consumers. The major cause of spoilage in canola is fungi because of high moisture content and the high oil content (40-45%) restricts other pests like insects from multiplying. Postharvest fungi can develop inside storage facilities and cause considerable damage to seeds under favorable conditions even after eliminating preharvest fungi by drying to safe moisture levels before storage.

The fungal infection in canola can reduce seed germination, oil quality, create unacceptable odors and can increase in free fatty acids and ergosterol content in seeds. The presence of fungi on the stored canola also helps mites to survive when they consume mold on canola seeds. The quality and quantity reduction due to the presence of fungi in canola results in reduced financial returns to the producers and if undetected can cause serious food safety issues to the consumers. The major fungal genera causing damage to canola in Canada are *Aspergillus* and *Penicillium. Aspergillus glaucus, Aspergillus candidus* and *Penicillium* spp. are predominantly found in stored canola in Canada (Pronyk et al., 2004; White et al., 1982). *Aspergillus glaucus* can thrive, multiply and decompose canola even at moderate relative humidity levels while *A. candidus* and *Penicillium* spp. require higher seed moisture contents (Pronyk et al., 2004; Sauer et al., 1992).

The detection of fungal infection at an early stage can reduce further damage to stored canola by applying suitable physical or chemical treatments. The traditional methods used for fungal detection such as microscopic culture methods and instrumental methods (gas chromatography, liquid chromatography, mass spectrometry) involve longer incubation time and tedious extraction procedures. There are various techniques developed to detect the fungal infection such as soft-X-rays (Navarankar et al., 2009), thermal imaging (Chelladurai et al., 2010), which are all non-invasive methods and require very short time to detect fungal damage; however, these can detect fungal infection only at advanced stages of deterioration. Polymerase Chain Reaction (PCR) methods (Hayat et al., 2012) which can even identify fungal species requires 24 h for DNA extraction and further processing.

Near-infrared (NIR) hyperspectral imaging is a combination of conventional imaging and spectroscopy which can provide spatial and spectral data of a given sample. NIR hyperspectral imaging system operates in the range from 700 to 2500 nm of the electromagnetic spectrum. Every material due to their physical and chemical nature reflect, transmit, absorb and emit energy in a particular manner at different wavelengths; hyperspectral imaging technique utilizes these effects to collect desirable data. The data acquired by NIR hyperspectral imaging can identify different chemical constituents of a material and it is also called chemical imaging. NIR hyperspectral imaging technique is a non-invasive or non-damaging method, and requires very limited sample preparation prior to imaging. Hyperspectral imaging was first utilized in remote sensing applications to map mineral resources and now it is extensively used in many sectors of agriculture, pharmaceuticals, medicine, environment, and food processing (Vadivambal and Jayas, 2015; Mahesh et al., 2015). NIR hyperspectral imaging used in the food processing sector involves many food quality and food safety parameters assessment applications.

NIR hyperspectral imaging has been used in detecting various quality parameters associated with raw grains such as prediction of oil and oleic acid concentrations in corn kernels (Weinstock et al., 2006) classification of sound and stained wheat kernels (Berman et al., 2007), wheat class classification using Linear Discriminant Analysis (LDA), Quadratic Discriminant Analysis (QDA), and Artificial Neural Network (ANN) Models (Mahesh et al., 2008), wheat class classification at different moisture levels (Mahesh et al., 2011), wheat class classification using wavelet texture features (Choudhary et al., 2009), identification of vitreous and non-vitreous durum wheat kernels (Shahin and Symons, 2008), classification of maize based on kernel hardness (Williams et al., 2009), evaluation of maize endosperm texture (Manley et al., 2009), detection of insect damaged wheat kernels (Singh et al., 2009), identification of pre-germinated barley (Arngren et al., 2011), classification of oat and groat kernels (Serranti et al., 2013), identification of rice seed cultivar (Kong et al., 2013) and classification of contaminants from wheat (Ravikanth et al., 2015).

NIR hyperspectral imaging techniques have also been used to detect pre- and post-harvest fungal infection in raw grains, detection of scab and other mold damaged wheat kernels (Delwiche, 2003), detection of scab damaged hard red spring wheat kernels (Delwiche and Hareland, 2004), detection of *A. glaucus*, *A. niger* and *Penicillium* spp. infected wheat kernels (Singh et al., 2007), classification of sound and *Fusarium* damaged wheat kernels (Peiris et al., 2009), detection of fungal-infected corn kernels (Tallada et al., 2011), fungal development in maize kernels (Williams et al., 2012), quantification of ergot bodies in cereals (Vermeulen et al., 2012), differentiation between species and strains of members of the genus *Fusarium* (Williams et al., 2012), detection of *Fusarium* head blight in wheat kernels (Barbedo et al., 2015) and detection of *Fusarium* damaged oats (Tekle et al., 2015).

Potential of NIR hyperspectral imaging technique has not yet been studied in any great detail for quality analysis in oilseeds. The study done by Senthilkumar et al. (2012) was a preliminary study which explored the potential of NIR hyperspectral imaging to classify healthy and heavily fungal infected high oil content canola seeds. The study used only *Aspergillus glaucus* infected canola samples. The classification accuracy between healthy and *A. glaucus* infected canola samples were more than 95% using LDA and QDA classifiers. NIR hyperspectral imaging technique to determine classification accuracies between healthy and artificially fungal infected canola by different species of fungi has not been reported. The objectives of this study were:

1. To determine the classification accuracy between healthy, *A. glaucus* and *Penicillium* spp. infected mixed variety canola seeds using NIR hyperspectral imaging, and

2. To determine the classification accuracy between different stages (two, four, six, eight and tenth weeks after inoculation) of fungal infected canola seeds.

4.2. Material and Methods

4.2.1 Sample preparation

Mixed variety canola seeds of the 2013 crop year were obtained from a grain elevator in Manitoba with a moisture content of 8.5%. Eleven kilograms of mixed variety canola to help fungi grow and multiply were conditioned to 14% (wet basis) moisture content by mixing a calculated amount of distilled water and were surface sterilized with 1% sodium hypochlorite solution to remove any pre-existing contaminants on canola seeds, then rinsed with distilled water and were then wiped using paper towels to remove excess water. The modified and sterilized canola seeds were divided into three subsamples, two subsamples of canola seeds were

artificially infected with *A. glaucus* and *Penicillium* spp. cultures obtained from the Cereal Research Centre, Agriculture and Agri Food Canada, Winnipeg, Manitoba and one subsample was preserved as healthy canola seeds (Senthilkumar et al., 2012). Both artificially infected subsamples were further divided equally and placed into five separate porous bags for each subsample. Samples were placed in between buffer samples on shelves in pails (20 L capacity) having KOH solution at the bottom to maintain 14% moisture content and to avoid fluctuations in the moisture content of canola (Sathya et al., 2009; Sun et al., 2014) (Fig. 4.1). We also avoided cross-contamination by sealing the pails and by placing the three replicates in three different environmental chambers maintained at 30ºC. There were 10 fungal-infected sample bags each weighing one kilogram and one healthy sample bag weighing one kilogram in each of the environmental chambers. The samples were labelled based on fungal species as follows; *A. glaucus* bag 1 and *Penicillium* spp. bag 1(Set 1), *A. glaucus* bag 2 and *Penicillium* spp. bag 2(Set 2), *A. glaucus* bag 3 and *Penicillium* spp. bag 3(Set 3), *A. glaucus* bag 4 and *Penicillium* spp. bag 4(Set 4), A. *glaucus* bag 5 and *Penicillium* spp. bag 5(Set 5), and healthy sample bag 1 (Set 6).

4.2.2 NIR hyperspectral imaging system

The NIR hyperspectral imaging system shown in Fig. 4.2 had three major parts, camera assembly, illumination, and data processing system. The NIR camera with InGaAS detector (Model No. SU640-1.7RT-D, Sensors Unlimited Inc., Princeton, NJ, USA) and 25 mm mounted lens (Electrophysics Corp., Fairfield, NJ, USA) attached to the two Liquid Crystal Tunable filters (LCTFs), (VariSpec, Cambridge Research and Instrumentation Inc., Woburn, MA, USA) made up the camera assembly. The NIR camera with a 640 X 480 array size and 27 µm pitch captured images in the wavelength range of 960 to 1700 nm. The LCTFs with 20 mm aperture size and 10 mm transmission bandwidth tuned on to the desired wavelength in the range of 900 to 1700 nm.

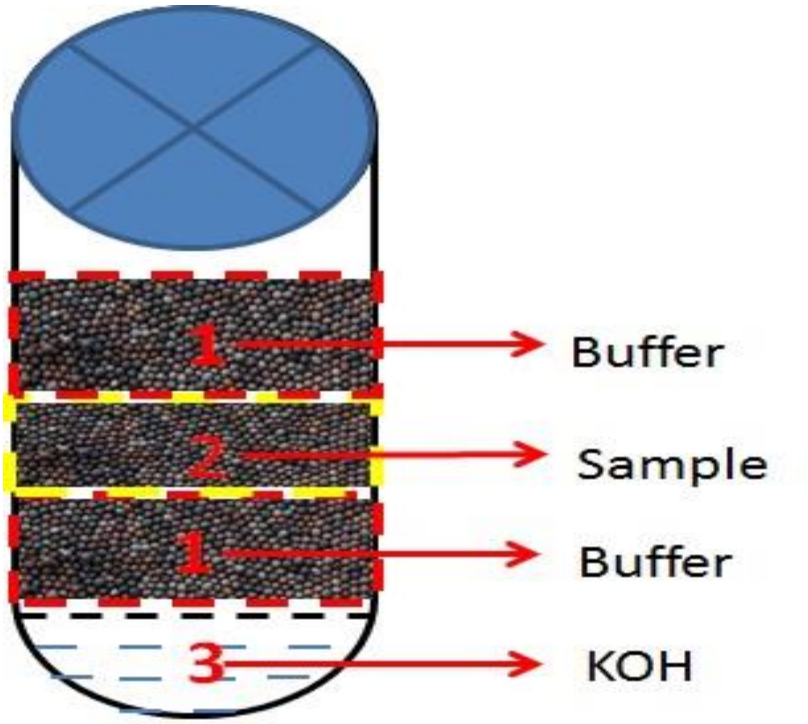

Fig. 4.1. Illustration of Canola seed placement between the buffer samples and KOH solution inside the 20 L pails

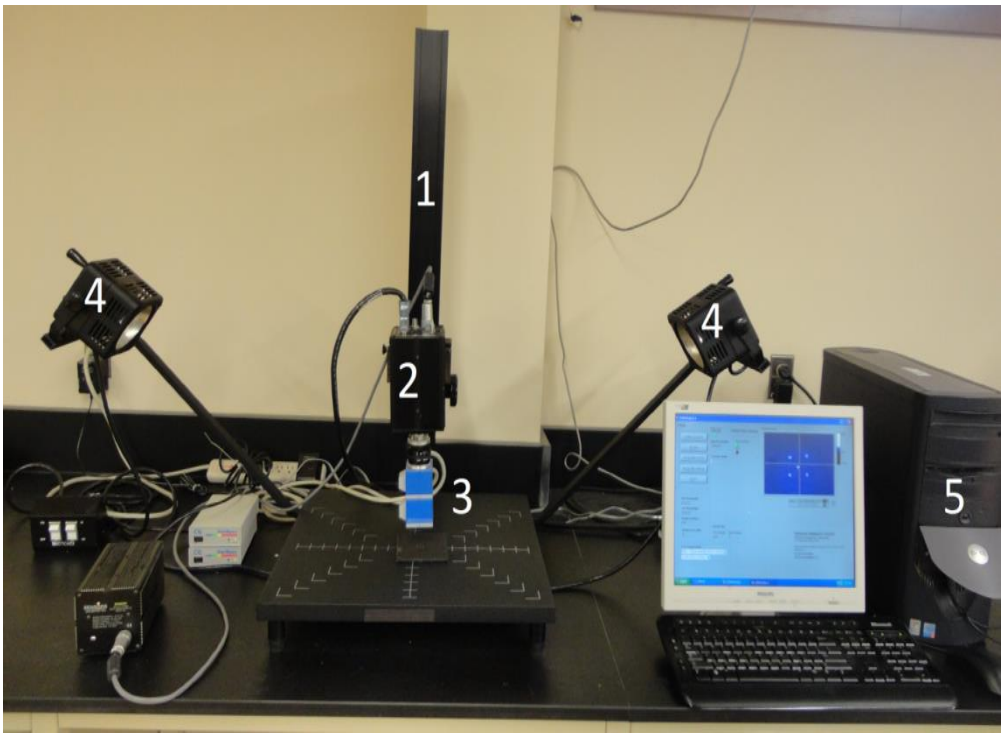

Fig. 4.2. NIR hyperspectral imaging system 1. Camera Stand, 2. NIR Camera, 3. LCTF Filters, 4. Tungsten- Halogen Lamps, 5. Data Acquisition and Processing System

The 300 W Tungsten Halogen lamps (Ushio Lighting Inc., Cypress, CA, USA), were used as the illumination source with the capacity to emit light in the 400 to 2500 nm wavelength range. The data processing system mainly had Lab VIEW Programme (Version 7.1, National Instruments Corp., Austin, TX, USA) and MATLAB software (The Mathworks, Inc., Natick, MA, USA). The Lab VIEW programme acquired images in the desired wavelength range and stored the acquired image data into the file and the MATLAB software was used to analyze the data files.

4.2.3 Image acquisition

The canola seeds from set 1 were subjected to imaging after two weeks since inoculation, set 2 after four weeks, set 3 after six weeks, set 4 after eight weeks and set 5 after ten weeks of fungal infection. The canola seeds from healthy sample bags were also subjected to imaging after conditioning the sample because there will be fungal growth after a few weeks in healthy canola seeds with 14% moisture content. The number of seeds subjected to imaging in each fungal infected set was 600 and for healthy sample it was 300. The seeds from each sample were subjected to single seed imaging by placing randomly selected five canola seeds without touching each other on a black board in the field of view of the camera as shown in Fig. 4.3 A. The camera acquired images in the wavelength range of 1000 to 1600 nm at 10 nm intervals to form one hypercube (two spatial dimensions and one wavelength dimension). A total of 660 hypercubes each containing 61 images of five non-touching canola seeds from each sample were acquired. The camera was aligned to the centre wavelength of 1300 nm and the baseline and dark count images were acquired before every image session.

A

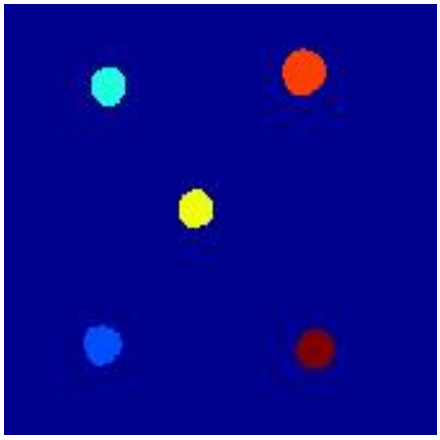

B

Fig. 4.3. Five non-touching canola seeds for imaging (A) and Labelled seeds excluding the background after applying image processing program (B)

4.2.4 Data analysis

The signal to noise ratio was removed during image acquisition by co-adding 10 scans in each of 61 wavelengths to form a single image slice. There were a few insensitive or dead pixels formed due to the sensor defect in the camera. The dead pixels were removed by applying a 3 X 3 median filter. The acquired images were in the three-dimensional hypercube form (two spatial and one wavelength). The original 660 hypercubes were transformed to two-dimensional data of individual canola seeds by a three step process; removing background from seed by means of automatic thresholding, labeling using *bwlabel* MATLAB function (Fig. 4.3 B) and reshaping by converting the intensity data into reflectance data (Senthilkumar et al., 2012).

The two-dimensional data of 3300 single seed images were subjected to Principal Component Analysis (PCA). The PCA provided significant wavelengths based on the highest factor loadings. Statistical features such as maximum, minimum, mean, median, standard deviation, and variance were extracted from the reflectance data corresponding to significant wavelengths. The classification of healthy and fungal infected samples using discriminant analysis was performed using the extracted statistical features.

4.2.5 Statistical discriminant analysis

Statistical discriminant classifiers linear, quadratic, and Mahalanobis were used to classify the healthy and different stages of *A. glaucus* and *Penicillium* spp. infected samples. Pair-wise, Two-class, and Six-class classification models were developed using Statistical Analysis Software (PROC DISCRIM, Version 9.1.3, SAS institute Inc., Cary, NC, USA). The classification models used 60 canola seeds as a testing set and 240 canola seeds as training set for each of the different stages of fungal infected canola seeds and healthy canola seeds.

4.2.6 Moisture content and germination measurement

Moisture content of canola was determined by oven drying 10 g of canola seeds in triplicate for 4 h at 130±1ºC (ASABE 2012). Germination of canola seeds was determined by placing triplicates of 25 canola seeds on Whatman No 3 filter paper soaked with 5.5 mL of distilled water in a petri dish (Wallace and Sinha 1962). The seeds were incubated for 7 d at room temperature (22±2 ºC) and percent germination was calculated after the incubation period.

4.2.7 Free fatty acid value (FAV) determination

The FAV of canola samples were determined using the method reported by Schroth et al. (1998). Five grams of dried and finely ground canola was used to extract oil using a fat extractor and petroleum ether (Goldfisch Fat Extractor, Laboratory Construction Co., Kansas City, MO). The extracted oil was mixed with 25 mL of TAP solution (50% ethanol and 50% toluene with phenolphthalein indicator) and titrated with a KOH solution. The FAV was then expressed as mg KOH/ 100 g of dry canola.

4.3. Results and Discussion

4.3.1 Moisture content, germination capacity, and free fatty acid value (FAV)

The canola samples kept inside the pails were tested for initial and final moisture content, the initial moisture content was 14 ± 0.2% (wet basis) and the final moisture content for all the samples were between 13.0± 0.3 to 13.5± 0.2%. The moisture content fluctuations were mostly reduced because of the presence of KOH solution inside the pales and placement of samples between the buffer bags (Sun et al., 2014). The germination capacity of fungal infected canola seeds reduced with the increase in fungal infection stages and the FAV of fungal infected canola

seeds increased with increase in fungal infection stages as shown in Table 4.1. The initial germination and FAV of healthy canola seeds were 97.5± 0.4% and 23± 1.1 mg KOH/100 g, respectively, but due to increased fungal infection in canola seeds the germination capacity was reduced to 0± 0% after 8 weeks of fungal infection and FAV increased to 79± 4.8 after 10 weeks of fungal infection in canola seeds. The germination capacity and FAV changes were indicators of fungal growth at different infection stages. Sun et al. (2014) studied the moisture content, germination and FAV changes in high oil content and low oil content canola seeds stored at 30ºC over the period of 20 wk with an initial moisture content of 14% by placing the canola seeds between buffer samples and having KOH at the bottom of the 20 L pails and reported the maximum change in moisture content at the end of 10 wk period to be one percentage point, the germination of canola seeds reached 0% at the end of 8 wk and FAV value reached 70 mg KOH/100 g at the end of 10 wk of storage. The moisture content, germination and FAV changes occurred in mixed variety canola seeds with 14% initial moisture content in this study were similar to the study on high oil content and low oil content canola seeds (Sun et al., 2014).

4.3.2 Average reflectance spectra and significant wavelengths

As a first step, Principal Component Analysis was done to extract four significant wavelengths 1100, 1130, 1250 and 1300 nm based on the highest factor loadings (Fig. 4.4 and Fig. 4.5) out of the 61 wavelengths in the range from 1000 to 1600 nm. The significant wavelengths found as a result of PCA were compared with the average spectra chart with identifiable peaks (Fig. 4.6 and Fig. 4.7). The peaks observed in Fig. 4.6 and Fig. 4.7 coincided with the identified significant wavelengths. The peak observed at 1300 nm can be related to fungal infection in canola seeds (Singh et al., 2007; Wang et al., 2003; Senthilkumar et al., 2012; Teena et al., 2014).

Table 4.1. Germination (%) and Free Fatty Acid Values (FAV) of healthy and different stages of *Aspergillus glaucus* and *Penicillium* spp. infected canola seeds.

Sample	Germination capacity (%)	FAV (mg KOH/100g)
Healthy	97.5±0.4	23±1.1
***A. glaucus* week 2**	79.0±0.8	40±0.5
***A. glaucus* week 4**	44.5±1.2	45±0.3
***A. glaucus* week 6**	25.0±0.3	46±1.1
***A. glaucus* week 8**	0.00±0.0	52±2.1
***A. glaucus* week 10**	0.00±0.0	70±2.8
***Penicillium* spp. week 2**	74.5±2.2	49±3.2
***Penicillium* spp. week 4**	38.0±1.8	51±3.6
***Penicillium* spp. week 6**	19.0±0.6	55±1.9
***Penicillium* spp. week 8**	0.00±0.0	58±2.1
***Penicillium* spp. week 10**	0.00±0.0	79±4.8

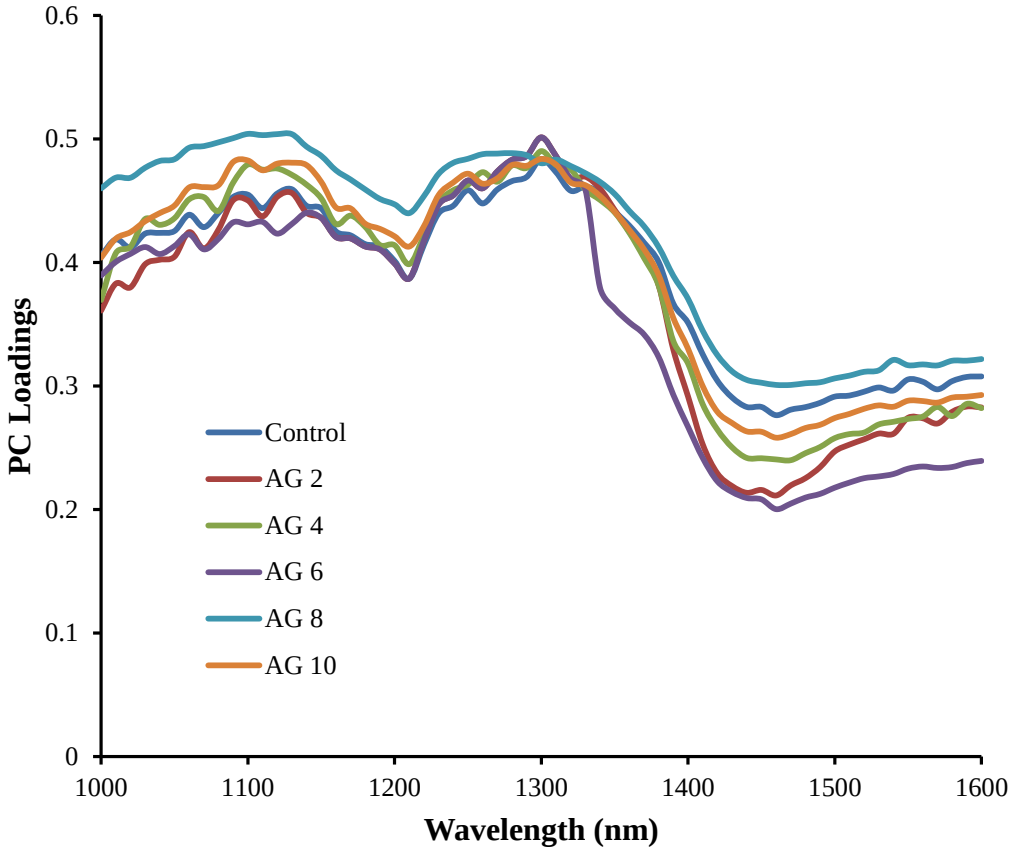

Fig. 4.4. First principal component (PC) loadings of healthy and different stages of *Aspergillus glaucus* infected canola (AG 2 to AG 10: *Aspergillus glaucus* Second to Tenth week post inoculation)

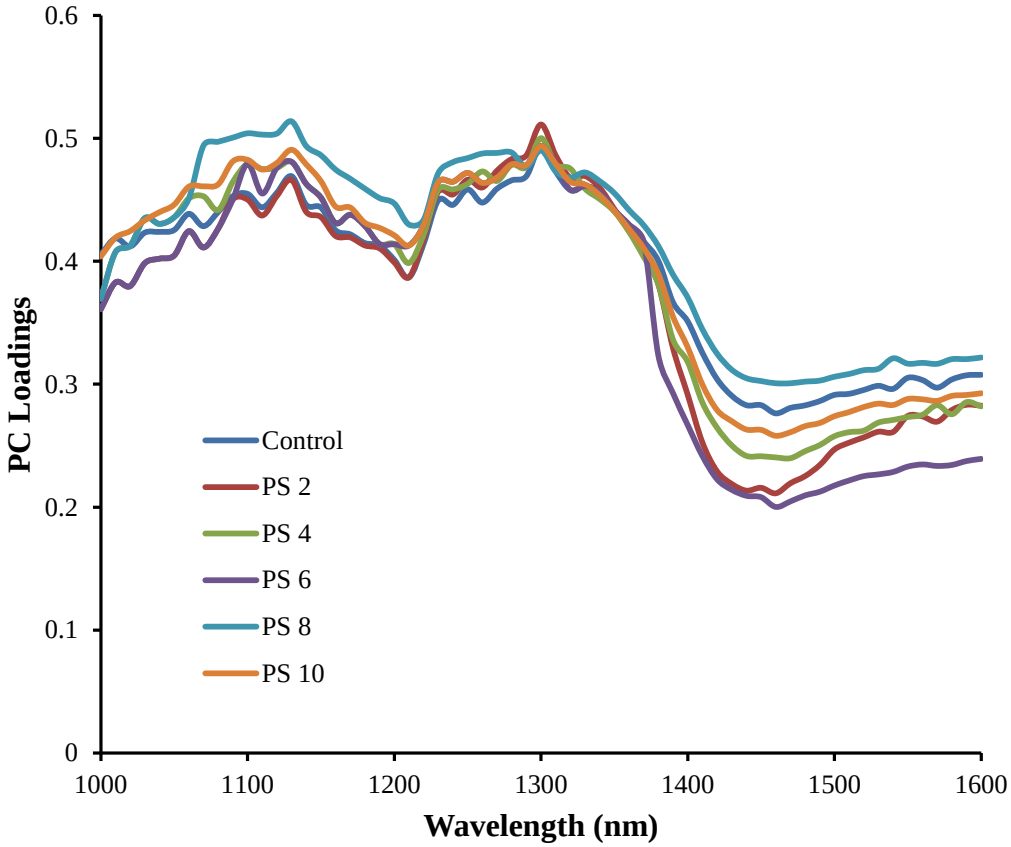

Fig. 4.5. First principal component (PC) loadings of healthy and different stages of *Penicillium* spp. infected canola (PS 2 to PS 10: *Penicillium* spp. Second to Tenth week post inoculation)

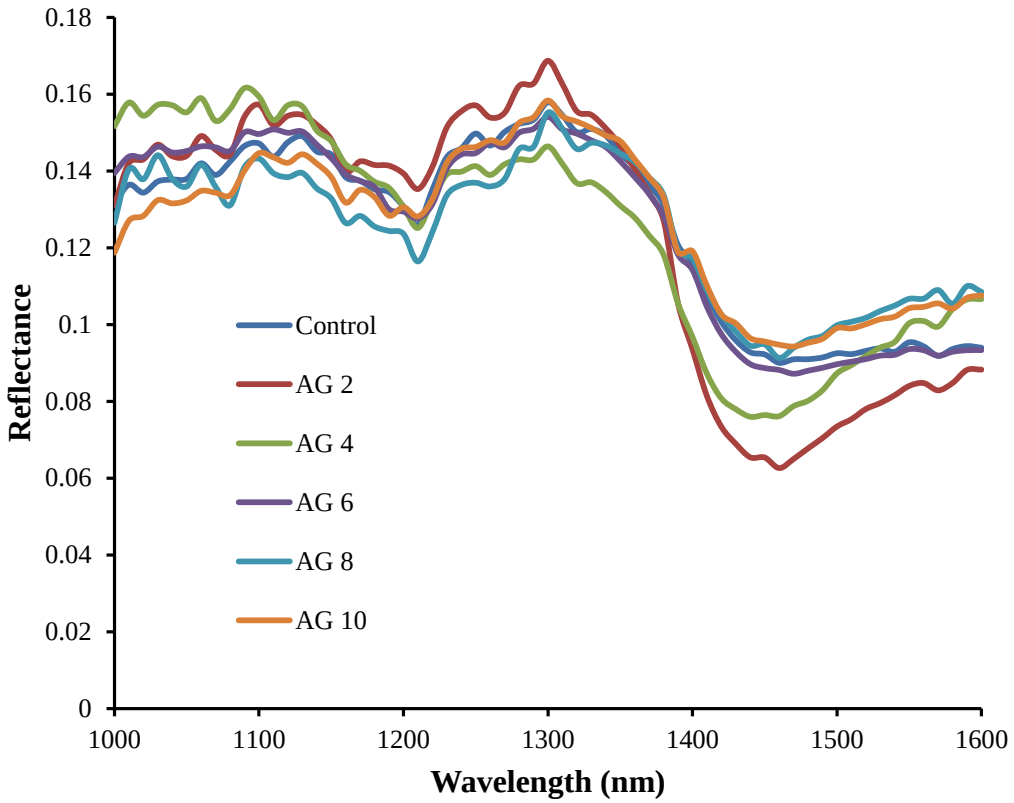

Fig. 4.6. Average spectra of healthy and different stages of *Aspergillus glaucus* infected samples (AG 2 to AG 10: *Aspergillus glaucus* Second to Tenth week post inoculation)

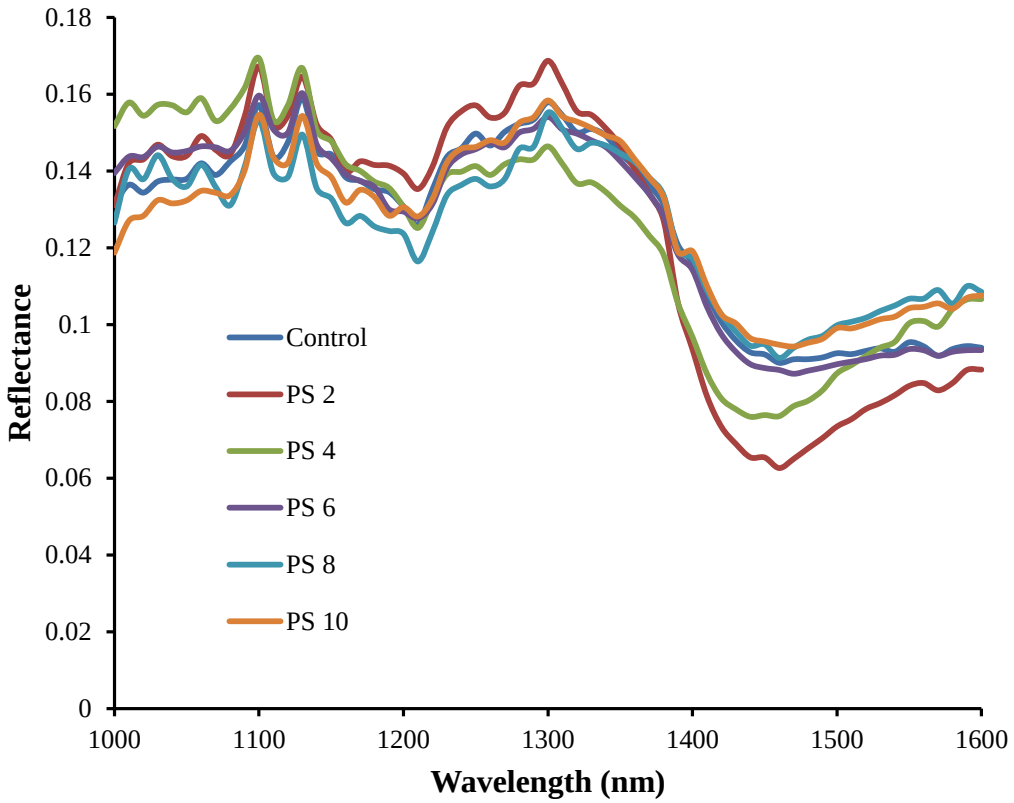

Fig. 4.7. Average spectra of healthy and different stages of *Penicillium* spp. infected samples (PS 2 to PS 10: *Penicillium* spp. Second to Tenth week post inoculation)

The peak observed at 1100 nm and 1130 nm can be related to moisture content of canola seeds (Senthilkumar et al., 2012; Teena et al., 2014). The NIR imaging system took nearly 2.5 min for image acquisition of all the 61 wavelengths, image processing, and applying PCA for all the five canola seeds. The time taken for future image analysis would reduce to nearly 1 min if we acquire and process images at the four identified significant wavelengths.

4.3.3 Pair-wise classification

Pair-wise classification model was first tested between healthy canola seeds and five infection stages of *A. glaucus* infected canola seeds as Healthy versus *A. glaucus* week 2, Healthy versus *A. glaucus* week 4, Healthy versus *A. glaucus* week 6, Healthy versus *A. glaucus* week 8 and Healthy versus *A. glaucus* week 10. The linear, quadratic and Mahalanobis classifiers classified healthy canola seeds with classification accuracy in the range between 93.5 to 100%; the lowest classification accuracy of 93.5% for healthy canola seeds was obtained in the Healthy versus *A. glaucus* week 2 pair (Table 4.2) and the classification accuracy of 100% of healthy canola seeds was obtained for healthy versus later stages of *A. glaucus* infected canola seeds. The three discriminant classifiers classified five stages of *A. glaucus* infected canola seeds with the classification accuracy in the range between 92.1 to 100%.

Second pair-wise classification model was tested between healthy and five infection stages of *Penicillium* spp. infected canola seeds in the similar pattern as followed for the healthy versus five stages of *A. glaucus* infected canola seeds. The linear, quadratic and Mahalanobis classifiers classified healthy canola seeds with a classification accuracy in the range between 98.1 to 100% and the discriminant classifiers classified five stages of *Penicillium* spp. infected canola seeds with a classification accuracy in the range between 96. 3 to 100%.

Table 4.2. Linear Discriminant Analysis (LDA), Quadratic Discriminant Analysis (QDA) and Mahalanobis classification accuracies (%) for pair-wise model between healthy and five infection stages of *Aspergillus glaucus* infected canola seeds.

Sample	Classification Accuracies (%) using statistical features from 1100, 1130,1250 and 1300 nm wavelengths*		
	LDA	**QDA**	**Mahalanobis**
Healthy	93.5	96.8	97.1
***A. glaucus* week 2**	92.1	93.6	94.5
Healthy	98.8	99.2	100
***A. glaucus* week 4**	97.9	99.6	100
Healthy	100	100	100
***A. glaucus* week 6**	100	100	100
Healthy	100	100	100
***A. glaucus* week 8**	100	100	100
Healthy	100	100	100
***A. glaucus* week 10**	100	100	100

* Sample size for each class was 300 seeds

Table 4.3. Linear Discriminant Analysis (LDA), Quadratic Discriminant Analysis (QDA) and Mahalanobis classification accuracies (%) for pair-wise model between healthy and five infection stages of *Penicillium* spp. infected canola seeds.

Sample	Classification Accuracies (%) using statistical features from 1100, 1130,1250 and 1300 nm wavelengths*		
	LDA	**QDA**	**Mahalanobis**
Healthy	98.1	98.2	98.4
***Penicillium* spp. week 2**	96.3	97.2	98.9
Healthy	100	100	100
***Penicillium* spp. week 4**	100	100	100
Healthy	100	100	100
***Penicillium* spp. week 6**	100	100	100
Healthy	100	100	100
***Penicillium* spp. week 8**	100	100	100
Healthy	100	100	100
***Penicillium* spp. week 10**	100	100	100

* Sample size for each class was 300 seeds

Table 4.4. Linear Discriminant Analysis (LDA), Quadratic Discriminant Analysis (QDA) and Mahalanobis classification accuracies (%) for pair-wise model between five infection stages of *Aspergillus glaucus* infected canola seeds.

Sample	Classification Accuracies (%) using statistical features from 1100, 1130,1250 and 1300 nm wavelengths*		
	LDA	**QDA**	**Mahalanobis**
***A. glaucus* week 2**	91.7	92.1	93.5
***A. glaucus* week 4**	96.4	97.3	98.6
***A. glaucus* week 2**	98.7	99.1	99.2
***A. glaucus* week 6**	99.1	99.4	99.7
***A. glaucus* week 2**	100	100	100
***A. glaucus* week 8**	100	100	100
***A. glaucus* week 2**	100	100	100
***A. glaucus* week 10**	100	100	100
***A. glaucus* week 4**	100	100	100
***A. glaucus* week 6**	100	100	100
***A. glaucus* week 4**	100	100	100
***A. glaucus* week 8**	100	100	100
***A. glaucus* week 4**	100	100	100
***A. glaucus* week 10**	100	100	100
***A. glaucus* week 6**	100	100	100
***A. glaucus* week 8**	100	100	100
***A. glaucus* week 6**	100	100	100
***A. glaucus* week 10**	100	100	100
***A. glaucus* week 8**	100	100	100
***A. glaucus* week 10**	100	100	100

* Sample size for each class was 300 seeds

The lowest classification accuracy of 98.1% for healthy canola seeds and 96.3% for *Penicillium* spp. infected canola seeds was obtained for Healthy versus *Penicillium* spp. week 2 pair and the highest for healthy versus the later stages of *Penicillium* spp. infected canola seeds (Table 4.3).

A third pair-wise model was tested between five infection stages of *A. glaucus* infected canola seeds as *A. glaucus* week 2 versus *A. glaucus* week 4, *A. glaucus* week 2 versus *A. glaucus* week 6, *A. glaucus* week 2 versus *A. glaucus* week 8, *A. glaucus* week 2 versus *A. glaucus* week 10, *A. glaucus* week 4 versus *A. glaucus* week 6, *A. glaucus* week 4 versus *A. glaucus* week 8, *A. glaucus* week 4 versus *A. glaucus* week 10, *A. glaucus* week 6 versus *A. glaucus* week 8, *A. glaucus* week 6 versus *A. glaucus* week 10 and *A. glaucus* week 8 versus *A. glaucus* week 10. The discriminant classifiers classified five stages of *A. glaucus* infected canola seeds with classification accuracy between 91.7% to 99.7 for the first two pairs and all the remaining pairs resulted in 100% classification accuracy (Table 4.4).

A fourth pair-wise model was tested between five infection stages of *Penicillium* spp. infected canola seeds in the similar pattern as followed by third pair-wise classification model. The discriminant classifiers classified five stages of *Penicillium* spp.-infected canola seeds with classification accuracy between 98.6 to 99.8% for the first pairs and all remaining pairs resulted in 100% classification accuracy (Table 4.5).

Fifth pair-wise model was tested between five stages of *A. glaucus* and *Penicillium* spp. infected canola seeds. The classification accuracy for *A. glaucus* week 2, *Penicillium* spp. week 2, *A. glaucus* week 4 and *Penicillium* spp. week 4 was between 91.9 and 99.9%. The classification accuracy of 100% was achieved for other stages of fungal infection (Table 4.6).

Table 4.5. Linear Discriminant Analysis (LDA), Quadratic Discriminant Analysis (QDA) and Mahalanobis Classification accuracies (%) for pair-wise model between five infection stages of *Penicillium* spp. infected canola seeds.

Sample	Classification Accuracies (%) using statistical features from 1100, 1130,1250 and 1300 nm wavelengths*		
	LDA	**QDA**	**Mahalanobis**
***Penicillium* spp. week 2**	99.4	99.2	99.8
***Penicillium* spp. week 4**	98.8	98.6	99.1
***Penicillium* spp. week 2**	100	100	100
***Penicillium* spp. week 6**	100	100	100
***Penicillium* spp. week 2**	100	100	100
***Penicillium* spp. week 8**	100	100	100
***Penicillium* spp. week 2**	100	100	100
***Penicillium* spp. week 10**	100	100	100
***Penicillium* spp. week 4**	100	100	100
***Penicillium* spp. week 6**	100	100	100
***Penicillium* spp. week 4**	100	100	100
***Penicillium* spp. week 8**	100	100	100
***Penicillium* spp. week 4**	100	100	100
***Penicillium* spp. week 10**	100	100	100
***Penicillium* spp. week 6**	100	100	100
***Penicillium* spp. week 8**	100	100	100
***Penicillium* spp. week 6**	100	100	100
***Penicillium* spp. week 10**	100	100	100
***Penicillium* spp. week 8**	100	100	100
***Penicillium* spp. week 10**	100	100	100

* Sample size for each class was 300 seeds

Table 4.6. Linear Discriminant Analysis (LDA), Quadratic Discriminant Analysis (QDA) and Mahalanobis Classification accuracies (%) for pair-wise model between five infection stages of *Aspergillus glaucus* and *Penicillium* spp. infected canola seeds.

Sample	**Classification Accuracies (%) using statistical features from 1100, 1130,1250 and 1300 nm wavelengths***		
	LDA	**QDA**	**Mahalanobis**
***A. glaucus* week 2**	92.5	93.1	93.7
***Penicillium* spp. week 2**	91.2	94.3	95.2
***A. glaucus* week 4**	95.8	96.6	97.5
***Penicillium* spp. week 4**	97.8	98.4	99.9
***A. glaucus* week 6**	100	100	100
***Penicillium* spp. week 6**	100	100	100
***A. glaucus* week 8**	100	100	100
***Penicillium* spp. week 8**	100	100	100
***A. glaucus* week 10**	100	100	100
***Penicillium* spp. week 10**	100	100	100

* Sample size for each class was 300 seeds

The classification accuracy of healthy canola seeds, five stages of *A. glaucus* and five stages of *Penicillium* spp. infected canola seeds increased with increase in fungal infection stages in the pair-wise classification. The quadratic and Mahalanobis discriminant classifiers gave better classification accuracy in the entire five tested pair-wise model when compared to linear discriminant classifier. Teena et al. (2014) also reported higher classification accuracy by quadratic discriminant classifier than linear discriminant classifier to classify healthy and fungal infected dates; however, Singh et al. (2007) reported higher classification accuracy by linear discriminant classifier than quadratic and Mahalanobis discriminant classifiers to classify healthy and fungal infected wheat kernels. The classification accuracies obtained were higher for pair-wise model tested between healthy versus *Penicillium* spp. infected canola seeds when compared to pair-wise model tested between healthy versus *Aspergillus glaucus* infected canola seeds because of higher intensity of fungal infection on the surface of *Penicillium* spp. infected canola seeds when observed by microscope and naked eyes. The results obtained in the fifth pair-wise model showed that fungal species can be classified using NIR hyperspectral imaging system at the later stages of fungal infection.

4.3.4 Two-class classification

The two-class classification model was tested to separate healthy samples from fungal infected samples. First two-class classification model was tested using 300 healthy canola seeds and 1500 *A. glaucus* infected canola seeds and the classification accuracy obtained by the linear, quadratic and Mahalanobis discriminant classifiers were 97.4, 97.6 and 98.5% for *A. glaucus* infected canola seeds and 98.1, 98.4 and 99.3%, respectively, for healthy canola seeds (Fig. 4.8).

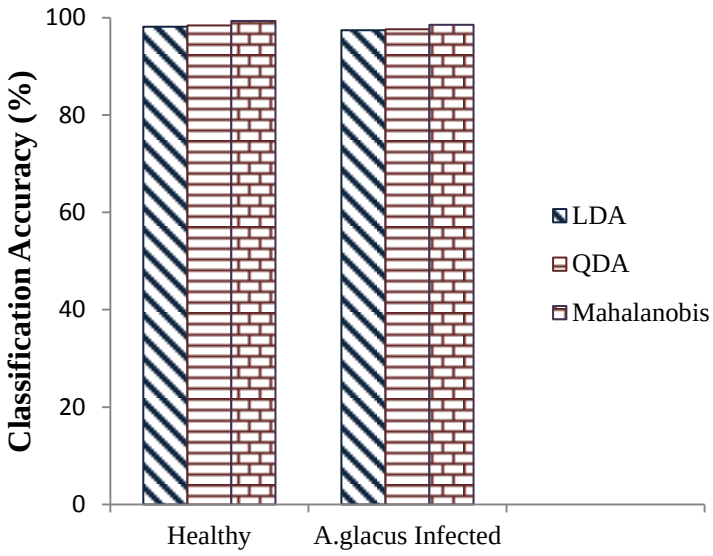

Fig. 4.8. Classification accuracy of two-class model: healthy and different stages of *A.glaucus* -infected samples

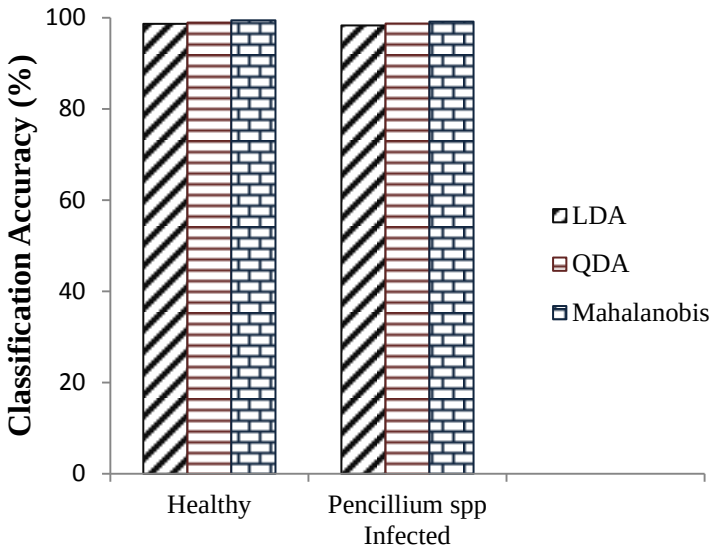

Fig. 4.9. Classification accuracy of two-class model: healthy and different stages of *Penicillium* spp.-infected samples

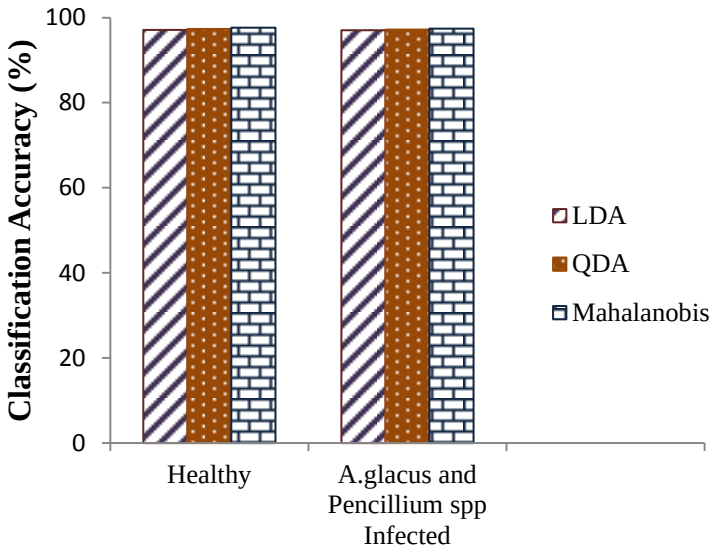

Fig. 4.10. Classification accuracy of two-class model: healthy and different stages of *A.glaucus* and *Penicillium* spp.- infected samples

Second two-class classification model was tested using 300 healthy canola seeds and 1500 *Penicillium* spp. infected canola seeds and the classification accuracy obtained by linear, quadratic and Mahalanobis classifiers were 98.3, 98.7 and 99.1% of *Penicillium* spp. infected canola seeds and 98.6, 98.9 and 99.4 %, respectively, for healthy canola seeds (Fig. 4.9). The third two-class classification model was tested using 300 healthy seeds and 3000 *A. glaucus* and *Penicillium* spp.-infected canola seeds and the classification accuracy obtained by linear, quadratic and Mahalanobis classifiers were 97, 97.2 and 97.4 for *A. glaucus* and *Penicillium* spp. infected canola seeds and 97.1, 97.3 and 97.6 %, respectively for healthy canola seeds (Fig. 4.10). The quadratic and Mahalanobis discriminant classifiers provided higher classification accuracies than the linear discriminant classifier for all the three two-class models tested between healthy and fungal infected canola seeds.

4.3.5 Six-class classification

A six-class classification model was used to classify healthy canola seeds and different stages of *A. glaucus* and *Penicillium* spp. infected canola seeds. First, six-class classification model was tested for 300 healthy canola seeds and 1500 canola seeds of two, four, six, eight and ten week *A. glaucus* infected canola seeds and the results obtained are given in Table 4.7. The classification accuracy of *A. glaucus* infected samples increased with increase in time from inoculation, which is an increase of *A. glaucus* infection stage. The classification accuracy of 100% was obtained for six, eight and ten week *A. glaucus* infected canola seeds using the quadratic and Mahalanobis discriminant classifiers whereas the linear discriminant classifier provided 100% classification accuracy for eight and tenth week *A. glaucus* infected canola seeds.

Table 4.7. Linear Discriminant Analysis (LDA), Quadratic Discriminant Analysis (QDA) and Mahalanobis Classification accuracies (%) for six-class model between healthy and five infection stages of *Aspergillus glaucus* infected canola seeds.

Sample	Healthy	Second Week	Fourth Week	Sixth week	Eight Week	Tenth Week
LDA						
Healthy	93.9	3.9	2.2	0	0	0
Second Week	12.8	80.3	6.9	0	0	0
Fourth Week	0	9.4	90.6	0	0	0
Sixth Week	0	0	3.2	96.8		
Eight Week	0	0	0	0	100	0
Tenth Week	0	0	0	0	0	100
QDA						
Healthy	94.2	5.3	0.5	0	0	0
Second Week	10.6	88.5	0.9	0	0	0
Fourth Week	0.2	3.7	96.1	0	0	0
Sixth Week	0	0	0	100	0	0
Eight Week	0	0	0	0	100	0
Tenth Week	0	0	0	0	0	100
Mahalanobis						
Healthy	95.8	2.4	1.8	0	0	0
Second Week	8.5	91.2	0.3	0	0	0
Fourth Week	0	1.9	98.1	0	0	0
Sixth Week	0	0	0	100	0	0
Eight Week	0	0	0	0	100	0
Tenth Week	0	0	0	0	0	100

* Sample size for each class was 300 seeds

Table 4.8. Linear Discriminant Analysis (LDA), Quadratic Discriminant Analysis (QDA) and Mahalanobis Classification accuracies (%) for six-class model between healthy and five infection stages of *Penicillium* spp. infected canola seeds.

Sample	Healthy	Second Week	Fourth Week	Sixth week	Eight Week	Tenth Week
LDA						
Healthy	96.4	2.8	0.8	0	0	0
Second Week	1.2	97.9	0.9	0	0	0
Fourth Week	0	0	100	0	0	0
Sixth Week	0	0	0	100	0	0
Eight Week	0	0	0	0	100	0
Tenth Week	0	0	0	0	0	100
QDA						
Healthy	97.1	1.8	1.1	0	0	0
Second Week	0.5	98.3	1.2	0	0	0
Fourth Week	0	0	100	0	0	0
Sixth Week	0	0	0	100	0	0
Eight Week	0	0	0	0	100	0
Tenth Week	0	0	0	0	0	100
Mahalanobis						
Healthy	98.4	1.1	0.5	0	0	0
Second Week	0.6	99.2	0.2	0	0	0
Fourth Week	0	0	100	0	0	0
Sixth Week	0	0	0	100	0	0
Eight Week	0	0	0	0	100	0
Tenth Week	0	0	0	0	0	100

* Sample size for each class was 300 seeds

Second six-class classification model was tested for 300 healthy canola seeds and 1500 canola seeds of two, four, six, eight and ten week *Penicillium* spp. infected canola and the results obtained are given in Table 4.8. The linear, quadratic and Mahalanobis discriminant classifiers provided 100% classification accuracy for four, six, eight and ten week Penicillium spp. infected canola seeds. The quadratic and Mahalanobis discriminant classifiers provided higher classification accuracies than the linear discriminant classifier for both six-class models tested between healthy and different stages of fungal infected canola seeds. The results obtained from the six-class model showed that NIR hyperspectral imaging system can be used to classify different stages of fungal infection in canola seeds. Teena et al. (2014) also reported the potential of NIR hyperspectral imaging to classify different stages of fungal infection in dates.

4.4. Conclusion

Healthy, *A. glaucus* and *Penicillium* spp. infected samples can easily be differentiated using near-infrared hyperspectral imaging system, in addition to that, it can also separate different infection stages of *A. glaucus* and *Penicillium* spp. infected canola seeds. The results obtained from this study prove that near-infrared hyperspectral imaging system can be used effectively in identifying fungal infection in canola at an early stage. Four significant wavelengths 1100, 1130, 1250 and 1300 nm were identified based on the highest factor loadings in the principal component analysis from the 61 wavelengths in the range of 1000 to 1600 nm. The classification accuracy increased with increase in fungal infection stages. The quadratic and Mahalanobis discriminant classifiers provided better classification accuracies in all the pair-wise, two-class and six-class models tested between healthy and different stages of fungal infected canola seeds when compared to the linear discriminant classifier.

References

Arngren, M., P.W. Hansen, B. Eriksen, J. Larsen, and R. Larsen. 2011. Analysis of pregerminated barley using hyperspectral image analysis. *Journal of Agricultural and Food Chemistry* 59: 11385-11394.

ASABE. 2012. Standard S352.2: Moisture Measurement Unground Grain and Seeds. ASABE: St. Joseph, Mich.

Barbedo, J. G.A., C.S. Tibola, and J.M.C. Fernandes. 2015. Detecting *Fusarium* head blight in wheat kernels using hyperspectral imaging. *Biosystems Engineering* 131: 65-76**.**

Berman, M., P.M. Connor, L.B. Whitbourn, D.A. Coward, B.G. Osborne, and M.D. Southan. 2007. Classification of sound and stained wheat grains using visible and near infrared hyperspectral image analysis. *Journal of Near Infrared Spectroscopy* 15: 351-358.

Chelladurai, V., D.S. Jayas, and N.D.G. White. 2010. Thermal imaging for detecting fungal infection in stored wheat. *Journal of Stored Products Research* 46: 174-179.

Choudhary, R., S. Mahesh, J. Paliwal, and D.S. Jayas. 2009. Identification of wheat classes using wavelet features from near infrared hyperspectral images of bulk samples. *Biosystems Engineering* 102: 115-127.

Delwiche, S.R. 2003. Classification of scab- and other mold-damaged wheat kernels by near-infrared reflectance spectroscopy. *Transactions of the ASAE* 46: 731-738.

Delwiche, S.R., and G.A. Hareland. 2004. Detection of scab-damaged hard red spring wheat kernels by near-infrared reflectance. *Cereal Chemistry* 81: 643-649.

Hayat, A., N. Paniel, A. Rhouati, J.L. Marty, and L. Barthelmebs. 2012. Recent advances in ochratoxin A-producing fungi detection based on PCR methods and ochratoxin A analysis in food matrices. *Food Control* 26: 401-415.

Kong, W.W., C. Zhang, F. Liu, P.C. Nie, Y. He. 2013. Rice seed cultivar identification using near-infrared hyperspectral imaging and multivariate data analysis. *Sensors* 13: 8916-8927.

Mahesh, S., D.S. Jayas, J. Paliwal and N.D.G. White. 2015. Hyperspectral imaging to classify and monitor quality of agricultural materials. *Journal of Stored Products Research* 61:17-26.

Mahesh, S., D.S. Jayas, J. Paliwal, and N.D.G. White. 2011. Identification of wheat classes at different moisture levels using near-infrared hyperspectral images of bulk samples. *Sensing and Instrumentation for Food Quality and Safety* 5: 1-9.

Mahesh, S., A. Manickavasagan, D.S. Jayas, J. Paliwal, and N.D.G. White. 2008. Feasibility of near-infrared hyperspectral imaging to differentiate Canadian wheat classes. *Biosystems Engineering* 101: 50-57.

Manley, M., P. Williams, D. Nilsson, and P. Geladi. 2009. Near infrared hyperspectral imaging for the evaluation of endosperm texture in whole yellow maize (*Zea maize* L.) kernels. *Journal of Agricultural and Food Chemistry* 57: 8761-8769.

Narvankar, D.S., C.B. Singh, D.S. Jayas, and N.D.G. White. 2009. Assessment of soft X-ray imaging for detection of fungal infection in wheat. *Biosystems Engineering* 103: 49-56.

Peiris, K.H.S., M.O. Pumphrey, and F.E. Dowell. 2009. NIR absorbance characteristics of deoxynivalenol and of sound and *Fusarium*-damaged wheat kernels. *Journal of Near Infrared Spectroscopy* 17: 213-221.

Pronyk, C., W.E. Muir, N.D.G. White, and D. Abramson. 2004. Carbon dioxide production and deterioration in stored canola. *Canadian Biosystems Engineering* 46: 3.25-3.33.

Ravikanth, L., C.B. Singh, D.S. Jayas, and N.D.G. White. 2015. Classification of contaminants from wheat using near-infrared hyperspectral imaging. *Biosystems Engineering* 135: 73-86.

Sathya, G., D.S. Jayas, and N.D.G. White. 2009. Safe storage guidelines for canola as the seeds slowly dry. *Canadian Biosystems Engineering* 51: 3.29-3.38.

Sauer, D.B., R.A. Meronuck, and C.M. Christensen. 1992. Microflora. In: Sauer, D.B. (Ed.), Storage of Cereal Grains and Their Products. American Association of Cereal Chemists, St. Paul, MN, pp. 313-340.

Senthilkumar, T., C.B. Singh, D.S. Jayas, and N.D.G. White. 2012. Detection of fungal infection in canola using near-infrared hyperspectral imaging. *Journal of Agricultural Engineering* 49: 21-27.

Serranti, S., D. Cesare, F. Marini, and G. Bonifazi. 2013. Classification of oat and groat kernels using NIR hyperspectral imaging. *Talanta* 103: 276-284.

Shahin, M.A., and S.J. Symons. 2008. Detection of hard vitreous and starchy kernels in amber durum wheat samples using hyperspectral imaging. *NIR News* 19: 16-18.

Singh, C.B., D.S. Jayas, J. Paliwal, and N.D.G. White. 2007. Fungal detection in wheat using near-infrared hyperspectral imaging. *Transactions of the ASAE* 50: 2171-2176.

Singh, C.B., D.S. Jayas, J. Paliwal, and N.D.G. White. 2009. Detection of insect-damaged wheat kernels using near-infrared hyperspectral imaging. *Journal of Stored Products Research* 45: 151-158.

Statistics Canada. Table 002-0001 - Farm cash receipts, annual (dollars), CANSIM (database). (Accessed: 2015-05-13)

Sun, K., F. Jian, D.S. Jayas, and N.D.G. White. 2014. Quality changes in high and low oil content canola during storage: Part I - safe storage time under constant temperatures. *Journal of Stored Products Research* 59: 320-327.

Tallada, J.G., D.T. Wicklow, T.C. Pearson, and P.R. Armstrong. 2011. Detection of fungus-infected corn kernels using near-infrared reflectance spectroscopy and color imaging. *Transactions of the ASABE* 54: 1151-1158.

Teena, M.A., A. Manickavasagan, L. Ravikanth, and D.S. Jayas. 2014. Near-infrered (NIR) hyperspectral imaging to classify fungal infected dates. *Journal of Stored Products Research* 59: 306-313.

Tekle, S., I. Måge, V.H. Segtnan, and A. Bjørnstad. 2015. Near-infrared hyperspectral imaging of *Fusarium*-damaged oats (*Avena sativa* L.). *Cereal Chemistry* 92: 73-80.

Vadivambal, R., and D.S. Jayas. 2016. Bio-Imaging: Principles, Techniques and Applications. CRC Press, Taylor and Francis Group Ltd., Oxford, UK. 395 p.

Vermeulen, P., J.A.F. Pierna, H.P.V. Egmond, P. Dardenne, and V. Baeten. 2012. Online detection and quantification of ergot bodies in cereals using near infrared hyperspectral imaging. *Food Additives and Contaminants* 29: 232-240.

Wang, D., F.E. Dowell, M.S. Ram, and W.T. Schapaugh. 2003. Classification of fungal damaged soybean seeds using near infrared spectroscopy. *International Journal of Food Properties* 7: 75-82.

Weinstock, B.A., J. Janni, L. Hagen, and S. Wright. 2006. Prediction of oil and oleic acid concentrations in individual corn (*Zea mays* L.) kernels using near-infrared reflectance hyperspectral imaging and multivariate analysis. *Applied Spectroscopy* 60: 9-16.

Williams, P., P. Geladi, G. Fox, and M. Manely. 2009. Maize kernel hardness classification by near infrared (NIR) hyperspectral imaging and multivariate data analysis. *Analytica Chimcia Acta* 653(2): 121-30.

Williams, P. J., P. Geladi, T.J. Britz, and M. Manley. 2012. Investigation of fungal development in maize kernels using NIR hyperspectral imaging and multivariate data analysis. *Journal of Cereal Science* 55(3): 272-278.

Chapter 5

Detection of fungal infection and ochratoxin A contamination in stored wheat using near-infrared hyperspectral imaging

This chapter is based on the following publication:

Senthilkumar, T., D.S. Jayas, P.G. Fields, N.D.G. White, and T. Gräfenhan. 2016. Detection of fungal infection and Ochratoxin A contamination in stored wheat using near-infrared hyperspectral imaging. *Journal of Stored Products Research,* 65: 30-39.

Abstract

A study was done to detect *Aspergillus glaucus*, and *Penicillium* spp., infection and ochratoxin A contamination in stored wheat using a Near-Infrared (NIR) Hyperspectral Imaging system. Fungal-infected samples were imaged every two weeks, and the three-dimensional hypercubes obtained from the image data were transformed into two-dimensional data. Principal component analysis was applied to the two-dimensional data and based on the highest factor loadings, 1280, 1300, and 1350 nm were identified as significant wavelengths. Six statistical features and ten histogram features corresponding to the significant wavelengths were extracted and subjected to linear, quadratic and Mahalanobis discriminant classifiers. All the three classifiers differentiated sterile kernels from fungal-infected kernels with a classification accuracy of more than 90%. The quadratic discriminant classifier provided classification accuracy higher than the linear and Mahalanobis classifiers for pair-wise, two-way and six-way classification models. The ochratoxin A contaminated samples had a unique significant wavelength at 1480 nm in addition to the two significant wavelengths corresponding to fungal infection. The peak at 1480 nm was identified only in the ochratoxin A contaminated samples. The ochratoxin A contaminated samples can be detected with 100% classification accuracy using the NIR hyperspectral imaging system. The NIR hyperspectral system can differentiate between different fungal infection stages and different levels of ochratoxin A contamination in stored wheat.

5.1 Introduction

Wheat is the second most important food crop and a source of protein in human nutrition with a world production of 715 million tonnes (Mt) in 2013 (FAOSTAT, 2013). Canada is the sixth largest producer and the third largest exporter of wheat in the world. Canada produced a record 37.5 Mt (FAOSTAT, 2013) and exported 20.3 Mt in 2013 (Statistics Canada, 2013). Seventy percent of the wheat produced and exported is of the Canada Western Red Spring (CWRS) class. Wheat is the second most valuable crop after canola in Canada and contributes CAD $11 billion to the economy (NRC Canada, 2013). Pests like fungi, insects, mites and rodents are a major cause of storage losses occurring in stored grain. It is necessary to protect the stored wheat from any pests from causing contamination or loss before it reaches consumers. Wheat grains dried to lower moisture content and stored at lower temperature levels will not allow pests to grow and multiply. However, some localized high moisture areas can occur inside the storage structure because of changes in exterior air temperatures leading to moisture migration and condensation. The localized areas will help the pests to grow and propagate, even though the average moisture content and temperature inside the storage structures is at desired low levels. Detection of pests inside the storage structure at an early stage will help producers to manage risks early by applying physical, chemical, or biological control methods.

Fungi affecting wheat grains can broadly be divided into pathogenic fungi active in the field and storage moulds. Field fungi get deactivated during the drying process before storage. Important species of molds causing damage to wheat grains in Canada are mainly members of the genera *Aspergillus* and *Penicillium*. Storage fungi usually grow and propagate when favorable conditions prevail inside the bulk grain. Fungal activity increases as the temperature and moisture content of stored wheat grains increases. The higher temperature and moisture

content help other pests like insects and mites to grow and multiply inside the bulk grain leading to further damage to stored grains.

The fungi present in grains causes quality changes like dull appearance, musty odors, seed germination loss, germ loss, discoloration, and increased free fatty acid value. The quality changes result in rejection for use as seeds, during processing and possibly yield lower grades for marketing. Other problems associated with fungal infection are aggregation of grains, heat damage and contamination with toxic metabolites. The aggregation of seeds creates uneven pressure inside the storage structures and eventually damages the structures during grain unloading. The heat damage can cause blackening of grains. Contamination with mycotoxins in grains can be a potential food safety issue for both humans and animals. All these effects caused by fungal infection in stored grains result in substantial economic losses to the farmers.

Mycotoxins are naturally occurring toxic metabolites produced by certain fungal species classified predominantly in the genera of *Fusarium*, *Aspergillus* and *Penicillium*. Mycotoxins can cause acute or chronic health issues in consumers. Ochratoxin A found in barley, oats, rye and wheat may have been produced by *Penicillium verrucosum* or a small number of *Aspergillus* species. In Canada because of its climatic conditions, ochratoxin A is produced by *P. verrucosum* and can be found occasionally in stored wheat, barley, oats and rye. Ochratoxin A toxicity studies conducted on laboratory animals caused nephrotoxicity, hepatotoxicity, teratogenicity, immunotoxicity, nephrocarcinogenicity, kidney and liver tumors (Boorman et al, 1992; Castegnaro et al, 1998; Bendele et al, 1985; JECFA, 2007; WHO 2001, O'Brien and Dietrich 2005). International agency on cancer research classified ochratoxin A as a potential carcinogen. The potential food safety risks resulted in implementation of maximum limits (0.5 to 10 µg/kg of food) for ochratoxin A in food products.

The traditional culture method and microscopic identification of fungal infections is a tedious and time consuming process requiring significant amount of expertise. The detection and quantitation of ochratoxin A in grain samples is a long process which involves extraction procedure using solvents and an identification process involving immuno- or chromatographic methods. There is a need for a more rapid technique to detect fungal infection and ochratoxin A contamination in stored wheat to avoid further infection and contamination by taking suitable corrective measures to disinfect the fungal infected grains and to discard ochratoxin A contaminated grain before it enters the supply chain. Near-infrared hyperspectral imaging also known as a chemical imaging technique is a non-destructive, non-chemical, and rapid method. NIR hyperspectral imaging is a combination of digital imaging and NIR spectroscopy, which extracts both spatial and spectral information from a sample and provides chemical composition of the sample.

Applications of near-infrared hyperspectral imaging technique in various fields were reported in a book by Vadivambal and Jayas (2016). Near-infrared hyperspectral imaging technique to detect different quality parameters, insect infestation, and fungal infection associated with different stored grains and oil seeds were reported by Mahesh et al. (2015), Senthilkumar et al. (2015) and Teena et al. (2013). NIR hyperspectral imaging technique in the wavelength range between 1000 and 2500 nm, was utilized to detect aflatoxin B1 in single maize kernels with classification accuracy between 80 and 96.1% (Wang et al., 2015a), Aflatoxin B1 concentration of as low as 10 ppb on maize kernel surfaces was identified using NIR hyperspectral imaging in the wavelength range between 1000 and 2500 nm with a classification accuracy of 88% (Wang et al, 2014). Wang et al. (2015b) identified wavelengths 1729 and 2344

nm corresponding to the presence of aflatoxin B1 in maize kernels. NIR hyperspectral imaging to identify other mycotoxins have not been reported in the literature.

Detection of fungal infection in wheat at an early stage and at different infection levels was not reported in the literature. NIR hyperspectral imaging was not utilized to detect ochratoxin A in any stored grains. Therefore, the objectives of this study were:

1. To detect different degrees of infection of *Aspergillus glaucus*, and *Penicillium* spp. infection in CWRS wheat using NIR hyperspectral imaging system, and
2. To detect ochratoxin A in *Pencillium verrucosum* infected wheat samples using a NIR hyperspectral imaging system.

5.2 Materials and Methods

5.2.1 Grain sample preparation for fungal detection study

Fifty one kilograms of 2013 crop year CWRS wheat with initial moisture content of 13.5% (wet basis) were obtained from Agriculture and Agri-Food Canada, Winnipeg, Manitoba. Wheat was conditioned to higher moisture content of 17% by adding a calculated amount of distilled water to help the growth of fungal cultures in stored wheat. The conditioned wheat grains were surface sterilized using 1% sodium hypochlorite solution and autoclaved at 120ºC for 20 min to remove any pre-existing contaminants from the wheat samples. Forty kilograms from the conditioned and sterilized samples were used as buffer samples and 1 kg wheat grain utilized as a control sample. The remaining 10 kg of wheat grains were divided into two samples of 5 kg each. The two samples were placed in two different environment chambers to avoid cross-contamination and were inoculated with two different fungal species, *Aspergillus glaucus*,

and *Penicillium* spp. obtained from the Grain Research Laboratory, Canadian Grain Commission, Winnipeg, MB, Canada. Pure fungal cultures were grown on potato dextrose agar; the fungi plus agar were placed in distilled water with 2 drops of Tween 20 in plastic misting bottles. Grain was sprayed until uniformly damp. The samples inoculated with *Aspergillus glaucus*, and *Penicillium* spp. were sealed and maintained at 30ºC±2 and 70% relative humidity inside the environmental chamber.

The two different samples inoculated with fungi were divided equally into five sub-samples of one kilogram each and were labelled as follows: Sample 1: *A. glaucus* sub-sample 1, *A. glaucus* sub-sample 2, *A. glaucus* sub-sample 3, *A. glaucus* sub-sample 4, *A. glaucus* sub-sample 5; Sample 2: *Penicillium* spp. sub-sample 1, *Penicillium* spp. sub-sample 2, *Penicillium* spp. sub-sample 3, *Penicillium* spp. sub-sample 4, *Penicillium* spp. sub-sample 5. Each fungal infected sub-sample was placed between two buffer wheat samples one on the top (2 kg) and the other on the bottom (2 kg) in a 20 L plastic pail with KOH solution with specific gravity to maintain the sub-samples at 17% moisture content throughout the study(Solomon, 1951). The sub-samples and buffer samples were separated by an iron mesh to avoid direct contact with KOH solution. The sample placement inside the plastic pail is illustrated in Fig.5.1.

5.2.2 Grain sample preparation for ochratoxin A detection study

Twenty five kilograms of CWRS wheat obtained from Agriculture and Agri-Food Canada, Winnipeg, Manitoba were conditioned to higher moisture content of 21.5% to help the fungi grow and produce mycotoxins (Nithya et al., 2011). The conditioned samples were surface sterilized using 1% sodium hypochlorite solution and autoclaved at 120ºC for 20 min. Twenty

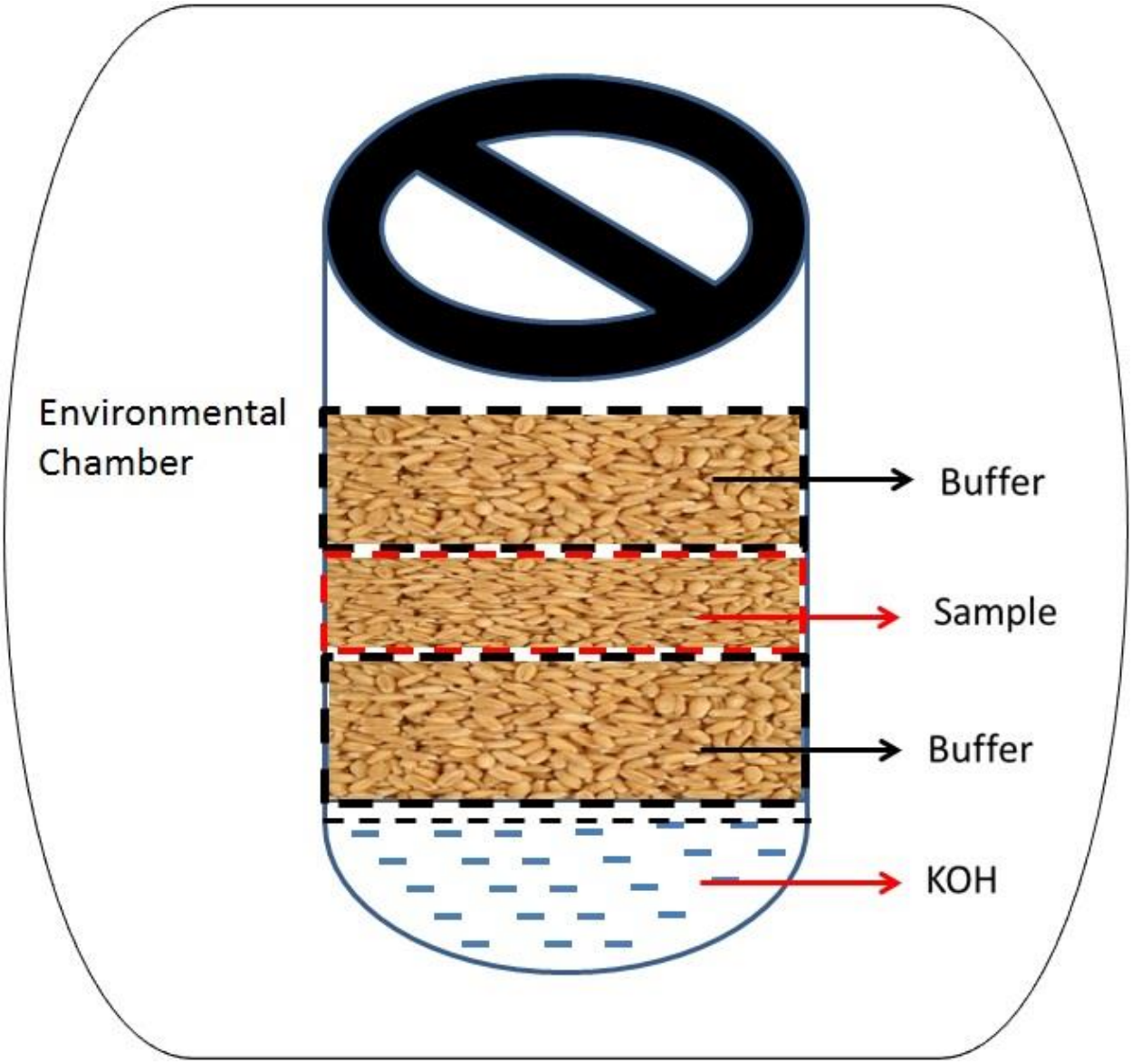

Fig. 5.1. Illustration of wheat sample placement between the buffer samples and KOH solution inside the 20 L pails.

kilograms of wheat grains were used as buffer samples to control moisture fluctuation in five samples inoculated with *P. verrucosum*, each weighing one kilogram. The samples were labelled as ochratoxin A sample 1, ochratoxin A sample 2, ochratoxin A sample 3, ochratoxin A sample 4, and ochratoxin A sample 5 and placed in the same way between the buffer samples as mentioned in section 2.1 and illustrated in Fig.5.1. The five samples prepared for ochratoxin A study were sealed and maintained at 20ºC±2 and 70% relative humidity. The moisture content between 20 and 22% and temperature around 20ºC were identified as the most conducive environment for ochratoxin A production by *P. verrucosum* (Czaban, 2006). The 1 kg control sample conditioned to 17% moisture content and autoclaved at 120ºC for 20 min was utilized for both fungal and ochratoxin A detection study.

5.2.3 NIR hyperspectral imaging system

The NIR hyperspectral imaging system is made up of four major components, Tungsten halogen lamp (300W, Ushio Lighting Inc., Cypress, CA, USA), NIR Camera (Model No. SU640-1.7RT-D, Sensors Unlimited Inc., Princeton, NJ, USA), Liquid Crystal Tunable Filters (LCTFs), (VariSpec, Cambridge Research and Instrumentation Inc., Woburn, MA, USA) and data processing unit. All the four major components were mounted on a camera stand. The NIR system used in this study is represented schematically in Fig.5.2. The tungsten halogen lamp were the source for emitting light in the wavelength range of 400 to 2500 nm. The NIR camera had an Indium Gallium Arsenide (InGaAs) detector and had a 25 mm mounted lens to capture images in the NIR wavelength region of 1000-1600 nm. The LCTFs helped to tune on to the

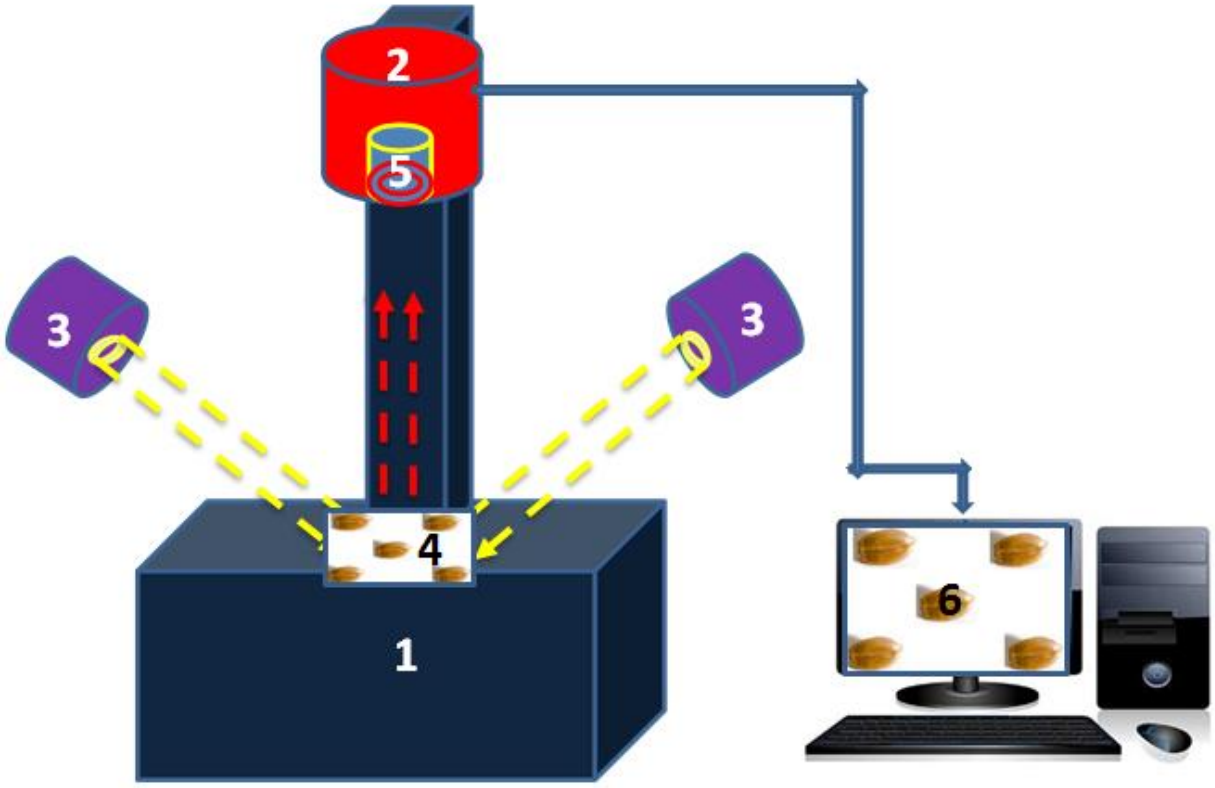

Fig. 5.2. Schematic representation of NIR hyperspectral imaging system 1. Camera Stand, 2. NIR Camera, 3. Tungsten- Halogen Lamps, 4. Wheat kernels, 5. LCTF Filters, 6. Data Acquisition and Processing System.

desired transmission bandwidth from 1000 to 1600 nm. The data processing unit had Lab VIEW Programme (Version 7.1, National Instruments Corp., Austin, TX, USA) to capture images and MATLAB software (The Mathworks, Inc., Natick, MA, USA) to process the acquired images.

2.4 Image acquisition and data analysis

Three hundred individual wheat kernels from each of the two fungal infected sub-sample 1 (*Penicillium* spp. sub-sample 1, and *Aspergillus glaucus* sub-sample 1,) were randomly selected and subjected to image acquisition after 2 weeks of fungal infection. Similarly, all two sub-sample 2 after 4 weeks, all two sub-sample 3 after 6 weeks, all two sub-sample 4 after 8 weeks and all two sub-sample 5 after 10 weeks after fungal infection were imaged. The number of fungal infected wheat kernels subjected to imaging were 3000 (10 sub-samples × 300) and 300 random wheat kernels from the control sample. The images acquired from 3300 individual kernels were used in the analysis. The wheat kernels were placed in a non-touching manner on a black board and were subjected to imaging. The black boards were thoroughly wiped with ethanol before and after every imaging session to avoid any cross contamination.

The wheat samples prepared for the ochratoxin A study were subjected to imaging as follows: ochratoxin A sample 1 after 18 weeks of fungal infection, ochratoxin A sample 2 after 20 weeks, ochratoxin A sample 3 after 22 weeks, ochratoxin A sample 4 after 24 weeks and ochratoxin A sample 5 after 26 weeks. Three hundred kernels from each ochratoxin A sample were randomly selected and subjected to single kernel imaging. The ochratoxin A sample wheat kernels subjected to imaging are 1500 (5 samples × 300).

The images were acquired in the wavelength range from 1000 to 1600 nm at 61 evenly distributed wavelengths. The data acquired were in the three-dimensional hypercube form. The three-dimensional hypercubes were transformed into two-dimensional data by means of

reshaping intensity data into reflectance data, and by automatic thresholding (Senthilkumar et al., 2012, 2015). The two-dimensional reflectance data of all the 4800 individual wheat kernels were subjected to Principal Component Analysis (PCA). Significant wavelengths were selected based on the highest factor loadings in the PCA. The six statistical features (mean, median, standard deviation, variance, maximum, and minimum) and ten histogram features corresponding to the significant wavelengths were extracted using a program written in MATLAB.

The extracted statistical and histogram features were used as inputs in linear, quadratic and Mahalanobis discriminant classifiers to discriminate between sterile, fungal infected, and ochratoxin A contaminated samples. Pair-wise, two-class, and six-class classification model programs were written using Statistical Analysis Software (PROC DISCRIM, Version 9.1.3, SAS institute Inc., Cary, NC, USA) and the models used 240 wheat kernels (80%) as training set and 60 wheat kernels (20%) as testing set for each of the sterile, five different stages of *A. glaucus* and *Penicillium* spp. infected samples and five different levels of ochratoxin A contaminated samples.

2.5 Moisture content, germination and ochratoxin A quantification

Wheat moisture content was determined every 2 weeks by oven drying 10 g of wheat kernels in triplicates for 19 h at 130±2ºC (ASABE, 2012). Wheat germination was determined by placing triplicates of 25 wheat kernels on Whatman No 3 filter paper soaked with 5.5 mL of distilled water in a 9 cm diameter petri dish (Wallace and Sinha, 1962). The wheat kernels were incubated for 4 d inside the polythene bag and the next 3 d without the polythene bag at room temperature (22±2 ºC) and percent germination was calculated. Ochratoxin A in wheat kernels were determined by testing the samples at Central Testing Laboratory, Winnipeg, Manitoba by employing an ELISA method.

5.3 Results and Discussion

5.3.1 Moisture content, seed germination, and ochratoxin A quantification

Moisture content of fungal infected wheat samples at the start of the study was 17.0 ± 0.3% and at the end of 10 weeks the moisture content was 17.0 ± 0.6%. The moisture content of the samples remained the same after 10 weeks because of the presence of buffer samples and KOH solution. A study on safe storage guidelines for durum wheat followed the same pattern of placing the samples between buffer samples and obtained similar results of constant moisture content up to 12 weeks of storage (Nithya et al., 2011). The germination at the start of the study was 92.5±0.3% and the germination reached 0% at the end of 8 weeks for all the fungal-infected samples. Germination gradually decreased with increase in fungal infection levels for all the fungal-infected samples (Table 5.1). The germination was measured to ensure that there was an increase in fungal infection levels over the period of 10 weeks. The *P. verrucosum* inoculated samples prepared for detecting ochratoxin A production were tested in a laboratory and the results obtained are given in ppb in Table 5.1.

5.3.2 Significant wavelengths

Three significant wavelengths 1280, 1300, and 1350 nm corresponding to the highest factor loadings in the first principal component analysis were obtained for *A. glaucus*, and Penicillium spp. inoculated samples (Fig. 5.3, and 5.4). The principal component analysis on ochratoxin A contaminated samples provided 1300, 1350 and1480 nm as significant wavelengths based on the highest factor loadings on all ochratoxin A contaminated samples (Fig. 5.5). The wavelength 1300 nm was attributed to fungal infection in soybean, wheat, canola and dates (Singh et al., 2007; Senthilkumar et al., 2015; Teena et al., 2014; Wang et al., 2003).

Table 5.1. Germination (%) of sterile, different infection periods (2, 4, 6, 8, and 10 weeks post inoculation) of *Aspergillus glaucus* (AG) and *Penicillium* spp. (PS) infected wheat kernels and different infection periods (18, 20, 22, 24, and 26 weeks post inoculation) of *Penicillium verrucosum* infected wheat kernels and ochratoxin A (OTA, ppb) as well as concentrations of OTA of *Penicillium verrucosum* infected wheat kernels. In the last column, nd means ochratoxin A was not detected).

Sample	Germination (%)	Ochratoxin A (ppb)
Sterile*	92.5±0.3	nd
AG week 2	70.0±0.5	nd
AG week 4	34.7±0.4	nd
AG week 6	13.0±0.2	nd
AG week 8	0.00±0.0	nd
AG week 10	0.00±0.0	nd
PS week 2	69.2±0.6	nd
PS week 4	28.0±0.9	nd
PS week 6	10.0±0.4	nd
PS week 8	0.00±0.0	nd
PS week 10	0.00±0.0	nd
OTA sample 1	0.00±0.0	72
OTA sample 2	0.00±0.0	100
OTA sample 3	0.00±0.0	382
OTA sample 4	0.00±0.0	430
OTA sample 5	0.00±0.0	600

* - germination before sterilization

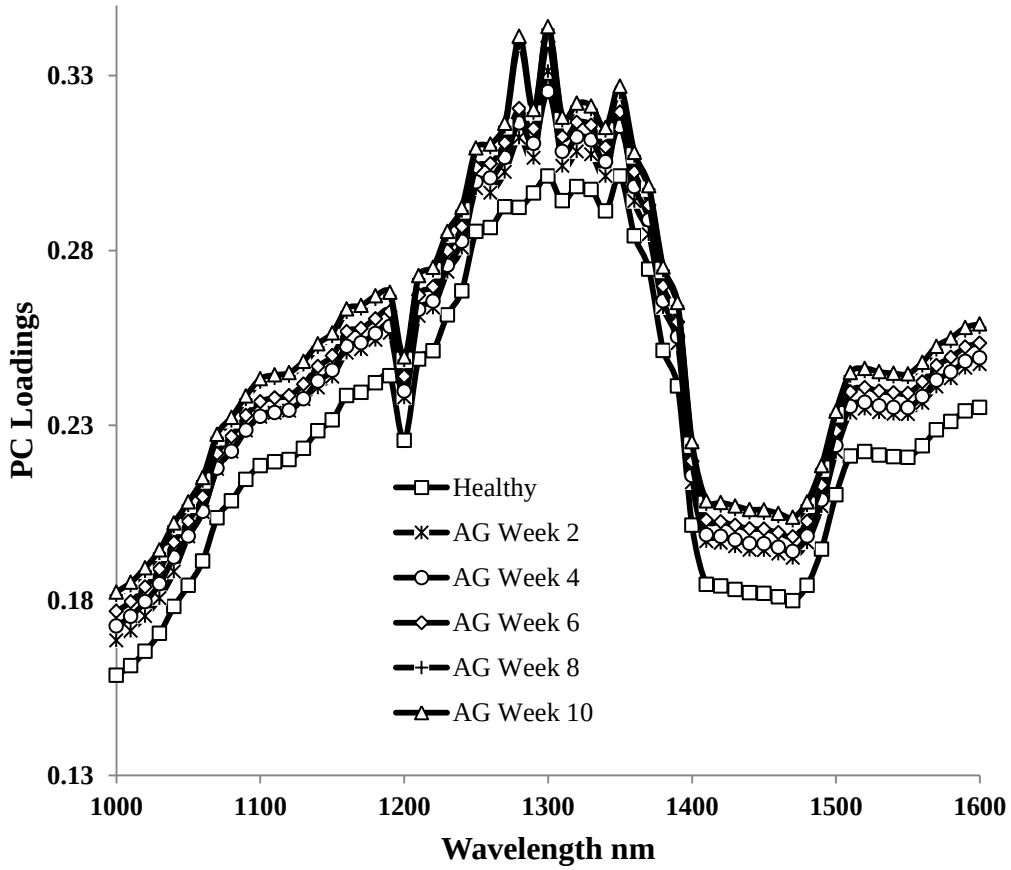

Fig. 5.3. First principal component (PC) loadings of sterile and different periods of *Aspergillus glaucus* infected wheat (AG 2 to AG 10: *Aspergillus glaucus* Second to Tenth week post inoculation).

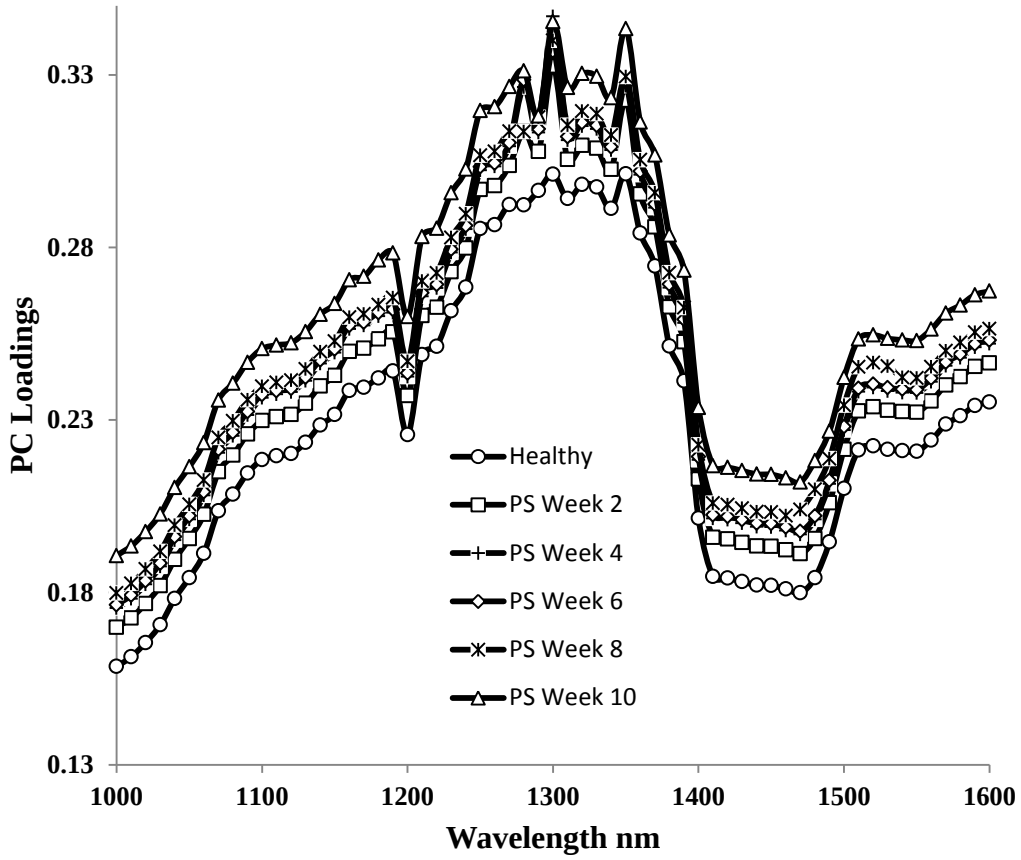

Fig. 5.4. First principal component (PC) loadings of sterile and different periods of *Penicillium* spp. infected wheat (PS 2 to PS 10: *Penicillium* spp. Second to Tenth week post inoculation).

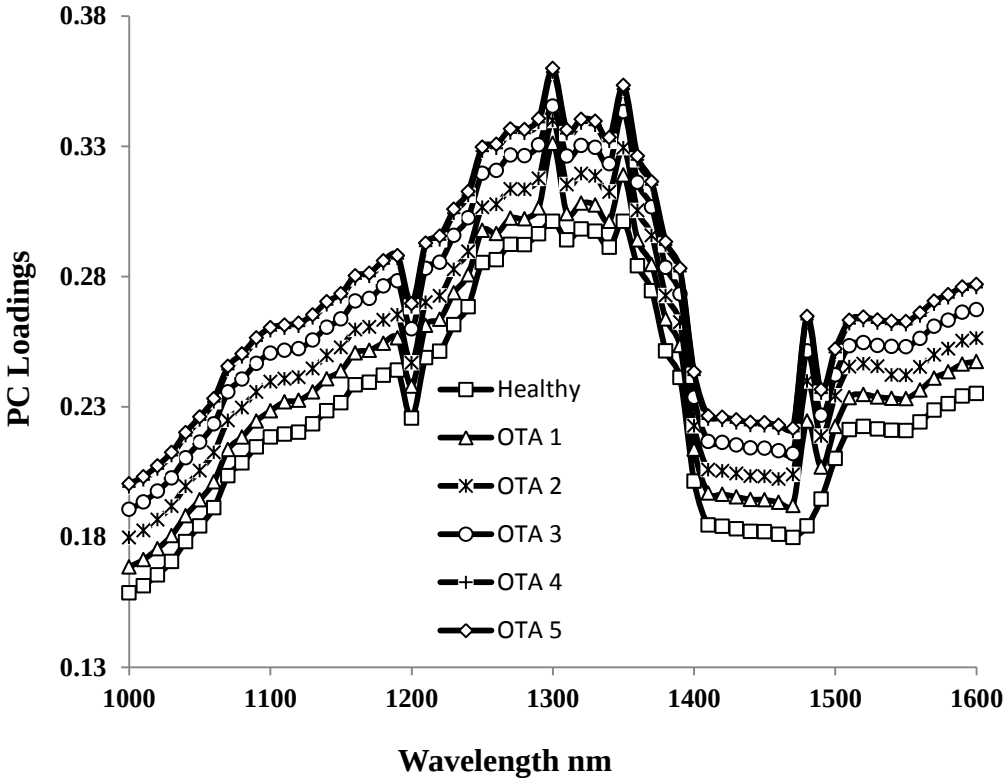

Fig. 5.5. First principal component (PC) loadings of sterile and five levels of ochratoxin A contaminated wheat kernels (OTA 1 to OTA 5: five levels of ochratoxin A contaminated wheat kernels).

The wavelength range between 1200 and 1360 nm and 1470 to 1500 nm was attributed to carbohydrate and protein content, respectively in wheat (Delwiche and Massie, 1996; Wang et al, 1999; Murray and Williams, 1987).

5.3.3 Pair-wise classification model

Five pair-wise models were developed, first pair-wise model to discriminate between sterile and different periods of fungal-infected samples, second pair-wise model to find the classification accuracy between different periods of fungal-infected samples, third pair-wise model to differentiate between *A.glaucus* and *Penicillium* spp. fungal-infected wheat kernels, fourth pair-wise model to differentiate between sterile and five levels of ochratoxin A contaminated wheat kernels, and fifth pair-wise model to differentiate between five levels of ochratoxin A contaminated wheat kernels.

The linear, quadratic and Mahalanobis pair-wise models developed to discriminate sterile wheat kernels from five different periods of *A. glaucus*-infected samples provided classification accuracy of 92.6 to 100% for sterile samples and 84.5 to 100% for *A. glaucus*-infected samples (Table 5.2). The linear, quadratic, and Mahalanobis classifiers completely differentiated sterile and *A. glaucus* infected samples with a classification accuracy of 100% after six weeks of *A. glaucus* infection. The *A. glaucus* infection at initial periods was less when compared to infection at later periods, so the classification accuracy increased with increase in infection levels. The quadratic classifiers provided the highest classification accuracy among the three classifiers (Singh et al., 2007). The classification accuracy of sterile samples was between 96.6 and 100% and for *Penicillium* spp. infected samples was between 93.9 and 100% for all the three discriminant pair-wise classification models developed to differentiate sterile and *Penicillium* spp. infected samples.

Table 5.2. Linear, quadratic and Mahalanobis classification accuracies (%) for pair-wise model between sterile and different infection periods (2, 4, 6, 8, and 10 weeks post inoculation) of *Aspergillus glaucus* (AG) infected wheat kernels using statistical and histogram features from 1280, 1300 and 1350 nm wavelengths. Sample size of sterile and each infection period were 300 kernels.

Pair-wise model	Sample	Statistical classification accuracies (%)		
		LDA	**QDA**	**Mahalanobis**
Sterile vs AG week 2	Sterile	93.2	96.5	92.6
	AG week 2	88.6	92.1	84.5
Sterile vs AG week 4	Sterile	98.1	98.8	97.8
	AG week 4	92.6	96.9	91.4
Sterile vs AG week 6	Sterile	100	100	100
	AG week 6	100	100	100
Sterile vs AG week 8	Sterile	100	100	100
	AG week 8	100	100	100
Sterile vs AG week 10	Sterile	100	100	100
	AG week 10	100	100	100

The classification accuracy reached 100% for both sterile and *Penicillium* spp. infected samples after four weeks of fungal infection. The quadratic classifier provided the highest classification accuracy among the three classifiers (Table 5.3). Singh et al. (2007) detected fungal infection in wheat at an advanced stage of mycelia growth using NIR hyperspectral imaging which had lower classification than this study, because in addition to statistical features we also used histogram features corresponding to significant wavelengths to differentiate sterile samples from fungal infected samples. The three discriminant classifiers differentiated sterile and all five levels of ochratoxin A contaminated wheat kernels with 100% classification accuracy (Table 5.4).

The linear, quadratic and Mahalanobis discriminant pair-wise models were developed to find classification accuracy between different periods of *A. glaucus* infected samples. The classification accuracy of 2 weeks *vs.* 4 weeks and 4 weeks *vs.* 6 weeks of *A. glaucus* infected samples were between 83.8 and 99.3%; and for all the other combinations was 100% (Table 5.5). The classification models developed to differentiate A. *glaucus* infected samples shortly after inoculation had lower classification accuracy than advanced periods of *A. glaucus* infected samples due to differences in mycelial growth and gradual deterioration of wheat kernels over the storage period. A study involving NIR hyperspectral imaging system to detect different periods of *A. glaucus* infected high oil content canola seeds had a similar pattern as observed in this study, low classification accuracy at early periods after inoculation and high classification accuracy at advanced periods of fungal growth (Senthilkumar et al., 2012). The three discriminant pair-wise models classified 2 weeks vs. 4 weeks of *Penicillium* spp. infected samples with a classification accuracy between 98.6 and 99.8% and 100% accuracy was achieved for all the remaining combinations (Table 5.6).

Table 5.3. Linear, quadratic, and Mahalanobis classification accuracies (%) for pair-wise model between sterile and different infection periods (2, 4, 6, 8, and 10 weeks post inoculation) of *Penicillium* spp. (PS) infected wheat kernels using statistical and histogram features from 1280, 1300 and 1350 nm wavelengths. Sample size of sterile and each infection period were 300 kernels.

Pair-wise model	Sample	Statistical classification accuracies (%)		
		LDA	**QDA**	**Mahalanobis**
Sterile vs PS week 2	Sterile	97.4	97.9	96.6
	PS week 2	96.2	98.9	93.9
Sterile vs PS week 4	**Sterile**	100	100	100
	PS week 4	100	100	100
Sterile vs PS week 6	**Sterile**	100	100	100
	PS week 6	100	100	100
Sterile vs PS week 8	**Sterile**	100	100	100
	PS week 8	100	100	100
Sterile vs PS week 10	**Sterile**	100	100	100
	PS week 10	100	100	100

Table 5.4. Linear, quadratic and Mahalanobis classification accuracies (%) for pair-wise model between sterile and different concentration levels (72, 100, 382, 430, 600 ppb) of ochratoxin A (OTA) contaminated wheat kernels using statistical and histogram features from 1300, 1350 and 1480 nm wavelengths. Sample size of sterile and each contamination level were 300 kernels.

Pair-wise model	Sample	Statistical classification accuracies (%)		
		LDA	**QDA**	**Mahalanobis**
Sterile vs OTA sample 1	Sterile	100	100	100
	OTA sample 1	100	100	100
Sterile vs OTA sample 2	**Sterile**	100	100	100
	OTA sample 2	100	100	100
Sterile vs OTA sample 3	**Sterile**	100	100	100
	OTA sample 3	100	100	100
Sterile vs OTA sample 4	**Sterile**	100	100	100
	OTA sample 4	100	100	100
Sterile vs OTA sample 5	**Sterile**	100	100	100
	OTA sample 5	100	100	100

Table 5.5 Linear, quadratic, and Mahalanobis classification accuracies (%) for pair-wise model between different infection periods (2, 4, 6, 8, and 10 weeks post inoculation) of *Aspergillus glaucus* (AG) infected wheat kernels using statistical and histogram features from 1280, 1300 and 1350 nm wavelengths. Sample size of each infection period was 300 kernels.

Pair-wise model	Sample	Statistical classification accuracies (%)		
		LDA	**QDA**	**Mahalanobis**
AG week 2 vs AG week 4	AG week 2	87.5	96.4	83.8
	AG week 4	98.0	98.3	97.9
AG week 2 vs AG week 6	AG week 2	100	100	100
	AG week 6	100	100	100
AG week 2 vs AG week 8	AG week 2	100	100	100
	AG week 8	100	100	100
AG week 2 vs AG week 10	AG week 2	100	100	100
	AG week 10	100	100	100
AG week 4 vs AG week 6	AG week 4	98.9	99.3	98.6
	AG week 6	99.0	99.5	98.9
AG week 4 vs AG week 8	AG week 4	100	100	100
	AG week 8	100	100	100
AG week 4 vs AG week 10	AG week 4	100	100	100
	AG week 10	100	100	100
AG week 6 vs AG week 8	AG week 6	100	100	100
	AG week 8	100	100	100
AG week 6 vs AG week 10	AG week 6	100	100	100
	AG week 10	100	100	100
AG week 8 vs AG week 10	AG week 8	100	100	100
	AG week 10	100	100	100

The quadratic pair-wise models developed to discriminate between different periods of all two fungal infected samples provided higher classification accuracy than the linear and Mahalanobis pair-wise models. The three discriminant pair-wise models classified ochratoxin A sample 1 vs ochratoxin A sample 2 with a classification accuracy between 98.9 and 100% and 100% accuracy was achieved for all the remaining combinations (Table 5.7). The three discriminant pair-wise models to differentiate between *A. glaucus* and *Penicillium* spp. fungal-infected wheat kernels provided classification accuracy between 71.3 and 80.2% for *A.glaucus* week 2 vs *Penicillium* spp. week 2, between 93.2 and 96.3% for *A.glaucus* week 4 vs *Penicillium* spp. week 4. The remaining combinations were differentiated with a complete classification accuracy of 100% (Table 5.8).

5.3.4 Two-class classification model

Four two-class models were developed, first to differentiate between sterile and combined samples of all five *A. glaucus* infection periods, second to differentiate between sterile and combined samples of all five *Penicillium* spp. infection periods, third to differentiate between sterile and combined samples of all five levels of ochratoxin A contaminated wheat kernels, and fourth to differentiate between sterile and combined samples of all five *A. glaucus,* and *Penicillium* spp. infection periods. The linear, quadratic and Mahalanobis discriminant classifiers differentiated sterile and all five *A. glaucus* infection periods with classification accuracy in the range between 96.8 and 97.9 % for sterile kernels and between 95.8 and 96.9 for all five *A. glaucus* infected wheat kernels (Fig. 5.6 A).

Table 5.6. Linear, quadratic, and Mahalanobis classification accuracies (%) for pair-wise model between different infection periods (2, 4, 6, 8, and 10 weeks post inoculation) of *Penicillium* spp. (PS) infected wheat kernels using statistical and histogram features from 1280, 1300 and 1350 nm wavelengths. Sample size of each infection period was 300 kernels.

Pair-wise model	Sample	Statistical classification accuracies (%)		
		LDA	**QDA**	**Mahalanobis**
PS week 2 vs PS week 4	PS week 2	99.4	99.8	99.1
	PS week 4	98.9	99.6	98.6
PS week 2 vs PS week 6	PS week 2	100	100	100
	PS week 6	100	100	100
PS week 2 vs PS week 8	PS week 2	100	100	100
	PS week 8	100	100	100
PS week 2 vs PS week 10	PS week 2	100	100	100
	PS week 10	100	100	100
PS week 4 vs PS week 6	PS week 4	100	100	100
	PS week 6	100	100	100
PS week 4 vs PS week 8	PS week 4	100	100	100
	PS week 8	100	100	100
PS week 4 vs PS week 10	PS week 4	100	100	100
	PS week 10	100	100	100
PS week 6 vs PS week 8	PS week 6	100	100	100
	PS week 8	100	100	100
PS week 6 vs PS week 10	PS week 6	100	100	100
	PS week 10	100	100	100
PS week 8 vs PS week 10	PS week 8	100	100	100
	PS week 10	100	100	100

Table 5.7.Linear, quadratic and Mahalanobis classification accuracies (%) for pair-wise model between different concentration levels (72, 100, 382, 430, 600 ppb) of ochratoxin A (OTA) contaminated wheat kernels using statistical and histogram features from 1300, 1350 and 1480 nm wavelengths. Sample size of each contamination level was 300 kernels.

Pair-wise model	Sample	Statistical classification accuracies (%)		
		LDA	**QDA**	**Mahalanobis**
OTA sample 1 vs OTA sample 2	OTA sample 1	99.8	100	99.4
	OTA sample 2	99.0	99.2	98.9
OTA sample 1 vs OTA sample 3	OTA sample 1	100	100	100
	OTA sample 3	100	100	100
OTA sample 1 vs OTA sample 4	OTA sample 1	100	100	100
	OTA sample 4	100	100	100
OTA sample 1 vs OTA sample 5	OTA sample 1	100	100	100
	OTA sample 5	100	100	100
OTA sample 2 vs OTA sample 3	OTA sample 2	100	100	100
	OTA sample 3	100	100	100
OTA sample 2 vs OTA sample 4	OTA sample 2	100	100	100
	OTA sample 4	100	100	100
OTA sample 2 vs OTA sample 5	OTA sample 2	100	100	100
	OTA sample 5	100	100	100
OTA sample 3 vs OTA sample 4	OTA sample 3	100	100	100
	OTA sample 4	100	100	100
OTA sample 3 vs OTA sample 5	OTA sample 3	100	100	100
	OTA sample 5	100	100	100
OTA sample 4 vs OTA sample 5	OTA sample 4	100	100	100
	OTA sample 5	100	100	100

Table 5.8. Linear, quadratic and Mahalanobis classification accuracies (%) for pair-wise model between different infection periods (2, 4, 6, 8, and 10 weeks post inoculation) of *Aspergillus glaucus* (AG), and *Penicillium* spp.(PS) infected wheat kernels using statistical and histogram features from 1280, 1300 and 1350 nm wavelengths. Sample size of each infection period was 300 kernels.

Pair-wise model	Sample	Statistical classification accuracies (%)		
		LDA	**QDA**	**Mahalanobis**
AG week 2 vs PS week 2	AG week 2	73.1	78.5	71.3
	PS week 2	79.2	80.2	78.4
AG week 4 vs PS week 4	AG week 4	94.8	95.8	93.2
	PS week 4	94.2	96.3	94.0
AG week 6 vs PS week 6	AG week 6	100	100	100
	PS week 6	100	100	100
AG week 8 vs PS week 8	AG week 8	100	100	100
	PS week 8	100	100	100
AG week 10 vs PS week 10	AG week 10	100	100	100
	PS week 10	100	100	100

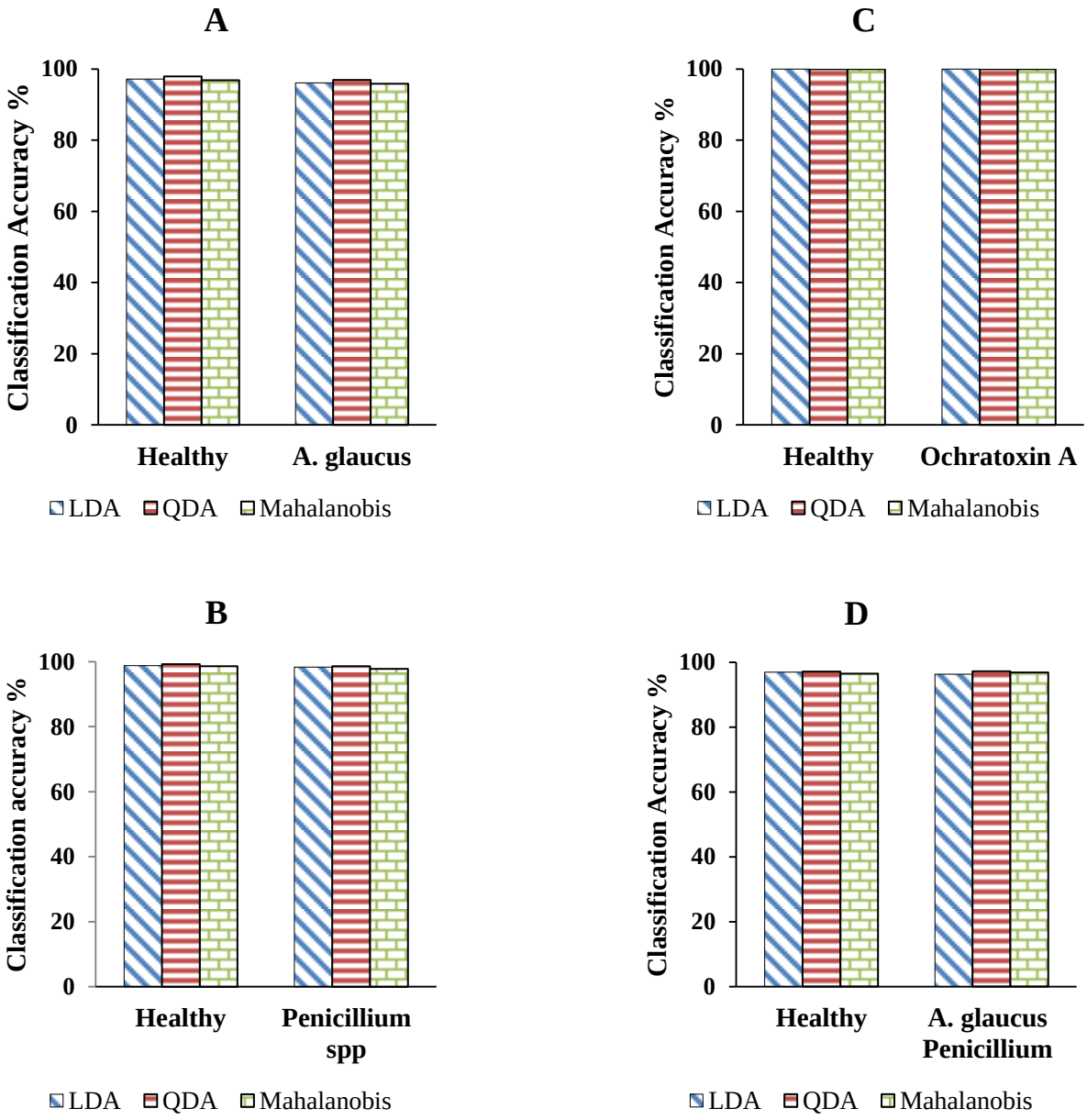

Fig. 5.6. Classification accuracy of two-class model: A- sterile and different periods of *A.glaucus* infected wheat kernels, B- sterile and different periods of *Penicillium* spp. infected wheat kernels, C- sterile and five levels of ochratoxin A contaminated wheat kernels, D- sterile and different periods of *A.glaucus,* and *Penicillium* spp. infected wheat kernels.

All the three discriminant classifiers differentiated sterile and combined samples of all five *Penicillium* spp. infection periods with classification accuracy between 98.6 and 99.1% for sterile samples and between 95.8 and 98.6% for combined samples of all five *Penicillium* spp. infected wheat kernels (Fig. 5.6B). The third two-class model differentiated sterile and combined samples of all five levels of ochratoxin A contaminated samples with a 100% classification accuracy for all three discriminant classifiers (Fig. 5.6C).

The fourth two-class classification model differentiated sterile and combined samples of all five periods of *A. glaucus,* and *Penicillium* spp. infected samples with a classification accuracy between 96.5 and 97.1% for sterile samples and between 96.3 and 97.2% for combined samples of all five periods of *A. glaucus,* and *Penicillium* spp. infected samples (Fig. 5.6D). The two-class quadratic discriminant classifier provided higher classification accuracy than the other two classifiers.

5.3.5 Six-class classification model

Three six-class models were developed, first six-class model was developed to discriminate between samples of all five *A.glaucus* infection periods and sterile sample, second six-class models was developed to discriminate between all five periods of *Penicillium* spp. infected wheat kernels and sterile sample and third six-class model was developed to discriminate between five levels of ochratoxin A contaminated wheat kernels and sterile sample. The classification accuracies obtained for the linear, quadratic and Mahalanobis discriminant six-class models are given in Table 5.9.

Table 5.9. Linear, quadratic and Mahalanobis classification accuracies (%) for six-class model between sterile and different infection periods (2, 4, 6, 8, and 10 weeks post inoculation) of *Aspergillus glaucus* (AG) infected wheat kernels using statistical and histogram features from 1280, 1300 and 1350 nm wavelengths. Sample size of sterile and each infection period were 300 kernels.

Statistical classifiers	Sample	Sterile	AG week 2	AG week 4	AG week 6	AG week 8	AG week 10
		Statistical classification accuracies (%)					
LDA							
	Sterile	94.0	3.9	2.1	0	0	0
	AG week 2	15.6	78.2	6.2	0	0	0
	AG week 4	0	8.7	91.3	0	0	0
	AG week 6	0	0	1.8	98.4	0	0
	AG week 8	0	0	0	0	100	0
	AG week 10	0	0	0	0	0	100
QDA							
	Sterile	95.1	3.7	1.2	0	0	0
	AG week 2	13.8	79.6	6.6	0	0	0
	AG week 4	0	6.1	93.9	0	0	0
	AG week 6	0	0	0.2	99.8	0	0
	AG week 8	0	0	0	0	100	0
	AG week 10	0	0	0	0	0	100
Mahalanobis							
	Sterile	93.4	3.9	2.7	0	0	0
	AG week 2	17.1	76.4	6.5	0	0	0
	AG week 4	1.2	10.4	88.4	0	0	0
	AG week 6	0	0	1.9	98.1	0	0
	AG week 8	0	0	0	0	100	0
	AG week 10	0	0	0	0	0	100

The six way classification of sterile samples resulted in 93.4 to 95.1 % accuracy of sterile sample with misclassifications of 3.7 to 3.9% into second week *A.glaucus* infected sample and 1.2 to 2.7 % into fourth week *A.glaucus* infected sample for all the three classifiers. This misclassification is due to the fact that during initial periods there were some uninfected wheat kernels inside the second and fourth week samples. The second week *A.glaucus* infected sample subjected to six way model classified 76.4 to 79.6 % of the sample correctly, and misclassified13.8 to 17.1% and 6.2 to 6.6% of *A.glaucus* infected 2 week sample as sterile sample and *A. glaucus* infected fourth week sample, respectively for all the three discriminant classifiers. The fourth week *A. glaucus* infected sample subjected to six-class model correctly classified 88.4 to 93.9% correctly and misclassified 6.1 to 10.4 % of fourth week *A. glaucus* infected sample as second week *A. glaucus* infected sample for all the three classifiers. Starting from sixth week of *A. glaucus* infected sample, the six class model correctly differentiated the remaining *A. glaucus* infected samples with a classification accuracy of more than 98%.

The three discriminant six-class models for all five periods of *Penicillium* spp. differentiated all the fungal infected samples and sterile samples with a classification accuracy of more than 95.9% for sterile sample and more than 97.4% for fungal infected sample for all the three discriminant classifiers (Table 5.10). The three discriminant six-class models differentiated sterile and five levels of ochratoxin A contaminated wheat kernels with a classification accuracy of 100% for sterile samples and more than 98.1% for all five levels of ochratoxin A contaminated wheat kernels (Table 5.11).

Table 5.10. Linear, quadratic, and Mahalanobis classification accuracies (%) for six-class model between sterile and different infection periods (2, 4, 6, 8, and 10 weeks post inoculation) of *Penicillium* spp. (PS) infected wheat kernels using statistical and histogram features from 1280, 1300 and 1350 nm wavelengths. Sample size of sterile and each infection period were 300 kernels.

Statistical classifiers	Sample	Sterile	PS week 2	PS week 4	PS week 6	PS week 8	PS week 10
		Statistical classification accuracies (%)					
LDA							
	Sterile	96.4	2.4	1.2	0	0	0
	PS week 2	0.9	98.2	0.9	0	0	0
	PS week 4	0	0	100	0	0	0
	PS week 6	0	0	0	100	0	0
	PS week 8	0	0	0	0	100	0
	PS week 10	0	0	0	0	0	100
QDA							
	Sterile	97.3	2.7	0	0	0	0
	PS week 2	0.5	98.9	0.6	0	0	0
	PS week 4	0	0	100	0	0	0
	PS week 6	0	0	0	100	0	0
	PS week 8	0	0	0	0	100	0
	PS week 10	0	0	0	0	0	100
Mahalanobis							
	Sterile	95.9	3.3	0.8	0	0	0
	PS week 2	0.8	97.4	1.8	0	0	0
	PS week 4	0	0	100	0	0	0
	PS week 6	0	0	0	100	0	0
	PS week 8	0	0	0	0	100	0
	PS week 10	0	0	0	0	0	100

Table 5.11. Linear, quadratic, and Mahalanobis classification accuracies (%) for six-class model between sterile and different concentration levels (72, 100, 382, 430, 600 ppb) of ochratoxin A (OTA) contaminated wheat kernels using statistical and histogram features from 1300, 1350, and 1480 nm wavelengths. Sample size of sterile and each contamination level were 300 kernels.

Statistical classifiers	Sample	Sterile	OTA Sample 1	OTA sample 2	OTA sample 3	OTA sample 4	OTA sample 5
		Statistical classification accuracies (%)					
LDA							
	Sterile	100.0	0.0	0.0	0	0	0
	OTA sample 1	0	98.1	1.9	0	0	0
	OTA sample 2	0	0.7	99.3	0	0	0
	OTA sample 3	0	0	0	100	0	0
	OTA sample 4	0	0	0	0	100	0
	OTA sample 5	0	0	0	0	0	100
QDA							
	Sterile	100	0	0	0	0	0
	OTA sample 1	0	98.5	1.5	0	0	0
	OTA sample 2	0	0.4	99.6	0	0	0
	OTA sample 3	0	0	0	100	0	0
	OTA sample 4	0	0	0	0	100	0
	OTA sample 5	0	0	0	0	0	100
Mahalanobis							
	Sterile	100	0	0	0	0	0
	OTA sample 1	0	98.3	1.7	0	0	0
	OTA sample 2	0	0.5	99.5	0	0	0
	OTA sample 3	0	0	0	100	0	0
	OTA sample 4	0	0	0	0	100	0
	OTA sample 5	0	0	0	0	0	100

5.4 Conclusions

A. glaucus and *Penicillium* spp. infected wheat samples can easily be differentiated from sterile wheat samples using near-infrared hyperspectral imaging system. NIR imaging system can also discriminate between different infection stages of *A. glaucus*, and *Penicillium* spp. infected wheat kernels. The results obtained from this study prove that near-infrared hyperspectral imaging system can be used effectively in identifying degree of fungal infection in wheat kernels at an early stage. Three significant wavelengths corresponding to *A. glaucus* and *Penicillium* spp. 1280, 1300 and 1350 nm were identified based on the highest factor loadings in the principal component analysis from the 61 wavelengths in the range between 1000 and 1600 nm. The quadratic discriminant classifiers provided better classification accuracies than the linear or Mahalanobis discriminant classifiers in all the pair-wise, two-class and six-class models tested between sterile and different periods of fungal infected wheat kernels. The ochratoxin A contaminated wheat kernels subjected to imaging and principal component analysis provided 1300, 1350, and 1480 nm as significant wavelengths. Ochratoxin A contaminated samples can be differentiated from sterile samples with a classification accuracy of more than 98 % at contamination levels as low as 72 ppb.

References

ASABE. 2012. Standard S352.2: Moisture Measurement Unground Grain and Seeds. ASABE, St. Joseph, Mich.

Bendele, A.M., W.W. Carlton, P. Krogh, and E.B. Lillehoj. 1985. ochratoxin A carcinogenesis in the (C57BL/6J X C3H) F1 mouse. *Journal of Natural Cancer Institute* 75: 733-742.

Boorman, G.A., M.R. McDonald, S. Imoto, and R. Persing. 1992. Renal lesions induced by ochratoxin A exposure in the F344 rat. *Toxicologic Pathology* 20: 236-245.

Castegnaro, M., U. Mohr, A. Pfohl-Leszkowicz, J. Esteve, J. Steinmann, T. Tillmann, J. Michelon, and H. Bartsch. 1998. Sex- and strain-specific induction of renal tumors by ochratoxin A in rats correlates with DNA adduction. *International Journal of Cancer* 77: 70-75.

Czaban, J., B. Wroblewska, A. Stochmal, and B. Janda. 2006. Growth of *Penicillium verrucosum* and production of ochratoxin A on nonsterilized wheat grain incubated at different temperatures and water activity. *Polish Journal of Microbiology* 55: 321-331.

Delwiche, S.R., and D.R. Massie. 1996. Classification of wheat by visible and near infrared reflectance from single kernels. *Cereal Chemistry* 73(3): 399-405.

FAOSTAT, 2013. Available at: http://faostat3.fao.org/download/Q/QC/E.

JECFA. 2007. Ochratoxin A, WHO Technical Report Series 947; IPCS, WHO: Geneva, Switzerland, 169-180.

Mahesh, S., D.S. Jayas, J. Paliwal and N.D.G. White. 2015. Hyperspectral imaging to classify

and monitor quality of agricultural materials. *Journal of Stored Products Research* 61: 17-26.

Murray, I., and P.C. Williams. 1987. Chemical principles of near-infrared technology. In Near-infrared Technology in the Agricultural and Food Industries, 17-34. St. Paul, MN: AACC.

Nithya, U., V. Chelladurai, D.S. Jayas, and N.D.G. White. 2011. Safe storage guidelines for durum wheat. *Journal of Stored Products Research* 47: 328-333.

NRC Canada, 2013. Factsheet - The Canadian Wheat Alliance. (accessed 20.09.2015).

O'Brien, E., and D.R. Dietrich. 2005. Ochratoxin A: The continuing enigma. *Critical Reviews in Toxicology* 35: 33–60.Senthilkumar T., C.B. Singh, D.S. Jayas, and N.D.G. White. 2012. Detection of fungal infection in wheat using near-infrared hyperspectral imaging. *Journal of Agricultural Engineering* 49(1): 21-27.

Senthilkumar**,** T., D.S. Jayas, and N.D.G. White. 2015. Detection of different periods of fungal infection in stored wheat using near-infrared hyperspectral imaging. *Journal of Stored Products Research* 63: 80-88.

Singh, C.B., D.S. Jayas, J. Paliwal, and N.D.G. White. 2007. Fungal detection in wheat using near-infrared hyperspectral imaging. *Transactions of the ASAE* 50: 2171-2176.

Solomon, M.E. 1951. Control of humidity with potassium hydroxide, sulphuric acid, or other solutions. *Bulletin of Entomologícal Research* 42: 543-554.

Statistics Canada, 2013. Table 001-0015 - Exports of grains, by final destination, monthly (tonnes), CANSIM (database). (accessed 20.09.2015).

Teena, M., A. Manickavasagan, A. Mothershaw, S. El Hadi, and D.S. Jayas. 2013. Potential of machine vision techniques for detecting fecal and microbial contamination of food products: a review. *Food and Bioprocess Technology* 6 (7): 1621-1634.

Teena, M.A., A. Manickavasagan, L. Ravikanth and D.S. Jayas. 2014. Near-infrered (NIR) hyperspectral imaging to classify fungal infected dates. *Journal of Stored Products Research* 59: 306-313.

Vadivambal, R., and D.S. Jayas. 2016. Bio-Imaging: Principles, Techniques and Applications. CRC Press, Taylor and Francis Group Ltd: Oxford, UK.

Wallace, H.A.H., and R.N. Sinha. 1962. Fungi associated with hot spots in farm stored grain. *Canadian Journal of Plant Science* 42: 130-141.

Wang, D., F.E. Dowell, and R.E. Lacey. 1999. Single wheat kernel colour classification using neural networks. *Transactions of the ASAE* 42: 233-240.

Wang, D., F.E. Dowell, M.S. Ram, and W.T. Schapaugh. 2003. Classification of fungal damaged soybean seeds using near infrared spectroscopy. *International Journal of Food Properties* 7: 75-82.

Wang, W., G.W. Heitschmidt, X. Ni, W.R. Windham, S. Hawkins, and X. Chu. 2014. Identification of aflatoxin B_1 on maize kernel surfaces using hyperspectral imaging. *Food Control* 42: 78-86.

Wang, W., X. Ni, K.C. Lawrence, S.C. Yoon, G.W. Heitschmidt, and P. Feldner. 2015a. Feasibility of detecting Aflatoxin B_1 in single maize kernels using hyperspectral imaging. *Journal of Food Engineering* 166: 182-192.

Wang, W., X. Ni, K.C. Lawrence, S.C. Yoon, G.W. Heitschmidt, and P. Feldner. 2015b. Near-infrared hyperspectral imaging for detecting Aflatoxin B_1 on maize kernels. *Food Control* 51: 347-355.

WHO. 2001. Ochratoxin A. Safety assessment of certain mycotoxins in food. WHO Food Additives Series No. 47. 281-415. Geneva: WHO.

Chapter 6

Detection of fungal infection and ochratoxin A contamination in stored barley using near-infrared hyperspectral imaging

Abstract

Aspergillus glaucus, and *Penicillium* spp. infections and ochratoxin A contamination were detected in stored barley using a Near-Infrared (NIR) hyperspectral imaging system. Fungal infected samples and ochratoxin A contaminated samples were subjected to single kernel imaging every two weeks, and acquired three-dimensional image data were transformed into two-dimensional data. The two-dimensional data corresponding to each fungal infected sample and ochratoxin A contaminated sample were subjected to principal component analysis (PCA) for data reduction, and to identify significant wavelengths. The significant wavelengths 1260, 1310, and 1360 nm corresponding to *A. glaucus, Penicillium* spp., and non-ochratoxin A producing *P. verrucosum* infected kernels and wavelengths 1310, 1360, and 1480 nm corresponding to ochratoxin A contaminated kernels obtained based on the highest principal components (PC) factor loadings. Statistical and histogram features from significant wavelengths were extracted and used as input for linear, quadratic, and Mahalanobis statistical classifiers. Pair-wise, two-class, and six-class classification models were developed to differentiate between sterile and infected kernels. The three classifiers differentiated sterile kernels with classification accuracy of more than 94%, fungal infected kernels with more than 80% at initial periods of fungal infection and attained 100% classification accuracy after four weeks of fungal infection. Ochratoxin A contaminated kernels can be differentiated from sterile kernels with a classification accuracy of 100%. Different periods of fungal infection and different levels of ochratoxin A contamination were discriminated with a classification accuracy of more than 82%.

6.1 Introduction

Canada is the fourth largest producer of barley grains (*Hordeum vulgare* L.) in the world with a total production of 10.2 million tonnes (Mt) in 2013 (FAOSTAT, 2013). There are three major barley grain classes based on its end use: feed, malting and food. More than 70% of the barley grown in Canada is used as animal feed, approximately 20% is used for malting and a small percentage of it is used for food, mainly to make instant baby formulas, pastas, and breakfast cereals (CMBTC, 2012; Anonymous, 2013). The Canadian food and feed barley brings CAD$800 million from cash receipts and another CAD$400 million from exports (Statistics Canada, 2013; Industry Canada, 2013). The malting barley alone contributes more than CAD $13.8 billion to the Canadian economy and generates 163,200 jobs in Canada (Palladini and Armstrong, 2013).

The barley chosen for malting should possess rigorous quality parameters like germination more than 95%, varietal purity, uniform kernel size, sterile, fully matured, bright, no heat damage, broken kernels below 5%, protein content between 10 and 13.5%, and moisture content below 13.5% (CMBTC, 2012). One of the major biological factors affecting the quality of barley is fungi. There are two types of fungi causing damage to barley grains, first are field fungi, which get eliminated by proper drying process before storage and the second are storage fungi occurring in the stored barley grains under unfavourable environmental conditions. Major species of molds causing damage to stored barley grains in Canada are primarily of *Aspergillus* and *Penicillium* genera. Fungal infection in stored barley grains reduces germination, imparts unacceptable odors, and has the potential to produce toxins in the grains. Barley grains lose their malting suitability within a few weeks of fungal infection. It is very important to protect the barley grains to prevent any quality deterioration before it gets processed for consumers.

Moisture content suitable for most fungal species to grow and multiply in barley grains is in the range between 14% and 20%, so the suitable moisture content to store barley is below 13.5%. The average moisture content inside the storage structures can be maintained below 13.5% moisture content, but some high moisture localized areas can occur inside the storage structure due to changes in external weather conditions and gradual moisture migration. The localized areas above 14% moisture content combined with higher temperature levels are conducive for fungal growth (CMBTC, 2012). Increase in fungal activity helps insects and mites to grow resulting in further quality deterioration in stored barley grains.

Aflatoxin discovery in 1960 in England turkey farms, killing nearly 100,000 turkey poults, compelled the scientific community to explore the secondary metabolites or mycotoxins produced by fungi (Sargeant, 1961), which led to the discovery of other major mycotoxins Deoxynivalenol, Zearalenone, Fumonisins and ochratoxin A. ochratoxin A, one of the most potent mycotoxins present in food and feed is being regulated in many countries by imposing maximum limits in food products. Ochratoxin A is primarily reported to be causing nephrotoxicity in many animals except ruminants (Krogh, 1992; Abrunhosa et al., 2010) and it is classified as a carcinogen (Group 2B) by the International Agency on Cancer Research because of its carcinogenicity in animals (IARC, 1993). The other problems caused by ochratoxin A are hepatotoxicity, teratogenicity, and immunotoxicity (JECFA, 2007; WHO, 2001). Ochratoxin A is produced by over 20 species in the genera *Penicillium* and *Aspergillus* (Cabañes et al., 2010), but in temperate regions like Canada ochratoxin A is predominantly produced by *Penicillium verrucosum* (Duarte et al., 2010). Small amounts of ochratoxin A is detected in Canadian wheat, barley, oats, and rye (Anonymous, 2013).

Any quality degradation in barley grains due to fungal infection will result in significant economic loss to the farmers and can cause potential health issues to the consumers because of mycotoxins. Detection of fungal infection and mycotoxin contamination at an early stage is very important to avoid further damage to the stored barley grains and to take necessary corrective actions. The traditional microscopic-culture method to detect fungal infections in barley or other grains is a time-consuming and laborious process. The chromatographic methods used to detect mycotoxin contamination in grains involve a tedious extraction procedure. A rapid method to detect fungal infection and ochratoxin A contamination is necessary to protect the stored barley grains. Near-Infrared (NIR) hyperspectral imaging technique is an emerging technology with a huge potential to detect various quality parameters in raw and processed food products.

NIR hyperspectral imaging system is a combination of both conventional imaging (spatial) and spectroscopy (spectral). NIR hyperspectral imaging is also called a chemical imaging system which can collect extrinsic spatial information like size and appearance as well as intrinsic spectral information like chemical constituents of a product. NIR hyperspectral imaging is a rapid, non-destructive, and a non-chemical method. Hyperspectral imaging was first used in remote sensing applications and later in agriculture, pharmaceuticals, and medical applications. Vadivambal and Jayas (2016) reported applications of NIR hyperspectral imaging in various sectors. The NIR hyperspectral imaging technique has not been utilized to its full potential in food safety applications like detection of microbiological organisms and their toxins in cereals, oilseeds and processed food products. The NIR hyperspectral imaging has been utilized to detect different quality parameters associated with cereals, oilseeds and pulses such as detection of different wheat classes (Mahesh et al., 2011), fungal infection in wheat (Singh et al., 2007; Senthilkumar et al., 2016), insect damage in wheat (Singh et al., 2009a), midge damage in

wheat (Singh et al., 2009b), fungal infection in canola (Senthilkumar et al., 2012; Senthilkumar et al., 2015), fungal infection in pulses (Karuppiah et al., 2016), insect infestation in mungbean (Kaliramest et al., 2013), and insect infestation in soybean (Chelladurai et al., 2014). NIR hyperspectral imaging has been used to detect barley kernel viability (McGoverin et al., 2011) and pregerminated barley (Arngren et al., 2011). The fungal infection and mycotoxin detection using NIR hyperspectral imaging in barley kernels has not been reported in the literature.

Therefore, the objectives of this study were:

1. To identify the significant wavelengths corresponding to the *Aspergillus glaucus*, *Penicillium* spp., and non-ochratoxin A producing *Penicillium verrucosum* infection in barley, and to find the classification accuracies between sterile and different periods of fungal infected barley samples,
2. To identify the significant wavelengths corresponding to the ochratoxin A contamination in barley grains and to find the classification accuracies between sterile and different concentrations of ochratoxin A contaminated barley samples, and
3. To find the classification accuracies between different concentration levels of ochratoxin A contaminated barley kernels and different periods of non-ochratoxin A producing *Penicillium verrucosum* infected barley kernels.

6.2 Materials and Methods

6.2.1 Grain sample preparation

One hundred and one kilograms of mixed variety of barley grains with initial moisture content of 13.7% (wet basis) of 2013 crop year were obtained from Agriculture and Agri-Food Canada for the fungal and ochratoxin A detection study. The total 101 kg of barley grains were divided as 50 kg of barley grains for the fungal detection study, 50 kg of barley grains for the ochratoxin A detection study and 1 kg utilized as a sterile control sample. The barley grains were conditioned to 17% moisture content (wet basis) for the fungal detection study and 21.5% moisture content (wet basis) for the ochratoxin A detection study by adding specific amounts of distilled water. The samples conditioned to 17 and 21.5% moisture content were surface sterilized by washing with 1% sodium hypochlorite solution for several minutes and were autoclaved at 120ºC for 20 min to remove any pre-existing contaminants in the barley grains.

Ten kilograms of barley grains out of the 50 kg of conditioned barley for the fungal detection study were divided equally into two main samples of 5 kg each (sample 1 and sample 2). The remaining 40 kg were utilized as buffer samples. The sample 1 was artificially infected with *Aspergillus glaucus* and sample 2 with *Penicillium* spp. cultures obtained from Grain Research Laboratory, Canadian Grain Commission, Winnipeg, MB and the two samples were placed in two different environmental chambers maintained at 30ºC ±2 ºC and 70±4% relative humidity to avoid any cross-contamination. Sample 1 and sample 2 were divided into 5 sub-samples each weighing 1 kg. Each of the 5 sub-samples infected by *A. glaucus* and 5 subamples infected by *Penicillium* spp. were placed between two buffer samples, one on the top and one at the bottom each weighing 2 kg. The sub-sample along with buffer samples were placed in 20 L

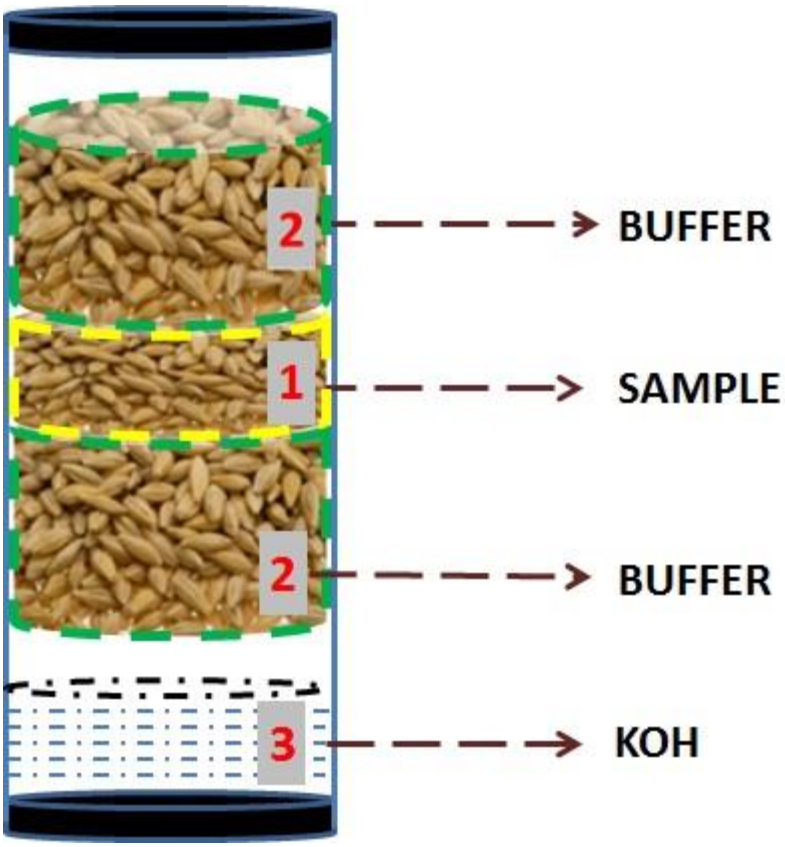

Fig. 6.1. Illustration of barley sample placement between the buffer samples and KOH solution inside the 20 L pails.

plastic pails with KOH solution to maintain the sub-samples at 17% moisture content throughout the study (Fig. 6.1).

Ten kilograms of barley grains out of the 50 kg of conditioned and sterilized barley grains for the ochratoxin A detection study were divided equally into two main samples of 5 kg each (sample 3 and sample 4). The remaining 40 kilograms were utilized as buffer samples. Sample 1 was artificially infected with ochratoxin A producing *P. verrucosum* (strain number: C618-1) and sample 2 with non-ochratoxin A producing *P. verrucosum* (strain number: C27-1) cultures obtained from Grain Research Laboratory, Canadian Grain Commission, Winnipeg, MB and the two samples were placed in two different environmental chambers maintained at 20ºC ±2 ºC and 70±4% relative humidity to avoid any cross-contamination. Sample 3 and sample 4 were divided into 5 sub-samples each weighing 1 kg. Each of the 5 sub-samples infected with ochratoxin A producing *P. verrucosum* (strain number: C618-1) and 5 sub-samples infected with non- ochratoxin A producing *P. verrucosum* (strain number: C27-1) were placed between two buffer samples, one on the top and one at the bottom each weighing 2 kg each. The sub-sample along with buffer samples were placed in 20 L plastic pails with KOH solution to maintain the sub-samples at 21.5% moisture content throughout the study. The 1 kg barley grains utilized as sterile control samples were conditioned to 17% moisture content and autoclaved at 120ºC for 20 min. The non-ochratoxin A producing *P.verrucosum* infected samples were used in this study to validate and identify the significant wavelengths particularly corresponding to ochratoxin A contamination. The sterile, *A.glaucus* infected, *Penicillium* spp infected, and Ochratoxin A contaminated samples are shown in Fig. 6.2.

Fig. 6.2. Sterile (A), *Aspergillus glaucus* (B) (after 4 weeks post inoculation) infected, *Penicillium* spp (C) (after 4 weeks post inoculation) infected and Ochratoxin A (D) (after 20 weeks post inoculation of *P. verrucosum* infected) contaminated barley kernels.

6.2.2 NIR hyperspectral imaging system and image acquisition.

NIR hyperspectral imaging system was made up of a NIR camera with Indium Gallium Arsenide (InGaAs) detector (Model No. SU640-1.7RT-D, Sensors Unlimited Inc., Princeton, NJ, USA), Liquid Crystal Tunable Filters (LCTFs) to tune on to desired wavelengths from 1000 to 1600 nm (VariSpec, Cambridge Research and Instrumentation Inc., Woburn, MA, USA), tungsten halogen lamps (used as a illumination source emitted light in the wavelength range between 400 and 2500 nm), a data processing system to capture images (LabVIEW program, version 7.1, National Instruments Corp., Austin, TX, USA) and to analyze the captured images (MATLAB, The Mathworks, Inc., Natick, MA, USA) (Fig. 6.3).

Three-hundred individual barley kernels (17% mc) from each of the two fungal infected (*A. glaucus* sub-sample 1 and *Penicillium* spp. sub-sample 1) sub-samples were randomly selected and subjected to image acquisition after 2 weeks of fungal infection and remaining sub-samples after 4, 6, 8, and 10 weeks of fungal infection, respectively. The number of barley kernels subjected to imaging for fungal detection study were 3000 (10 sub-samples×300). The barley sub- samples prepared for the ochratoxin A study (21.5% mc) were subjected to imaging after 18, 20, 22, 24, and 26 weeks. Three hundred kernels from each of the OTA producing *P. verrucosum* and non-OTA producing *P. verrucosum* infected sub-samples were randomly selected and subjected to single kernel imaging. The individual barley kernels subjected to imaging for OTA study were 3000 (10 sub-samples × 300). Three hundred barley kernels from sterile samples (17% mc) were subjected to image acquisition and used to compare both fungal infected and OTA contamination samples. We took utmost attention by wiping the black surface

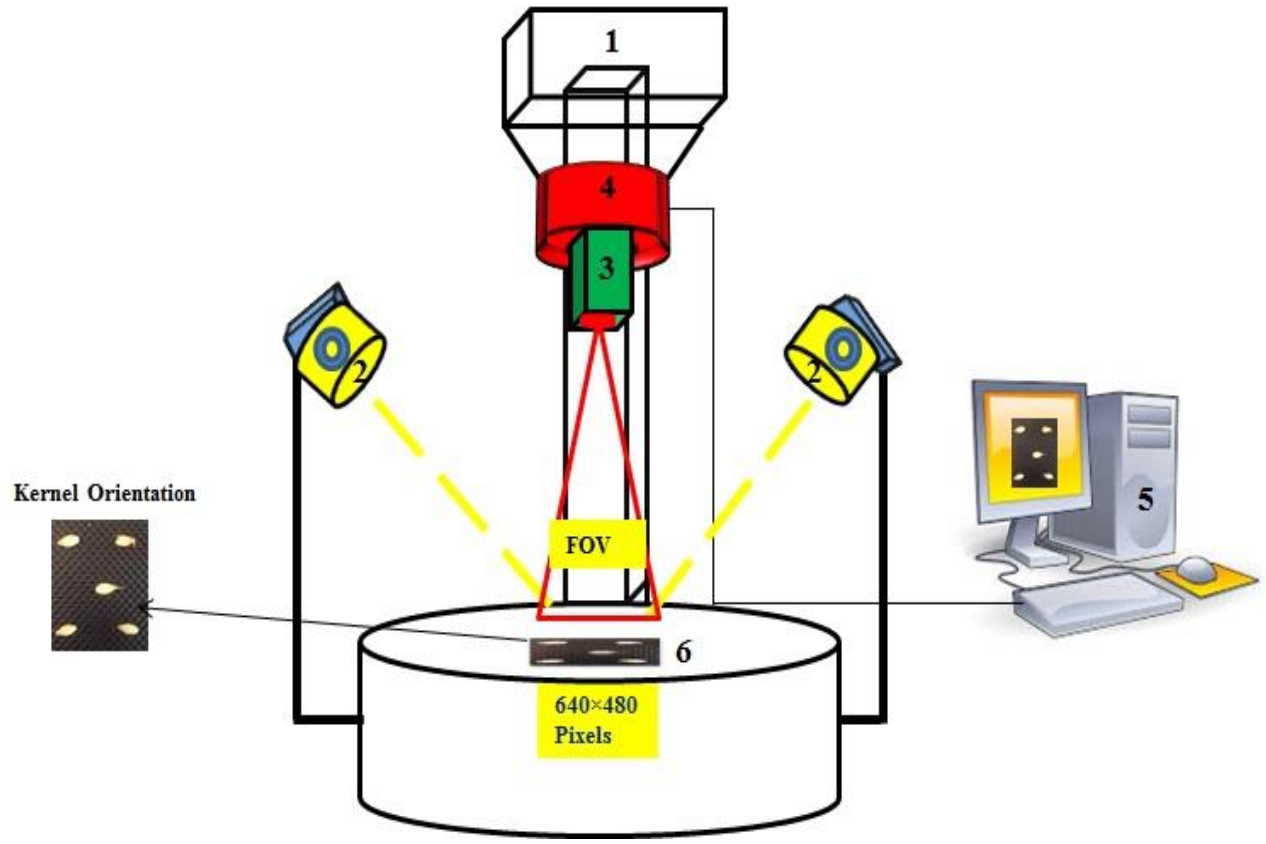

Fig. 6.3. Schematic representation of NIR hyperspectral imaging system 1. Camera Stand, 2. Tungsten- Halogen Lamps, 3. LCTF Filters, 4. NIR Camera, 5. Data Acquisition and Processing System, 6. Barley Sample.

with ethanol, used for imaging after every imaging session to avoid any cross-contamination. The single kernel imaging were done by placing five barley kernels in a non-touching manner on a black board and images were acquired using NIR imaging system in the wavelength range between 1000 and 1600 nm at 61 evenly distributed wavelengths at 10 nm interval.

6.2.3 Data analysis

The acquired image data were in the 3D hypercube form (two spatial and one wavelength). The three-dimensional intensity data were transformed into image format and then to binary image to get the desired two-dimensional reflectance data. Principal Component Analysis (PCA) was applied to the reflectance data to select the most significant wavelengths. Six statistical features (mean, median, standard deviation, variance, maximum, and minimum) and 10 histogram features corresponding to significant wavelengths were extracted and used in classification using linear, quadratic and Mahalanobis discriminant statistical classifiers. Pair-wise, two-class and six-class models were developed using PROC DISCRIM (Statistical Analysis Software (SAS), Version 9.1.3, SAS Institute Inc., Cary, NC) procedure to discriminate between different samples. All the models used 80% of barley kernels as training set and 20% of barley kernels as testing set in quintuplicates (five different training and testing sets) from the 300 kernels of each sub-samples in fungal detection and OTA detection studies.

6.2.4 Moisture content, germination and ochratoxin A quantification

Moisture content of barley kernels was determined every 2 weeks by oven drying 10 g of barley kernels in triplicates for 20 h at 130±1ºC (ASABE, 2012). Germination was determined by placing triplicates of 25 barley kernels on Whatman No 3 filter paper soaked in 5.5 mL of distilled water in a 9 cm diameter Petri dish (Wallace and Sinha, 1962). The barley kernels were

incubated for 7 d at room temperature (22±2 ºC). Ochratoxin A concentrations in barley kernels were tested at Central Testing Laboratory, Winnipeg, Manitoba by using an ELISA method.

6.3 Results and Discussion

6.3.1 Moisture content, germination, and ochratoxin A concentrations

Moisture content of fungal infected barley samples at the start of the study was 17.0 ± 0.3% and at the end of 10 weeks the moisture content was 17.0 ± 0.8%. The moisture content of the samples remained the same after 10 weeks because of the presence of buffer samples and KOH solution. A study on detection of fungal infection on Canadian Western Red Spring (CWRS) wheat using NIR hyperspectral imaging followed the same method of placing the samples between buffer samples and achieved constant moisture content up to 10 weeks of storage (Senthilkumar et al., 2016). The germination at the start of the study was 91.5±0.5% and the germination reached 0% at the end of 4 weeks for all the fungal-infected samples. Ochratoxin A concentrations were 140, 251, 536, 620, and 814 ppb in *P. verrucosum* (ochratoxin A producing strain, 21.5% moisture content) infected barley kernels after 18, 20, 22, 24, and 26 weeks post inoculation, respectively.

6.3.2 Significant wavelengths

The first principal component loadings provided three significant wavelengths 1260, 1310, and 1360 nm based on the highest principal component factor loadings corresponding to *A. glaucus*, *Penicillium* spp., and non-ochratoxin A producing *P. verrucosum* infected samples (Fig. 6.4, 6.5, and 6.6).

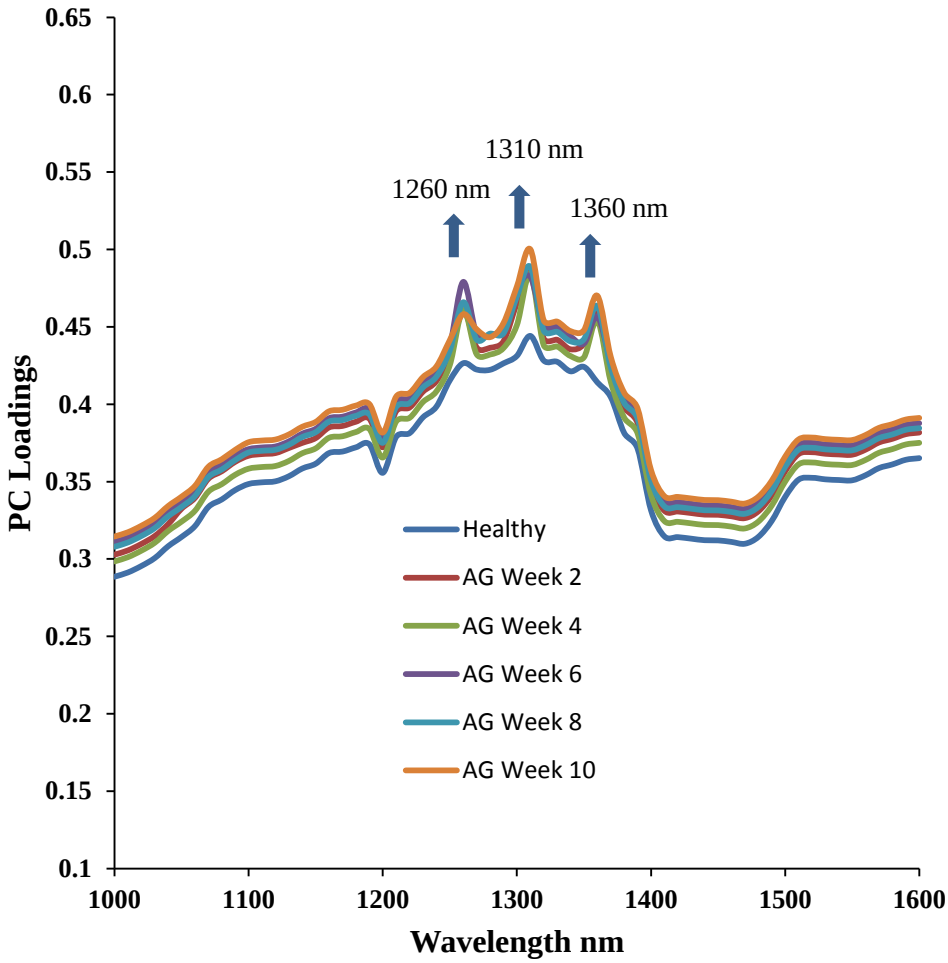

Fig. 6.4. First principal component (PC) loadings of sterile and different infection periods of *Aspergillus glaucus* infected barley kernels (AG 2 to AG 10).

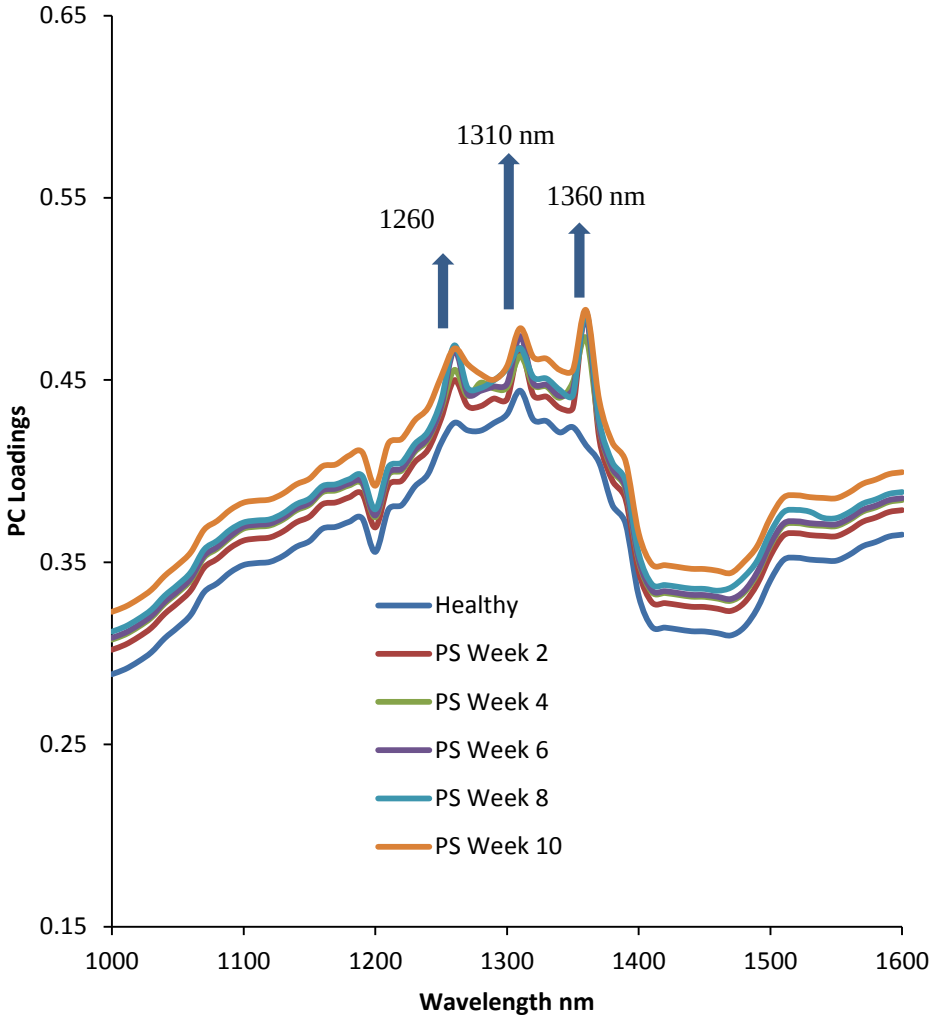

Fig. 6.5. First principal component (PC) loadings of sterile and different infection periods of *Penicillium* spp. infected barley kernels (PS 2 to PS 10).

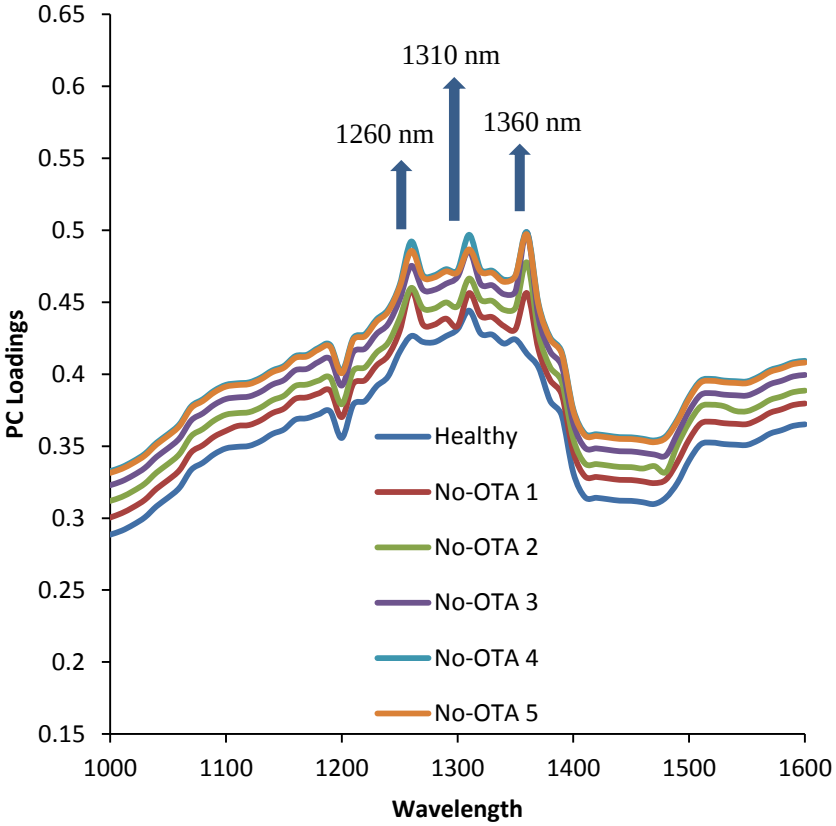

Fig. 6.6. First principal component (PC) loadings of sterile and different infection periods of Non-ochratoxin A producing *Penicillium verrucosum* infected barley kernels (No-OTA 1 to No-OTA 5).

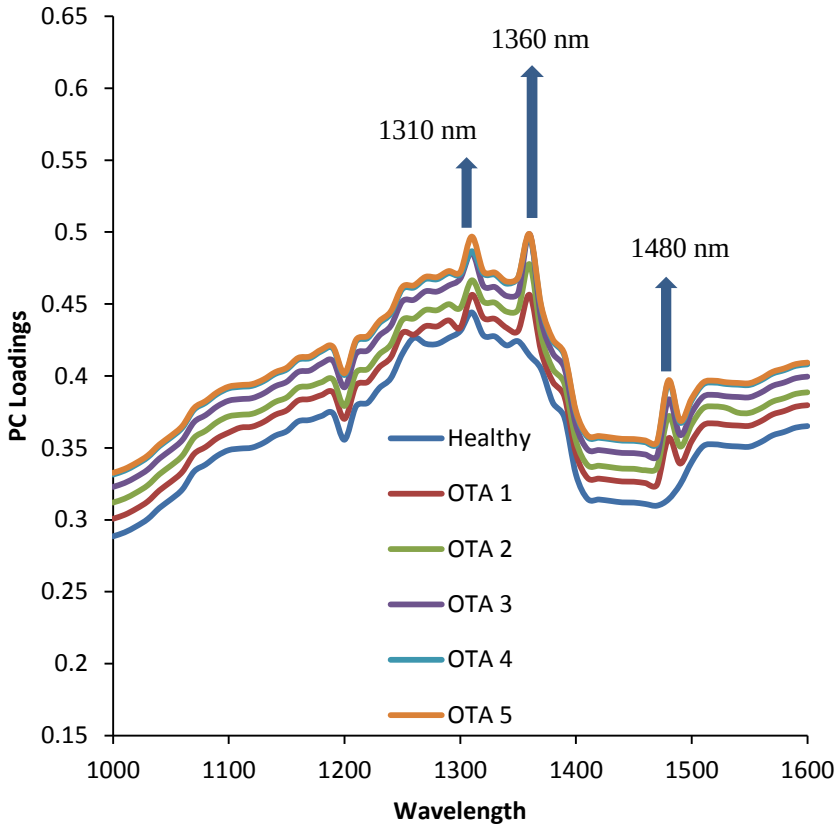

Fig. 6.7. First principal component (PC) loadings of sterile and five concentration levels of ochratoxin A contaminated barley kernels (OTA 1 to OTA 5).

The first principal component loadings corresponding to ochratoxin A contaminated samples provided 1310, 1360 and 1480 nm as significant wavelengths based on the highest principal component factor loadings (Fig. 6.7). The wavelength 1310 nm can be associated with fungal infection in barley kernels (Singh et al., 2007; Senthilkumar et al., 2012; 2015; 2016)

The wavelengths 1260 and 1360 nm are associated with carbohydrate content in barley kernels (Delwiche and Massie, 1996) and wavelength 1480 nm is associated with protein content in barley kernels (Wang et al., 1999; Murray and Williams, 1987). The significant wavelength 1480 nm was found only in the ochratoxin A contaminated samples and not in non-ochratoxin A producing *P. verrucosum* infected samples. NIR hyperspectral imaging system used to detect ochratoxin A contamination in wheat samples also reported the unique significant 1480 nm wavelength (Senthilkumar et al., 2016).

6.3.3 Pair-wise classification models

Ten pair-wise models were developed, the first pair-wise model to differentiate between sterile and different periods of *A.glaucus* infected samples, the second between sterile and *Penicillium* spp, the third between sterile and different levels of ochratoxin A contaminated samples, the fourth between sterile and different infection periods of non-ochratoxin A producing *P. verrucosum* infected samples, the fifth between different infection periods of *A. glaucus* infected samples, the sixth between different infection periods of *Penicillium* spp. infected samples, the seventh between different levels of ochratoxin A contaminated samples, the eighth between different infection periods of non-ochratoxin A producing *P. verrucosum* infected samples, the ninth between different infection periods of *A. glaucus* and *Penicillium* spp. infected samples, and the tenth between different levels of ochratoxin A contaminated

samples and different infection periods of non-ochratoxin A producing *P. verrucosum* infected samples.

Classification accuracies for the first pair-wise model are given in Table 6.1. The first pair-wise model classified sterile kernels with a classification accuracy in the range from 94.7±0.6 to 100±0.0%, and different infection levels of *A. glaucus* infected kernels in the range from 83.3±0.8 to 100±0.0%. The classification accuracy between sterile and different infection levels of *A. glaucus* infected kernels increased with increase in fungal infection levels. The second pair-wise model classified sterile kernels with a classification accuracy in the range from 96.5±0.8 to 100±0.0% and different infection levels of *Penicillium* spp. infected kernels in the range from 98.1±0.9 to 100±0.0% (Table 6.2). The third and fourth pair-wise models classified sterile kernels, different levels of ochratoxin A contaminated kernels, different infection periods of non-ochratoxin A producing *P. verrucosum* infected kernels with a classification accuracy of 100±0.0%.

The fifth pair-wise model classified different infection periods of *A. glaucus* infected kernels with a classification accuracy in the range from 92.6±0.9 to 100±0.0% (Table 6.3). The sixth pair-wise model classified different infection periods of *Penicillium* spp. infected kernels with a classification accuracies in the range from 98.4±0.7 to 100±0.0% (Table 6.4). The seventh pair-wise model classified different levels of ochratoxin A contaminated kernels with classification accuracy in the range from 98.2±0.7 to 100±0.0% (Table 6.5). The eighth pair-wise model classified different infection periods of non-ochratoxin A producing *P. verrucosum* infected kernels with classification accuracy in the range from 98.8±0.7 to 100±0.0% (Table 6.6).

Table 6.1. Classification accuracies (mean ± standard deviation, %) for pair-wise model between sterile and five infection periods (2, 4, 6, 8, and 10 weeks post inoculation,17% moisture content) of *Aspergillus glaucus* (AG) infected barley kernels using statistical and histogram features extracted from 1260, 1310, and 1360 nm wavelengths. Sample size of sterile and each infection period were 300 kernels.

Pair-wise model	Sample	Classification accuracies		
		Linear	**Quadratic**	**Mahalanobis**
Sterile vs AG week 2	Sterile	95.1±0.4	96.4±0.3	94.7±0.6
	AG week 2	83.8±0.3	84.3±0.2	83.3±0.8
Sterile vs AG week 4	Sterile	98.3±0.6	99.1±0.8	98.1±0.7
	AG week 4	95.9±0.3	97.1±0.5	95.2±0.4
Sterile vs AG week 6	Sterile	100±0.0	100±0.0	100±0.0
	AG week 6	100±0.0	100±0.0	100±0.0
Sterile vs AG week 8	Sterile	100±0.0	100±0.0	100±0.0
	AG week 8	100±0.0	100±0.0	100±0.0
Sterile vs AG week 10	Sterile	100±0.0	100±0.0	100±0.0
	AG week 10	100±0.0	100±0.0	100±0.0

Table 6.2. Classification accuracies (mean ± standard deviation, %) for pair-wise model between sterile and five infection periods (2, 4, 6, 8, and 10 weeks post inoculation, 17% moisture content) of *Penicillium* spp.(PS) infected barley kernels using statistical and histogram features extracted from 1260, 1310, and 1360 nm wavelengths. Sample size of sterile and each infection period were 300 kernels.

Pair-wise model	Sample	Classification accuracies		
		Linear	**Quadratic**	**Mahalanobis**
Sterile vs PS week 2	Sterile	97.6±0.3	98.3±0.1	96.5±0.8
	PS week 2	98.8±0.8	99.4±0.4	98.1±0.9
Sterile vs PS week 4	Sterile	100±0.0	100±0.0	100±0.0
	PS week 4	100±0.0	100±0.0	100±0.0
Sterile vs PS week 6	Sterile	100±0.0	100±0.0	100±0.0
	PS week 6	100±0.0	100±0.0	100±0.0
Sterile vs PS week 8	Sterile	100±0.0	100±0.0	100±0.0
	PS week 8	100±0.0	100±0.0	100±0.0
Sterile vs PS week 10	Sterile	100±0.0	100±0.0	100±0.0
	PS week 10	100±0.0	100±0.0	100±0.0

Table 6.3. Classification accuracies (mean ± standard deviation, %) for pair-wise model between five infection periods (2, 4, 6, 8, and 10 weeks post inoculation, 17% moisture content) of *Aspergillus glaucus* (AG) infected barley kernels using statistical and histogram features extracted from 1260, 1310, and 1360 nm wavelengths. Sample size of each infection period was 300 kernels.

Pair-wise model	Sample	Classification accuracies		
		Linear	**Quadratic**	**Mahalanobis**
AG week 2 vs AG week 4	AG week 2	93.2±0.6	95.2±0.4	92.6±0.9
	AG week 4	97.1±0.8	98.4±0.5	94.5±0.4
AG week 2 vs AG week 6	AG week 2	100±0.0	100±0.0	100±0.0
	AG week 6	100±0.0	100±0.0	100±0.0
AG week 2 vs AG week 8	AG week 2	100±0.0	100±0.0	100±0.0
	AG week 8	100±0.0	100±0.0	100±0.0
AG week 2 vs AG week 10	AG week 2	100±0.0	100±0.0	100±0.0
	AG week 10	100±0.0	100±0.0	100±0.0
AG week 4 vs AG week 6	AG week 4	98.4±0.4	99.1±0.7	98.1±0.3
	AG week 6	99.1±0.5	99.4±0.3	98.7±0.8
AG week 4 vs AG week 8	AG week 4	100±0.0	100±0.0	100±0.0
	AG week 8	100±0.0	100±0.0	100±0.0
AG week 4 vs AG week 10	AG week 4	100±0.0	100±0.0	100±0.0
	AG week 10	100±0.0	100±0.0	100±0.0
AG week 6 vs AG week 8	AG week 6	100±0.0	100±0.0	100±0.0
	AG week 8	100±0.0	100±0.0	100±0.0
AG week 6 vs AG week 10	AG week 6	100±0.0	100±0.0	100±0.0
	AG week 10	100±0.0	100±0.0	100±0.0
AG week 8 vs AG week 10	AG week 8	100±0.0	100±0.0	100±0.0
	AG week 10	100±0.0	100±0.0	100±0.0

Table 6.4. Classification accuracies (mean ± standard deviation, %) for pair-wise model between five infection periods (2, 4, 6, 8, and 10 weeks post inoculation, 17% moisture content) of *Penicillium* spp.(PS) infected barley kernels using statistical and histogram features extracted from 1260, 1310, and 1360 nm wavelengths. Sample size of each infection period was 300 kernels.

Pair-wise model	Sample	Classification accuracies		
		Linear	**Quadratic**	**Mahalanobis**
PS week 2 vs PS week 4	PS week 2	99.1±0.9	99.7±1.0	98.6±0.5
	PS week 4	98.9±0.4	99.5±0.8	98.4±0.7
PS week 2 vs PS week 6	PS week 2	100±0.0	100±0.0	100±0.0
	PS week 6	100±0.0	100±0.0	100±0.0
PS week 2 vs PS week 8	PS week 2	100±0.0	100±0.0	100±0.0
	PS week 8	100±0.0	100±0.0	100±0.0
PS week 2 vs PS week 10	PS week 2	100±0.0	100±0.0	100±0.0
	PS week 10	100±0.0	100±0.0	100±0.0
PS week 4 vs PS week 6	PS week 4	100±0.0	100±0.0	100±0.0
	PS week 6	100±0.0	100±0.0	100±0.0
PS week 4 vs PS week 8	PS week 4	100±0.0	100±0.0	100±0.0
	PS week 8	100±0.0	100±0.0	100±0.0
PS week 4 vs PS week 10	PS week 4	100±0.0	100±0.0	100±0.0
	PS week 10	100±0.0	100±0.0	100±0.0
PS week 6 vs PS week 8	PS week 6	100±0.0	100±0.0	100±0.0
	PS week 8	100±0.0	100±0.0	100±0.0
PS week 6 vs PS week 10	PS week 6	100±0.0	100±0.0	100±0.0
	PS week 10	100±0.0	100±0.0	100±0.0
PS week 8 vs PS week 10	PS week 8	100±0.0	100±0.0	100±0.0
	PS week 10	100±0.0	100±0.0	100±0.0

Table 6.5. Classification accuracies (mean ± standard deviation, %) for pair-wise model between five concentration levels (140, 251, 536, 620, 814 ppb) of ochratoxin A contaminated barley kernels (OTA) using statistical and histogram features from 1310, 1360, and 1480 nm wavelengths. Sample size of each concentration level was 300 kernels.

Pair-wise model	Sample	Classification accuracies		
		Linear	**Quadratic**	**Mahalanobis**
OTA 1 vs OTA 2	OTA 1	99.1±0.3	99.5±0.6	98.7±0.8
	OTA 2	98.6±0.8	99.1±0.9	98.2±0.7
OTA 1 vs OTA 3	OTA 1	100±0.0	100±0.0	100±0.0
	OTA 3	100±0.0	100±0.0	100±0.0
OTA 1 vs OTA 4	OTA 1	100±0.0	100±0.0	100±0.0
	OTA 4	100±0.0	100±0.0	100±0.0
OTA 1 vs OTA 5	OTA 1	100±0.0	100±0.0	100±0.0
	OTA 5	100±0.0	100±0.0	100±0.0
OTA 2 vs OTA 3	OTA 2	100±0.0	100±0.0	100±0.0
	OTA 3	100±0.0	100±0.0	100±0.0
OTA 2 vs OTA 4	OTA 2	100±0.0	100±0.0	100±0.0
	OTA 4	100±0.0	100±0.0	100±0.0
OTA 2 vs OTA 5	OTA 2	100±0.0	100±0.0	100±0.0
	OTA 5	100±0.0	100±0.0	100±0.0
OTA 3 vs OTA 4	OTA 3	100±0.0	100±0.0	100±0.0
	OTA 4	100±0.0	100±0.0	100±0.0
OTA 3 vs OTA 5	OTA 3	100±0.0	100±0.0	100±0.0
	OTA 5	100±0.0	100±0.0	100±0.0
OTA 4 vs OTA 5	OTA 4	100±0.0	100±0.0	100±0.0
	OTA 5	100±0.0	100±0.0	100±0.0

Table 6.6. Classification accuracies (mean ± standard deviation, %) for pair-wise model between five infection levels (18, 20, 22, 24, and 26 weeks post inoculation, 21.5% moisture content) of non-ochratoxin A producing *Penicillium verrucosum* infected barley kernels (No-OTA) using statistical and histogram features extracted from 1260, 1310, and 1360 nm wavelengths. Sample size of each infection period was 300 kernels.

Pair-wise model	Sample	Classification accuracies		
		Linear	**Quadratic**	**Mahalanobis**
No-OTA 1 vs No-OTA 2	No-OTA 1	99.3±0.6	99.7±0.8	98.9±0.8
	No-OTA 2	99.1±0.9	99.2±0.7	98.8±0.7
No-OTA 1 vs No-OTA 3	No-OTA 1	100±0.0	100±0.0	100±0.0
	No-OTA 3	100±0.0	100±0.0	100±0.0
No-OTA 1 vs No-OTA 4	No-OTA 1	100±0.0	100±0.0	100±0.0
	No-OTA 4	100±0.0	100±0.0	100±0.0
No-OTA 1 vs No-OTA 5	No-OTA 1	100±0.0	100±0.0	100±0.0
	No-OTA 5	100±0.0	100±0.0	100±0.0
No-OTA 2 vs No-OTA 3	No-OTA 2	100±0.0	100±0.0	100±0.0
	No-OTA 3	100±0.0	100±0.0	100±0.0
No-OTA 2 vs No-OTA 4	No-OTA 2	100±0.0	100±0.0	100±0.0
	No-OTA 4	100±0.0	100±0.0	100±0.0
No-OTA 2 vs No-OTA 5	No-OTA 2	100±0.0	100±0.0	100±0.0
	No-OTA 5	100±0.0	100±0.0	100±0.0
No-OTA 3 vs No-OTA 4	No-OTA 3	100±0.0	100±0.0	100±0.0
	No-OTA 4	100±0.0	100±0.0	100±0.0
No-OTA 3 vs No-OTA 5	No-OTA 3	100±0.0	100±0.0	100±0.0
	No-OTA 5	100±0.0	100±0.0	100±0.0
No-OTA 4 vs No-OTA 5	No-OTA 4	100±0.0	100±0.0	100±0.0
	No-OTA 5	100±0.0	100±0.0	100±0.0

Table 6.7. Classification accuracies (mean ± standard deviation, %) for pair-wise model between five infection periods (2, 4, 6, 8, and 10 weeks post inoculation, 17% moisture content) of *Aspergillus glaucus*(AG*)*, and *Penicillium* spp.(PS) infected barley kernels using statistical and histogram features extracted from 1260, 1310, and 1360 nm wavelengths. Sample size of each infection period was 300 kernels.

Pair-wise model	Sample	Classification accuracies		
		Linear	**Quadratic**	**Mahalanobis**
AG week 2 vs PS week 2	AG week 2	83.4±0.9	86.2±0.5	82.3±1.2
	PS week 2	84.9±0.4	87.1±0.6	84.5±0.7
AG week 4 vs PS week 4	AG week 4	92.1±0.7	94.4±0.8	91.6±0.9
	PS week 4	94.6±0.4	97.9±0.6	93.4±0.4
AG week 6 vs PS week 6	AG week 6	100±0.0	100±0.0	100±0.0
	PS week 6	100±0.0	100±0.0	100±0.0
AG week 8 vs PS week 8	AG week 8	100±0.0	100±0.0	100±0.0
	PS week 8	100±0.0	100±0.0	100±0.0
AG week 10 vs PS week 10	AG week 10	100±0.0	100±0.0	100±0.0
	PS week 10	100±0.0	100±0.0	100±0.0

Table 6.8. Classification accuracies (mean ± standard deviation, %) for pair-wise model between five contamination levels (140, 251, 536, 620, 814 ppb) of ochratoxin A contaminated kernels (OTA), and five infection periods (18, 20, 22, 24, and 26 weeks post inoculation, 21.5% moisture content) of non-ochratoxin A producing *Penicillium verrucosum* infected barley kernels (No-OTA) using statistical and histogram features extracted from 1260, 1310, 1360, and 1480 nm wavelengths. Sample size of each infection period and each concentration level were 300 kernels.

Pair-wise model	Sample	Classification accuracies		
		Linear	**Quadratic**	**Mahalanobis**
OTA 1 vs No-OTA 1	OTA 1	99.2±0.2	99.5±0.3	99.0±0.4
	No-OTA 1	99.6±0.5	99.8±0.4	99.3±0.2
OTA 2 vs No-OTA 2	OTA 2	100±0.0	100±0.0	100±0.0
	No-OTA 2	100±0.0	100±0.0	100±0.0
OTA 3 vs No-OTA 3	OTA 3	100±0.0	100±0.0	100±0.0
	No-OTA 3	100±0.0	100±0.0	100±0.0
OTA 4 vs No-OTA 4	OTA 4	100±0.0	100±0.0	100±0.0
	No-OTA 4	100±0.0	100±0.0	100±0.0
OTA 5 vs No-OTA 5	OTA 5	100±0.0	100±0.0	100±0.0
	No-OTA 5	100±0.0	100±0.0	100±0.0

The ninth pair-wise model classified different infection periods of *A. glaucus*, and *Penicillium* spp. infected barley kernels with classification accuracies in the range from 82.3±1.2 to 100±0.0% (Table 6.7). The tenth pair-wise model classified between different contamination levels of ochratoxin A contaminated kernels, and no-ochratoxin A producing *P. verrucosum* infected barley kernels with classification accuracies in the range from 99.0±0.4 to 100±0.0% (Table 6.8).

The classification accuracy between sterile and different infection periods of fungal infected barley kernels increased with increase in fungal infection periods. The *Penicillium* spp. infected barley kernels; ochratoxin A contaminated barley kernels, and non-ochratoxin A producing *P. verrucosum* infected kernels can be easily separated from sterile kernels at an early stage than *A. glaucus* infected kernels due to difference in mycelial growth on the barley kernels (Senthilkumar et al., 2016). Different periods of fungal infected kernels and different concentration levels of ochratoxin A contaminated kernels can be easily differentiated due to difference in fungal infection levels, and ochratoxin A concentration levels. The same pattern of differentiation between different infection periods were observed in fungal infected dates, canola, and wheat (Teena et al., 2014; Senthilkumar at al., 2012; 2015; 2016). There was a trend for classification accuracies of quadratic statistical classifiers to be higher than the linear and Mahalanobis statistical classifiers for all the pair-wise models (Singh et al., 2007; Senthilkumar et al., 2016).

6.3.4 Two-class classification models

Six two-class models were developed, the first to discriminate between sterile and combined samples of all five infection periods of *A. glaucus* infected barley kernels, the second between sterile and combined samples of all five infection periods of *Penicillium* spp. infected

barley kernels, the third between sterile and combined samples of all five concentration levels of ochratoxin A contaminated barley kernels, the fourth between sterile and combined samples of all five infection periods of *n*on-ochratoxin A producing *P. verrucosum* infected barley kernels, the fifth between sterile and combined samples of all five infection periods of *A. glaucus* and *Penicillium* spp. infected barley kernels, and the sixth between sterile and combined samples of all five concentration levels of ochratoxin A contaminated barley kernels and all five infection periods of non-ochratoxin A producing *P. verrucosum* infected barley kernels. The linear, quadratic and Mahalanobis statistical classification accuracies (mean±standard deviation, %) for all the two-class models are given in Table 6.9.

The first two-class model discriminated sterile kernels with classification accuracy between 97.2±0.5 and 98.9±0.6% and combined samples of all infection periods of *A. glaucus* infected kernels with classification accuracy between 96.8±0.7 and 97.9±0.4% for all the three statistical classifiers. The second two-class model discriminated sterile kernels with classification accuracy between 98.1±0.6 and 99.1±0.3% and combined samples of all infection periods of *Penicillium* spp. with classification accuracy between 97.7±0.9 and 98.9±0.5%. The third and fourth two-class models discriminated sterile kernels, combined samples of all five concentration levels of ochratoxin A contaminated barley kernels, and combined samples of all five infection periods of non-ochratoxin A producing *P. verrucosum* infected barley kernels with a classification accuracy of 100±0.0%. The fifth two-class model discriminated sterile kernels with classification accuracy between 97.4±0.9 and 99±0.0% and combined samples of

Table 6.9. Classification accuracies (mean ± standard deviation, %) for two-class model between sterile and combined samples of all five infection periods of fungal infected kernels (AG, PS, No-OTA) and all five concentration levels of ochratoxin A contaminated kernels (OTA). Sample size of sterile, each infection period and each concentration level were 300 kernels.

Two-class model	Sample	Classification accuracies		
		Linear	**Quadratic**	**Mahalanobis**
Sterile vs AG (week 2-10)	Sterile	97.8±0.4	98.9±0.6	97.2±0.5
	AG (week 2-10)	97.2±0.3	97.9±0.4	96.8±0.7
Sterile vs PS (week 2-10)	Sterile	98.6±0.3	99.1±0.3	98.1±0.6
	PS (week 2-10)	98.3±0.6	98.9±0.5	97.7±0.9
Sterile vs OTA(140-814 ppb)	Sterile	100±0.0	100±0.0	100±0.0
	OTA (140-814 ppb)	100±0.0	100±0.0	100±0.0
Sterile vs No-OTA(week 18 -26)	Sterile	100±0.0	100±0.0	100±0.0
	No-OTA (week 18 -26)	100±0.0	100±0.0	100±0.0
Sterile vs AG+ PS (week 2-10)	Sterile	98.4±0.4	99.0±0.0	97.4±0.9
	AG+ PS (week 2-10)	97.9±0.5	98.4±0.4	96.8±0.6
Sterile vs OTA(140-814 ppb)+No-OTA(week 18 -26)	Sterile	100±0.0	100±0.0	100±0.0
	OTA(140-814 ppb) +No-OTA(week 18-26)	100±0.0	100±0.0	100±0.0

all five infection periods of *A. glaucus* and *Penicillium* spp. infected barley kernels with classification accuracy between 96.8±0.6 and 98.4±0.4%. The sixth two-class model discriminated both sterile kernels and combined samples of all five concentration levels of ochratoxin A contaminated barley kernels and all five infection periods of non-ochratoxin A producing *P. verrucosum* infected barley kernels with a classification accuracy of 100±0.0%.

The classification accuracies between sterile and combined samples of all five infection periods of *Penicillium* spp., were higher than the classification accuracies between sterile and combined samples of all five infection periods of *A. glaucus* due to differences in mycelial growth. Both visual and microscopical observations showed that the mycelial growths on *Penicillium* spp., infected barley kernels were higher than the *A.glaucus* infected barley kernels. The classification accuracies between sterile and combined samples of five concentration levels of ochratoxin A contaminated barley kernels and between sterile and combined samples of five infection periods of non-ochratoxin A producing *P. verrucosum* infected barley kernels were 100±0.0% due to high level of fungal infection in these barley kernels (18 to 26 weeks of fungal infection). There was a trend for classification accuracies of quadratic statistical classifiers to be higher than the other two statistical classifiers for all the six two-class models (Senthilkumar et al., 2016).

6.3.5 Six-class classification models

Four six-class models were developed, first to differentiate between all five infection periods of *A. glaucus* infected barley kernels and sterile kernels, second to differentiate between all five infection periods of *Penicillium* spp. infected barley kernels and sterile kernels, third to differentiate between all five concentration levels of ochratoxin A contaminated (ochratoxin A

Table 6.10. Classification accuracies (mean ± standard deviation, %) for six-class model between sterile and different infection periods (2, 4, 6, 8, and 10 weeks post inoculation, 17% moisture content) of *Aspergillus glaucus* (AG) infected barley kernels using statistical and histogram features extracted from 1260, 1310, and 1360 nm wavelengths. Sample size of sterile and each infection period were 300 kernels.

Statistical classifiers	Sample	Sterile	AG week 2	AG week 4	AG week 6	AG week 8	AG week 10
		Classification accuracies					
Linear							
	Sterile	97.1±0.3	3.2±0.5	0±0.0	0±0.0	0±0.0	0±0.0
	AG week 2	13.5±0.4	80.1±0.7	6.7±0.4	0±0.0	0±0.0	0±0.0
	AG week 4	0±0.0	8.9±0.4	92.1±0.5	0±0.0	0±0.0	0±0.0
	AG week 6	0±0.0	0±0.0	2.1±0.3	98.9±0.5	0±0.0	0±0.0
	AG week 8	0±0.0	0±0.0	0±0.0	0±0.0	100±0.0	0±0.0
	AG week 10	0±0.0	0±0.0	0±0.0	0±0.0	0±0.0	100±0.0
Quadratic							
	Sterile	98.6±0.5	1.9±0.5	0±0.0	0±0.0	0±0.0	0±0.0
	AG week 2	13.4±0.4	82.3±0.4	5.6±0.3	0±0.0	0±0.0	0±0.0
	AG week 4	0±0.0	5.5±0.5	94.8±0.4	0±0.0	0±0.0	0±0.0
	AG week 6	0±0.0	0±0.0	0±0.0	100±0.0	0±0.0	0±0.0
	AG week 8	0±0.0	0±0.0	0±0.0	0±0.0	100±0.0	0±0.0
	AG week 10	0±0.0	0±0.0	0±0.0	0±0.0	0±0.0	100±0.0
Mahalanobis							
	Sterile	96.8±0.5	3.9±0.7	0±0.0	0±0.0	0±0.0	0±0.0
	AG week 2	15.8±0.2	78.9±0.3	5.9±0.4	0±0.0	0±0.0	0±0.0
	AG week 4	0±0.0	8.9±0.3	91.8±0.4	0±0.0	0±0.0	0±0.0
	AG week 6	0±0.0	0±0.0	2.7±0.5	98.5±0.2	0±0.0	0±0.0
	AG week 8	0±0.0	0±0.0	0±0.0	0±0.0	100±0.0	0±0.0
	AG week 10	0±0.0	0±0.0	0±0.0	0±0.0	0±0.0	100±0.0

Table 6.11. Classification accuracies (mean ± standard deviation, %) for six-class model between sterile and different infection periods (2, 4, 6, 8, and 10 weeks post inoculation, 17% moisture content) of *Penicillium* spp. (PS) infected barley kernels using extracted statistical and histogram features from 1260, 1310, and 1360 nm wavelengths. Sample size of sterile and each infection period were 300 kernels.

Statistical classifiers	Sample	Sterile	PS week 2	PS week 4	PS week 6	PS week 8	PS week 10
		Classification accuracies					
Linear							
	Sterile	98.1±0.3	2.9±0.5	0±0.0	0±0.0	0±0.0	0±0.0
	PS week 2	1.8±0.4	98.7±0.6	0.2±0.5	0±0.0	0±0.0	0±0.0
	PS week 4	0±0.0	0±0.0	100±0.0	0±0.0	0±0.0	0±0.0
	PS week 6	0±0.0	0±0.0	0±0.0	100±0.0	0±0.0	0±0.0
	PS week 8	0±0.0	0±0.0	0±0.0	0±0.0	100±0.0	0±0.0
	PS week 10	0±0.0	0±0.0	0±0.0	0±0.0	0±0.0	100±0.0
Quadratic							
	Sterile	98.9±0.4	1.6±0.5	0±0.0	0±0.0	0±0.0	0±0.0
	PS week 2	0.9±0.3	99.2±0.5	0.2±0.6	0±0.0	0±0.0	0±0.0
	PS week 4	0±0.0	0±0.0	100±0.0	0±0.0	0±0.0	0±0.0
	PS week 6	0±0.0	0±0.0	0±0.0	100±0.0	0±0.0	0±0.0
	PS week 8	0±0.0	0±0.0	0±0.0	0±0.0	100±0.0	0±0.0
	PS week 10	0±0.0	0±0.0	0±0.0	0±0.0	0±0.0	100±0.0
Mahalanobis							
	Sterile	97.8±0.3	2.8±0.4	0±0.0	0±0.0	0±0.0	0±0.0
	PS week 2	1.8±0.6	98.4±0.8	0.5±0.2	0±0.0	0±0.0	0±0.0
	PS week 4	0±0.0	0±0.0	100±0.0	0±0.0	0±0.0	0±0.0
	PS week 6	0±0.0	0±0.0	0±0.0	100±0.0	0±0.0	0±0.0
	PS week 8	0±0.0	0±0.0	0±0.0	0±0.0	100±0.0	0±0.0
	PS week 10	0±0.0	0±0.0	0±0.0	0±0.0	0±0.0	100±0.0

Table 6.12. Classification accuracies (mean ± standard deviation, %) for six-class model between sterile and different concentration levels (140, 251, 536, 620, 814 ppb, 21.5% moisture content) of ochratoxin A contaminated barley kernels (OTA) using statistical and histogram features extracted from 1310, 1360, and 1480 nm wavelengths. Sample size of sterile and each contamination level were 300 kernels.

Statistical classifiers	Sample	Sterile	OTA 1	OTA 2	OTA 3	OTA 4	OTA 5
		Classification accuracies					
Linear							
	Sterile	100.0±0.0	0.0±0.0	0.0±0.0	0±0.0	0±0.0	0±0.0
	OTA 1	0±0.0	98.7±0.4	1.8±0.5	0±0.0	0±0.0	0±0.0
	OTA 2	0±0.0	0±0.0	100±0.0	0±0.0	0±0.0	0±0.0
	OTA 3	0±0.0	0±0.0	0±0.0	100±0.0	0±0.0	0±0.0
	OTA 4	0±0.0	0±0.0	0±0.0	0±0.0	100±0.0	0±0.0
	OTA 5	0±0.0	0±0.0	0±0.0	0±0.0	0±0.0	100±0.0
Quadratic							
	Sterile	100±0.0	0±0.0	0±0.0	0±0.0	0±0.0	0±0.0
	OTA 1	0±0.0	98.8±0.7	1.6±0.3	0±0.0	0±0.0	0±0.0
	OTA 2	0±0.0	0±0.0	100±0.0	0±0.0	0±0.0	0±0.0
	OTA 3	0±0.0	0±0.0	0±0.0	100±0.0	0±0.0	0±0.0
	OTA 4	0±0.0	0±0.0	0±0.0	0±0.0	100±0.0	0±0.0
	OTA 5	0±0.0	0±0.0	0±0.0	0±0.0	0±0.0	100±0.0
Mahalanobis							
	Sterile	100±0.0	0±0.0	0±0.0	0±0.0	0±0.0	0±0.0
	OTA 1	0±0.0	98.2±0.6	2.4±0.5	0±0.0	0±0.0	0±0.0
	OTA 2	0±0.0	0±0.0	100±0.0	0±0.0	0±0.0	0±0.0
	OTA 3	0±0.0	0±0.0	0±0.0	100±0.0	0±0.0	0±0.0
	OTA 4	0±0.0	0±0.0	0±0.0	0±0.0	100±0.0	0±0.0
	OTA 5	0±0.0	0±0.0	0±0.0	0±0.0	0±0.0	100±0.0

Table 6.13. Classification accuracies (mean ± standard deviation, %) for six-class model between sterile and different infection periods (18, 20, 22, 24, and 26 weeks post inoculation, 21.5% moisture content) of Non-OTA producing *P. verrucosum* infected barley kernels (No-OTA) using statistical and histogram features extracted from 1260, 1310, and 1360 nm wavelengths. Sample size of Sterile and each infection period were 300 kernels.

Statistical classifiers	Sample	Sterile	No-OTA 1	No-OTA 2	No-OTA 3	No-OTA 4	No-OTA 5
		Classification accuracies					
Linear							
	Sterile	100.0±0.0	0.0±0.0	0.0±0.0	0±0.0	0±0.0	0±0.0
	No-OTA 1	0±0.0	98.8±0.4	1.8±0.6	0±0.0	0±0.0	0±0.0
	No-OTA 2	0±0.0	0±0.0	100±0.0	0±0.0	0±0.0	0±0.0
	No-OTA 3	0±0.0	0±0.0	0±0.0	100±0.0	0±0.0	0±0.0
	No-OTA 4	0±0.0	0±0.0	0±0.0	0±0.0	100±0.0	0±0.0
	No-OTA 5	0±0.0	0±0.0	0±0.0	0±0.0	0±0.0	100±0.0
Quadratic							
	Sterile	100±0.0	0±0.0	0±0.0	0±0.0	0±0.0	0±0.0
	No-OTA 1	0±0.0	99.1±0.8	1.4±0.6	0±0.0	0±0.0	0±0.0
	No-OTA 2	0±0.0	0±0.0	100±0.0	0±0.0	0±0.0	0±0.0
	No-OTA 3	0±0.0	0±0.0	0±0.0	100±0.0	0±0.0	0±0.0
	No-OTA 4	0±0.0	0±0.0	0±0.0	0±0.0	100±0.0	0±0.0
	No-OTA 5	0±0.0	0±0.0	0±0.0	0±0.0	0±0.0	100±0.0
Mahalanobis							
	Sterile	100±0.0	0±0.0	0±0.0	0±0.0	0±0.0	0±0.0
	No-OTA 1	0±0.0	98.1±0.5	2.2±0.4	0±0.0	0±0.0	0±0.0
	No-OTA 2	0±0.0	0±0.0	100±0.0	0±0.0	0±0.0	0±0.0
	No-OTA 3	0±0.0	0±0.0	0±0.0	100±0.0	0±0.0	0±0.0
	No-OTA 4	0±0.0	0±0.0	0±0.0	0±0.0	100±0.0	0±0.0
	No-OTA 5	0±0.0	0±0.0	0±0.0	0±0.0	0±0.0	100±0.0

producing *P. verrucosum* infected) barley kernels and sterile kernels, and fourth to differentiate between all five infection periods of non-OTA producing *P. verrucosum* infected barley kernels and sterile kernels. The linear, quadratic, and Mahalanobis statistical classification accuracies for first six-class model are given in Table 6.10. The first six-class model classified sterile kernels with a classification accuracy between 96.8±0.5 and 98.6±0.5%, second week *A. glaucus* infected barley kernels between 78.9±0.3 and 82.3±0.4%, fourth week *A. glaucus* infected barley kernels between 91.8±0.4 and 94.8±0.4%, sixth week *A. glaucus* infected barley kernels between 98.5±0.2 and 100±0.0%, eight and tenth week *A. glaucus* infected barley kernels with 100%. The second week *A. glaucus* infected barley kernels were misclassified into sterile kernels, and fourth week *A. glaucus* infected barley kernels whereas the fourth week *A. glaucus* infected barley kernels were misclassified into second week *A. glaucus* infected barley kernels, this misclassification is due to the fact that during initial periods of fungal infection there were some uninfected barley kernels present in the sample bags. The second six class model classified sterile kernels with classification accuracies between 97.8±0.3 and 98.9±0.4, second week *Penicillium* spp. infected barley kernels between 98.4±0.8 and 99.2±0.5, fourth, sixth, eight and tenth week *Penicillium* spp. infected barley kernels with 100±0.0% for all three statistical classifiers (Table. 6.11). The third six class model classified sterile kernels with a classification accuracy of 100±0.0%, first level of ochratoxin A contaminated barley kernels between 98.2±0.6 and 98.8±0.7%, second, third, fourth and fifth level of ochratoxin A contaminated barley kernels with 100±0.0% (Table. 6.12). The fourth six class model classified sterile kernels with a classification accuracy of 100±0.0%, 18 weeks of non-ochratoxin A producing *P.verrucosum* between 98.1±0.5 and 99.1±0.8%, 20 weeks, 22 weeks, 24 weeks, and 26 weeks of non-ochratoxin A producing *P. verrucosum* with 100±0.0% (Table 6.13). The

Penicillium spp. infected kernels, ochratoxin A contaminated kernels, non-ochratoxin A producing *P. verrucosum* were easily differentiated from sterile kernels at an earlier stage than *A. glaucus* infected barley kernels due to more mycelial growth in *Penicillium* spp., ochratoxin A contaminated kernels, and non-ochratoxin A producing *P. verrucosum* infected kernels (Senthilkumar et al., 2015; 2016). There was a trend for classification accuracies of quadratic statistical classifiers to be higher than the linear and Mahalanobis statistical classifiers for all six-class models.

6.4 Conclusions

The NIR hyperspectral imaging system used in the range from 1000 to 1600 nm at 61 evenly distributed wavelengths can easily separate sterile kernels from fungal infected and ochratoxin A contaminated kernels. The significant wavelengths corresponding to ochratoxin A contaminated kernels were different from *A. glaucus, Penicillium* spp., and non-ochratoxin A producing *P. verrucosum* infected kernels. The wavelength 1480 nm was unique in ochratoxin A contaminated kernels. The *Penicillium* spp. infected kernels, non-ochratoxin A producing *P. verrucosum* infected kernels, and ochratoxin A contaminated kernels can be separated from sterile kernels at an earlier stage than *A. glaucus* infected kernels. There was a trend for classification accuracies of quadratic statistical classifiers to be higher than the linear and Mahalanobis statistical classifiers for all the classification models. The time taken for image acquisition, processing and data analysis for 5 kernels is less than 2 min, and the time taken will be reduced further to less than 1 min if images were scanned only for significant wavelengths. The results prove that the NIR hyperspectral imaging has the potential to differentiate between

different fungal infection periods and different levels of ochratoxin A concentrations in barley kernels at an earlier stage.

References

Abrunhosa, L., R.R.M. Paterson, and A. Venâncio. 2010. Biodegradation of ochratoxin A for food and feed decontamination. *Toxins* 2: 1078-1099.

Anonymous. (2013). Grains of Canada-Canadian Barley. Available from: https://www.grainscanada.gc.ca/barley-orge/bom-mbo-eng.htm. Accessed 11.11.2015.

Arngren, M., P.W. Hansen, B. Eriksen, J. Larsen, and R. Larsen. 2011. Analysis of pregerminated barley using hyperspectral image analysis. *Journal of Agricultural and Food Chemistry* 59(21): 11385-11394.

ASABE. 2012. Standard S352.2: Moisture measurement unground grain and seeds. St. Joseph, Michigan: ASABE.

Cabañes, F.J., M.R. Bragulat, and G. Castella. 2010. Ochratoxin A producing species in the genus *Penicillium. Toxins* 2: 1111-1120.

Chelladurai, V., K. Karuppiah, D.S. Jayas, P.G. Fields, and N.D.G. White. 2014. Detection of *Callosobruchus maculatus* (F.) infestation in soybean using soft X-ray and NIR hyperspectral imaging techniques. *Journal of Stored Products Research* 57: 43-48.

CMBTC. 2012. *Canadian Barley Malting and Brewing Technical Guide*. (5th ed.).Winnipeg: CMBTC. Available from: http://cmbtc.com/CMBTC_Site/Technical_Guide_files/Barley%20Guide_Oct.%2022%202012.pdf. Accessed 11.11.2015

Delwiche, S.R., and D.R. Massie. 1996. Classification of wheat by visible and near infrared reflectance from single kernels. *Cereal Chemistry* 73(3): 399-405.

Duarte, S.C., A. Pena, and C.M. Lino. 2010. A review on ochratoxin A occurrence and effects of processing of cereal and cereal derived food products. *Food Microbiology* 27: 187-198.

FAOSTAT. 2013. Food and Agricultural commodities production. Food and Agricultural Organization of the United Nations. Available from http://faostat3.fao.org/browse/Q/QC/E. Accessed 11.11.15

IARC. 1993 Some naturally occurring substances: Food items and constituents, heterocyclic aromatic amines and mycotoxins. *IARC Monographs on the Evaluation of Carcinogenic Risks to Humans*. 489-521. WHO: Lyon.

Industry Canada. 2013. Trade data Online. Available from: https://www.ic.gc.ca/app/scr/tdst/tdo/crtr.html?&productType=HS6&lang=eng.Accessed 11.11.2015.

JECFA. 2007. Ochratoxin A, *WHO Technical Report Series 947 IPCS* . 169-180. WH0: Geneva.

Kaliramesh, S., V. Chelladurai, D.S. Jayas, K. Alagusundaram, N.D.G. White, and P.G. Fields. 2013. Detection of infestation by *Callosobruchus maculatus* in mungbean using near-infrared hyperspectral imaging. *Journal of Stored Products Research* 52: 107-111.

Karuppiah, K., T. Senthilkumar, D.S. Jayas, and N.D.G. White. 2016. Detection of fungal infection in five different pulses using near-infrared hyperspectral imaging. *Journal of Stored Products Research* 65: 13-18.

Krogh, P. 1992. Role of ochratoxinin disease causation. *Food and Chemical Toxicology* 30: 213-224.

Mahesh, S., D.S. Jayas, J. Paliwal, and N.D.G. White. 2011. Identification of wheat classes at

different moisture levels using near-infrared hyperspectral images of bulk samples. *Sensing and Instrumentation for Food Quality and Safety* 5(1): 1-9.

McGoverin, C., P. Engelbrecht, P. Geladi, and M. Manley. (2011).Characterization of non-viable whole barley, wheat and sorghum grains using near-infrared hyperspectral data and chemometrics. *Analytical and Bioanalytical Chemistry* 401(7): 2283-2289.

Murray, I., and P.C. Williams. 1987. Chemical principles of near-infrared technology. *Near-infrared Technology in the Agricultural and Food Industries*.17-34. AACC : St. Paul, MN.

Palladini, J., and M. Armstrong. 2013. *From Farm to Glass: The Value of Beer in Canada*. 1-34. Conference Board of Canada: Ottawa

Ravikanth L., C.B. Singh, D.S. Jayas, and N.D.G. White. 2015. Classification of contaminants from wheat using near-infrared hyperspectral imaging. *Biosystems Engineering* 135: 73-86.

Sargeant, K., A. Sheridan, and J. Okelly. 1961. Toxicity associated with certain samples of groundnuts. *Nature* 192: 1096-1097.

Senthilkumar, T., C.B. Singh, D.S. Jayas, and N.D.G. White. 2012. Detection of fungal infection in canola using near-infrared hyperspectral imaging. *Journal of Agricultural Engineering* 49(1): 21-27.

Senthilkumar, T., D.S. Jayas, and N.D.G. White. 2015. Detection of different stages of fungal infection in stored canola using near-infrared hyperspectral imaging. *Journal of Stored Products Research* 63: 80-88.

Senthilkumar, T., D.S. Jayas, N.D.G. White, P.G. Fields, and T. Gräfenhan. 2016. Detection of fungal infection and ochratoxin A contamination in stored wheat using near-infrared hyperspectral imaging. *Journal of Stored Products Research* 65: 30-39.

Singh, C. B., D.S. Jayas, J. Paliwal and N.D.G. White. 2007. Fungal detection in wheat using near-infrared hyperspectral imaging. *Transactions of the ASABE* 50(6): 2171-2176.

Singh, C. B., D.S. Jayas, J. Paliwal, and N.D.G. White. 2009a. Detection of insect-damaged wheat kernels using near-infrared hyperspectral imaging. *Journal of Stored Product Research* 45(3): 151-158.

Singh, C. B., D.S. Jayas, J. Paliwal, and N.D.G. White. 2009b. Detection of sprouted and midge-damaged wheat kernels using near-infrared hyperspectral imaging. *Cereal Chemistry* 86(3): 256-260.

Statistics Canada. 2013. Table 002-0001 - Farm cash receipts, annual (dollars), CANSIM (database). (Accessed: 2015-09-20).

Teena, M.A., A. Manickavasagan, L. Ravikanth, and D.S. Jayas. 2014. Near-infrered (NIR) hyperspectral imaging to classify fungal infected dates. *Journal of Stored Products Research* 59: 306-313.

Vadivambal, R., and D.S. Jayas. 2016. *Bio-Imaging: Principles, Techniques and Applications*. CRC Press, Taylor and Francis Group Ltd: Oxford, UK.

Wang, D., F.E. Dowell, and R.E. Lacey. 1999. Single wheat kernel colour classification using neural networks. *Transactions of the ASAE 42*: 233-240.

Wang, D., F.E. Dowell, M.S. Ram, and W.T. Schapaugh. 2003. Classification of fungal damaged soybean seeds using near infrared spectroscopy. I*nternational Journal of Food Properties* 7: 75-82.

WHO. 2001. Ochratoxin A. Safety assessment of certain mycotoxins in food. *WHO Food Additives Series No.* 47. 281-415. WHO: Geneva

Chapter 7

General discussion and conclusions

7.1 Discussion

The preliminary study done to assess the potential of NIR hyperspectral imaging system to detect *A. glaucus* infection in high oil content canola provided promising results. In the preliminary study we took images after 2, 4, 6, 8, and 10 weeks post inoculation from the same sample and moisture content of the samples were not maintained throughout the study. The preliminary study also utilized six statistical features, and it did not utilize the histogram features, because statistical features alone provided promising results. The later studies reported in chapter 4 to 6 involving canola, wheat and barley utilized different samples for different periods of fungal infection and different concentrations of ochratoxin A contamination. The studies reported in chapter 4 to 6 maintained the moisture content of grains throughout the study by placing the samples between buffer samples inside the 20 L plastic pails filled with KOH solution.

The study reported in Chapter 4 involving detection of fungal infection in mixed variety canola seeds utilized only the six statistical features to obtain higher classification accuracy. The study reported in chapter 5 and 6 involving detection of fungal infection and ochratoxin A contamination in wheat and barley utilized both statistical and histogram features to obtain higher classification accuracies. The study involving NIR hyperspectral imaging system to detect fungal infection in wheat, dates and pulses utilized both statistical and histogram features to get higher classification accuracies (Singh et al., 2007; Teena et al., 2014; Kannan et al., 2016).

Studies done to develop safe storage guidelines for mixed variety canola, high oil content canola, and durum wheat used a similar method as in the present study to place the samples inside the 20 L pail filled with KOH solution and between buffer samples to maintain the sample

moisture content up to ten weeks (Sathya et al., 2009; Nithya et al., 2011; Sun et al., 2014). Germination capacity and FAV of different periods of fungal infected canola seeds were determined to confirm the increase in fungal infection over the period of ten weeks. It is a well-established fact that germination decreases with increase in fungal infection and FAV increases with increase in fungal infection (Sun et al., 2014; Nithya et al., 2011). These confirmation tests were not performed in previous studies involving the detection of fungal infection in wheat using NIR hyperspectral imaging system (Singh et al., 2007).

The NIR hyperspectral imaging system used in the range from 1000 to 1600 nm at 10 nm intervals took considerably less time of two minutes to detect fungal and ochratoxin A contamination in cereals and oilseeds, and it can be reduced to one minute if the NIR hyperspectral imaging system is used to acquire images only at the significant wavelengths, whereas traditional microbiological method requires 7 to 15 days and modern polymerase chain reaction (PCR) based methods require 24 h to detect fungal infection (Hayat et al., 2012) ; the traditional chromatographic, immune and aptamer based methods require 2 h to detect ochratoxin A contamination (Hayat et al., 2012). The results obtained in this study show that the NIR hyperspectral imaging system can detect fungal and ochratoxin A contamination in cereals and oilseeds faster than any other available methods. The wavelength 1300 nm found to be significant based on highest principal component loadings in canola, wheat, and barley studies can be attributed to fungal infection in canola, wheat and barley. The wavelength 1300 nm corresponds to C-H bond of cereals and oilseeds and the original C-H bond get altered due to presence of fungal infection in cereals and oilseeds and it is reflected in the NIR spectrum (Wang et al., 2003). Different studies involving the use of NIR hyperspectral imaging system to detect fungal infection in wheat, soybeans, dates, and pulses provided the similar wavelength of 1300

nm to be significant based on highest principal component loadings (Singh et al., 2007; Teena et al., 2014; Wang et al., 2003; Kannan et al., 2016).

The NIR hyperspectral imaging system detected *Penicillium* spp. infected canola, wheat and barley samples with higher classification accuracy than *A. glaucus* infected canola, wheat and barley samples due to difference in mycelial growth, and similar trend was observed in studies on detection of fungal infection in wheat and pulses using NIR hyperspectral imaging system (Singh et al., 2007; Kannan et al., 2016). The *A. glaucus* infected canola, wheat, and barley kernels can be differentiated from the healthy kernels with 100% classification accuracy after four weeks post inoculation, and *Penicillium* spp. infected canola, wheat, and barley can be differentiated from the healthy kernels with 100% classification accuracies after two weeks post inoculation. There was a trend for classification accuracy between healthy and fungal infected canola and barley kernels to be higher than fungal infected wheat and healthy kernels, and it can be confirmed from visual and microscopic inspection that canola and barley spoil much faster than wheat due to their chemical nature. The amount of ochratoxin A produced in barley kernels (140 ppb) are higher than wheat kernels (72 ppb) after 18 weeks post inoculation, due to faster spoilage of barley kernels.

NIR hyperspectral imaging system operated in the range from 1000 to 2500 nm was used to detect aflatoxin B_1 in maize kernels at a very low concentration level of 10 ppb with a classification accuracy of 88% (Wang et al, 2014). Ergot alkaloids in rye, wheat, and oat were detected using NIR hyperspectral imaging system operated in the range between 970 and 2500 nm and a higher correlation of 0.94 between predicted and supplied values was obtained (Vermeulen et al., 2013). There are no reported studies in the literature about detection of ochratoxin A contamination in grains using NIR hyperspectral imaging system; the present study

used the NIR hyperspectral imaging system to detect different concentrations of ochratoxin A contamination in wheat and barley and identified a unique significant wavelength 1480 nm to detect ochratoxin A contamination. The wavelengths 1470, 1480, and 1500 nm were related to protein content of cereals (Wang et al., 1999; Delwiche and Massie, 1996; Murray and Williams, 1987), the peak observed at 1480 nm in ochratoxin A contaminated wheat and barley is due to change in protein composition in ochratoxin A contaminated wheat and barley and it is reflected in the NIR spectrum and identified as significant wavelength based on principal component loadings.

There was a trend for quadratic and Mahalanobis discriminant statistical classifiers to give higher accuracies than linear discriminant statistical classifiers for all the studies involving canola, wheat and barley, and a similar trend was reported in the studies to detect fungal infection in dates and wheat using NIR hyperspectral imaging system (Singh et al., 2007; Teena et al., 2014). The wavelengths 1100, 1130, 1250, and 1300 nm were identified to be significant for detection of fungal infection in canola kernels, wavelengths 1280, 1300, and 1350 nm were identified to be significant for detection of fungal infection in wheat kernels, and wavelengths 1260, 1310, and 1360 nm were identified to be significant for detection of fungal infection in barley kernels. The identified significant wavelengths for different cereals and oilseeds are not similar due to differences in chemical composition of canola, wheat and barley kernels subjected to NIR hyperspectral imaging. Wheat and barley are rich in carbohydrates, 69.7 and 55.8% of total composition, respectively (Haard et al., 1999); whereas canola is rich in oil content with an average oil content of 44.5% and average crude protein content of 19.6% (Canola Council of Canada, 2008). The peaks observed in average spectra and variation in significant wavelengths for canola, wheat and barley are due to the differences in chemical composition of these grains.

Table 7.1. Significant wavelengths corresponding to fungal infection and mycotoxin contamination in different crops in the present study and other studies in the literature.

Crops	Infection	Significant wavelengths (nm)							Source
Canola	Fungi		1100 1130	1250	1300				Present study
Wheat	Fungi			1280	1300 1350				Present study
Barley	Fungi			1260	1310 1360				Present study
Wheat	Fungi			1284	1316 1347				Singh et al., 2007
Chick pea	Fungi		1110	1250	1300	1440	1550		Kannan et al., 2016
Green pea	Fungi		1110	1250 1290	1300 1320	1440	1550		Kannan et al., 2016
Lentils	Fungi	1010 1060	1110	1220 1250	1300		1510 1550		Kannan et al., 2016
Pinto bean	Fungi	1030	1110 1180	1240 1250	1300	1420 1450			Kannan et al., 2016
Kidney bean	Fungi	1020	1110	1200 1250	1300	1440 1450			Kannan et al., 2016
Dates	Fungi		1120		1300			1610 1650	Teena et al., 2014
Soybean	Fungi				1330	1465		1600	Wang et al., 2003
Wheat	Ochratoxin A				1300 1350	1480			Present study
Barley	Ochratoxin A				1310 1360	1480			Present study
Maize	Aflatoxin B_1							1729 2344	Wang et al., 2015

The wavelengths 1250, 1310, 1360 nm identified to be significant can be attributed to carbohydrate content and wavelength 1330 nm can be attributed to kernel hardness in grains, as reported in published literatures involving NIR hyperspectral imaging system to detect different quality parameters associated with various cereals and oilseeds (Wang et al., 1999; Delwiche and Massie, 1996; Murray and Williams, 1987) (Table 7.1).

The previous studies involving the use of NIR hyperspectral imaging detected advanced stages of fungal infection in wheat, maize and soybean (Singh et al., 2007; Williams et al., 2012; Wang et al., 2003), whereas in this present study the fungal infection at an early stage of two weeks post inoculation was detected. The previous studies involving the use of NIR hyperspectral imaging system was used to detect only one stage of fungal infection (Singh et al., 2007; Williams et al., 2012; Wang et al., 2003), but in this study different periods of fungal infected samples were studied to find the classification accuracy between different periods of fungal infected samples and healthy samples and also between different periods of fungal infected samples. The detection of fungal infection at an early stage can be helpful in implementing suitable corrective measures to avoid further spoilage of stored grains. The present study used KOH solution and buffer samples to maintain the moisture content of samples throughout the study, but previous studies involving the use of NIR hyperspectral imaging system to detect fungal infection in cereals and oil seeds did not maintain the moisture content throughout the study (Singh et al., 2007; Williams et al., 2012; Wang et al., 2003).

This study identified a unique wavelength 1480 nm for detection of ochratoxin A in wheat and barley kernels which was not reported in the literature. The correlation between the unique wavelength 1480 nm and ochratoxin A contamination was confirmed by analyzing the data obtained from the non-ochratoxin A producing *P. verrucosum* strain infected barley kernels,

and results obtained proves that the wavelength 1480 nm was linked only with the presence of ochratoxin A in barley samples and not with the non-ochratoxin A producing *P. verrucosum* strain infected barley kernels. The present study discriminated different concentrations of ochratoxin A contaminated kernels from healthy kernels with a classification accuracies of 100%; similar studies utilizing NIR hyperspectral imaging to detect aflatoxin B1 and ergot alkaloids did not report comparison between different concentrations of mycotoxin contaminated samples and healthy samples (Wang et al, 2014; Vermeulen et al., 2013).

The classification accuracy between fungal infected canola, wheat, and barley samples and healthy samples increased with increase in fungal infection periods. The fungal infection levels at initial stages were lower and it increased over the period of ten weeks, the increased levels of fungal infection caused more damage to the canola, wheat, and barley and it is reflected in the NIR spectral data. The similar trend of increase in classification accuracy with the increase in fungal infection level was observed in the study involving detection of fungal infection in dates using NIR hyperspectral imaging system (Teena et al., 2014). The classification accuracies between different periods of A. glaucus infected canola, wheat and barley at initial periods (up to 6 weeks post inoculation) were below 95% and increased to 100% at later periods (after 8 weeks post inoculation) of *A. glaucus* infected canola, wheat and barley; the same trend was observed in a study involving *Aspergillus* and *Penicillium* spp infected pulses using NIR hyperspectral imaging system (Karuppiah et al., 2016). In this present study, the NIR hyperspectral imaging system can differentiate between different periods of *Penicillium* spp infected canola, wheat, and barley with a classification accuracies of 100% after four weeks post inoculation, the *Penicillium* spp infected samples had more mycelial growth than *A. glaucus* infected samples, so the classification accuracies between different periods of *Penicillium* spp infected samples were

higher than classification accuracies obtained for *A. glaucus* infected samples (Karuppiah et al., 2016).

The laboratory model NIR hyperspectral imaging system can easily be modified into a push-broom imaging system by attaching the NIR hyperspectral imaging system to a belt conveyor for commercial purpose. The initial installation cost can be higher, but the non-invasive and non-chemical NIR hyperspectral imaging system can be economical in the long run. There will not be any grain losses due to grain sampling for fungal and ochratoxin A detection. In addition to fungal and mycotoxin detection, various quality parameters like kernel hardness (Williams et al., 2009), protein content (Mahesh et al., 2011), insect damaged wheat kernels (Singh et al., 2009), and presence of physical contaminants (Ravikanth et al., 2015) can be determined in a single scanning using NIR hyperspectral imaging system.

The major limitation of hyperspectral imaging system when compared to other available methods is the handling of large amount of data. The main features of extraction is the requirement of more time for computation. Once a proper extraction and computational algorithms were created, the imaging and classification process become easier. There should be extreme caution during the handling of fungal and ochratoxin A contaminated samples by wearing proper hand gloves and mask. This present study detected ochratoxin A contaminated samples at a lowest concentration level of 72 ppb, but in real time situation it should detect in the range around 5 ppb (Health Canada, 2009). The NIR hyperspectral imaging system available for this present study can operate in the NIR region of 960 to 1700 nm, if there is an availability of NIR hyperspectral imaging system which can operate in the complete NIR region of 700 to 2500 nm, the classification accuracy might have increased at the initial stages of fungal infection. In

this study the classification algorithm was tested only for single kernel imaging, but to replicate the real time scenario bulk samples should be tested with the developed classification algorithms.

.

7.2 Conclusions

Fungal infected canola, wheat, and barley kernels and ochratoxin A contaminated wheat and barley kernels can easily be differentiated from healthy canola, wheat, and barley kernels using a Near-Infrared (NIR) hyperspectral imaging system in the wavelength region between 1000 and 1600 nm with acquired images at 61 evenly distributed wavelengths at 10 nm interval.

The NIR hyperspectral imaging system can also discriminate between *A. glaucus* and *Penicillium* spp. infected canola, wheat, and barley kernels at different periods of post inoculation; discriminate between different concentrations levels of ochratoxin A contamination in wheat, and barley kernels. The classification accuracy between healthy and fungal infected samples increased with increase in fungal infection periods.

Generally, the quadratic and Mahalanobis discriminant statistical classifiers gave higher accuracies than the linear discriminant statistical classifiers for all the pair-wise, two-class, and six-class models developed to differentiate between healthy and fungal infected canola kernels and the quadratic and linear discriminant statistical classifiers gave higher accuracies than the Mahalanobis discriminant statistical classifiers for all the classification models developed to differentiate between healthy, fungal infected, and ochratoxin A contaminated wheat, and barley kernels.

The time taken for image acquisition, processing and data analysis for five kernels was less than 2 min, and the time taken could be reduced to less than 1 min, if images were scanned at the identified significant wavelengths only. The wavelength 1480 nm was significant in ochratoxin A contaminated wheat and barley kernels but was not significant in other fungal infected kernels and non-ochratoxin A producing *P. verrucosum* infected kernels. The *Penicillium* spp. infected

canola, wheat, and barley kernels; ochratoxin A contaminated wheat and barley kernels, and non-ochratoxin A producing *P. verrucosum* infected wheat and barley kernels can easily be separated from healthy kernels at an earlier period post inoculation than the *A. glaucus* infected canola, wheat, and barley kernels due to differences in mycelial growth on canola, wheat, and barley kernels.

The NIR system classified healthy canola, wheat, and barley kernels with > 90%; fungal infected samples with > 80%; and ochratoxin A contaminated wheat, and barley kernels with > 98% classification accuracies. The germination of fungal infected canola, wheat, and barley kernels decreased with increase in fungal infection period. Fat Acidity Values of fungal infected canola kernels increased with increase in fungal infection periods. Moisture content of canola, wheat, and barley kernels were maintained at conditioned moisture content at nearly constant levels throughout the study period.

7.3 Recommendations for future studies

This present study utilized staring single kernel NIR hyperspectral imaging system to detect fungal infection in cereals and oilseeds and ochratoxin A in cereals and proved to be a promising method. The future studies can be focused on using a push-broom NIR hyperspectral imaging system, replicating a real time situation with a NIR hyperspectral imaging system attached to a grain conveyor belt.

The present study detected ochratoxin A contaminated wheat kernels with concentrations as low as 72 ppb in wheat and 140 ppb in barley kernels, the future studies can be focused on detecting ochratoxin A contamination in different grains with concentrations as low as 5 ppb (maximum limit specified by many countries (Health Canada, 2009)).

The present study provided significant wavelengths to detect fungal infection in canola, wheat and barley and ochratoxin A contamination in wheat and barley. The future studies can be done to identify significant wavelengths corresponding to fungal infection and ochratoxin A contamination in durum wheat, oats, rye, soybean, and maize kernels. The data obtained from all these studies can be useful in developing an on-line system to detect fungal infection and ochratoxin A contamination in various grains.

In the present study, the staring single kernel NIR hyperspectral imaging system utilized NIR region from 1000 to 1600 nm, the future studies can utilize the complete NIR region from 700 to 2500 nm to improve classification accuracies.

References

Canola Council of Canada. 2008. Socio-Economic Value Report. Available online: http://www.canolacouncil.org/uploads/Canola_in_Canada_Socio_Economic_Value_Report_January_08.pdf.

Delwiche, S. R., and D.R. Massie. 1996. Classification of wheat by visible and near-infrared reflectance from single kernels. *Cereal Chemistry* 73: 399-405.

Haard, N.F., S.A. Odunfa, C.H. Lee, R.Q. Ramirez, A.L. Quinone, and C.W. Radarte. 1999. Fermented Cereals: A Global Perspective. FAO: Rome.

Hayat, A., N. Paniel, A. Rhouati, J.L. Marty, and L. Barthelmebs.2012. Recent advances in ochratoxin A-producing fungi detection based on PCR methods and ochratoxin A analysis in food matrices. *Food Control* 26(2): 401-415.

Health Canada. 2009. Proposed maximum limits for Ochratoxin A in food products. Ottawa, Canada: Health Canada.

Karuppiah, K., T. Senthilkumar, D.S. Jayas, and N.D.G. White. 2016. Detection of fungal infection in five different pulses using near-infrared hyperspectral imaging. *Journal of Stored Products Research* 65: 13-18.

Mahesh, S., D.S. Jayas, J. Paliwal, and N.D.G. White. 2011. Identification of wheat classes at different moisture levels using near-infrared hyperspectral images of bulk samples. *Sensing and Instrumentation for Food Quality and Safety* 5(1): 1-9.

Murray, I., and P.C. Williams. 1987. Chemical principles of near-infrared technology. In Near-

infrared Technology in the Agricultural and Food Industries, eds. Williams P C; Norris K H. American Association of Cereal Chemists Inc, St. Paul, MN, pp. 17-34.

Nithya, U., V. Chelladurai, D.S. Jayas, and N.D.G. White. 2011. Safe storage guidelines for durum wheat. *Journal of Stored Products Research* 47: 328-333.

Ravikanth, L., C.B. Singh, D.S. Jayas, and N.D.G. White. 2015. Classification of contaminants from wheat using near-infrared hyperspectral imaging. *Biosystems Engineering* 135: 73-86.

Sathya, G., D.S. Jayas, and N.D.G. White. 2009. Safe storage guidelines for canola as the seeds slowly dry. *Canadian Biosystems Engineering* 51: 3.29-3.38.

Singh, C. B., D.S. Jayas, J. Paliwal and N.D.G. White. 2007. Fungal detection in wheat using near-infrared hyperspectral imaging. *Transactions of the ASABE* 50(6): 2171-2176.

Singh, C. B., D.S. Jayas, J. Paliwal, and N.D.G. White. 2009a. Detection of insect-damaged wheat kernels using near-infrared hyperspectral imaging. *Journal of Stored Product Research* 45(3): 151-158.

Sun, K., F. Jian, D.S. Jayas, and N.D.G. White. 2014. Quality changes in high and low oil content canola during storage: Part I - safe storage time under constant temperatures. *Journal of Stored Products Research* 59: 320-327.

Teena, M.A., A. Manickavasagan, L. Ravikanth, and D.S. Jayas. 2014. Near-infrered (NIR) hyperspectral imaging to classify fungal infected dates. *Journal of Stored Products Research* 59: 306-313.

Vermeulen, P.H., J. A. F. Pierna, H. P. Van-Egmond, J. Zegers, P. Dardenne, and V. Baeten.

2013. Validation and transferability study of a method based on near-infrared hyperspectral imaging for the detection and quantification of ergot bodies in cereals. *Analytical and Bioanalytical Chemistry* 405(24): 7765-7772.

Wang, D., F.E. Dowell., and R.E. Lacey. 1999. Single wheat kernel color classification using neural networks. *Transactions of ASAE* 42: 233-240.

Wang, D., F.E. Dowell, M.S. Ram, and W.T. Schapaugh. 2003. Classification of fungal damaged soybean seeds using near infrared spectroscopy. I*nternational Journal of Food Properties* 7: 75-82.

Wang, W., G.W. Heitschmidt, X. Ni, W.R. Windham, S. Hawkins, and X. Chu. 2014. Identification of aflatoxin B_1 on maize kernel surfaces using hyperspectral imaging. *Food Control* 42: 78-86.

Williams, P., P. Geladi, G. Fox, and M. Manely. 2009. Maize kernel hardness classification by near infrared (NIR) hyperspectral imaging and multivariate data analysis. *Analytica Chimcia Acta* 653(2): 121-30.

Williams, P. J., P. Geladi, T.J. Britz, and M. Manley. 2012. Investigation of fungal development in maize kernels using NIR hyperspectral imaging and multivariate data analysis. *Journal of Cereal Science* 55(3): 272-278.

Appendix

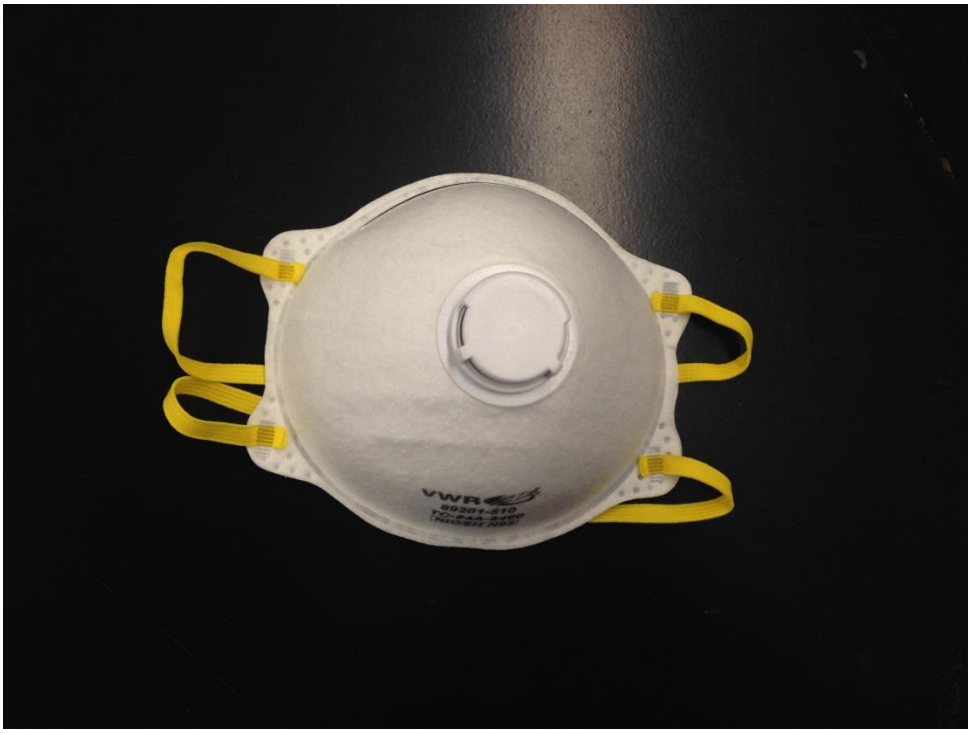

Fig. A.1. Disposable respirator with valve

Fig. A.2. Disposable gloves